Adaptive Reservoir Operation in the Transboundary Nile River Basin

Hisham Eldardiry

A dissertation

submitted in partial fulfillment of the

requirements for the degree of

Doctor of Philosophy

University of Washington

2021

Reading Committee:

Faisal Hossain, Chair

Bart Nijssen

Maoyi Huang

Program Authorized to Offer Degree:

Department of Civil and Environmental Engineering

University of Washington

Abstract

Adaptive Reservoir Operation in the Transboundary Nile River Basin

Hisham Eldardiry

Chair of the Supervisory Committee:
Professor Faisal Hossain
Department of Civil and Environmental Engineering

The Nile River Basin (NRB) is home to more than 200 million people sharing the water resources for agriculture, industry, municipal uses, in-stream navigation, and hydropower generation. A central and existential water management issue for the region is maintaining a sustainable supply of water against increasing population, recurring drought, and climate change. Recent published datasets on future dams reveal an increasingly impounded NRB for hydropower development by upstream and transboundary nations, notably Ethiopia. The most downstream country, Egypt, therefore needs to adapt the operation of High Aswan Dam (HAD), which is key to the country's water security, to planned dams, such as the Grand Ethiopian Renaissance Dam (GERD). *The overarching goal of this dissertation is to derive an adaptive reservoir operating policy under the combined impacts from climate variability, population*

pressures and planned dams. First, a modeling framework was developed to simulate streamflow and understand reservoir operations in the NRB using satellite earth observations and macroscale hydrologic modeling. The satellite-based framework yielded a reasonable skill in deriving monthly HAD releases in good agreement with measured discharge downstream of the dam. Building upon this satellite-based modeling, the second study evaluated the hydrological potential of the Upper Blue Nile (UBN) basin for meeting the declared hydropower production design from the GERD (5150 MW). The results indicated the hydrology of the UBN limited the hydropower potential of GERD and thus the initial plans to upgrade the GERD capacity (from 5250MW to 6000MW to 6450 MW) have not been beneficial to improving the dam's hydropower production. The third study presented a blueprint for adapting HAD operation under the impacts of filling/operation of the GERD based on a Water Supply Stress Index (WaSSI). To adapt to a faster GERD filling scenario (e.g., 3-year filling), HAD needs to modify its operation in summer months by elevating the downstream stress level (store more and release less), e.g., $WaSSI_{AG}$=0.70. Such adaptation can also help HAD recover its normal operating level in four years after GERD is completely filled compared to 7 years with no adaptation scenario. Additionally, maintaining HAD storage at higher levels prior to GERD filling can significantly reduce the HAD recovery period to only 2 years. In the fourth study, a Forecast-based Adaptive Reservoir Operation (FARO) approach is introduced to explore how HAD can improve its operation by using long-term streamflow forecasts. The FARO results showed that the forecast horizon for HAD operation, using perfect forecasts, ranges between 5- and 12-month lead time in low and high demand scenarios, respectively, beyond which the forecast information no longer improves the release decision. . The forecast value to HAD operation is more pronounced in the months following the flooding season (October through December). The work presented in this

dissertation provides a tangible way forward for existing dams to adapt their operations to real-world transboundary challenges while inspiring a win-win deal and considering the equitable rights of development in the Nile countries.

TABLE OF CONTENTS

LIST OF FIGURES

LIST OF TABLES

ACKNOWLEDGEMENTS

"In the name of Allah, Most Gracious, Most Merciful"

I would like to thank Almighty Allah for giving me the opportunity, determination, and strength to do my research and accomplish this achievement. I would like to express my deep and sincere gratitude to my supervisor, Dr. Faisal Hossain, for his continued support, encouragement, and his inspiring guidance throughout the period of my study. It was a great privilege to work under his supervision.

I would also like to offer my special thanks to Dr. Bart Nijssen and Dr. Maoyi Huang for being part of my dissertation committee and providing me with insightful feedback. I also want to thank Benjamin Brunjes for his time as my Graduate School Representative.

I thank my fellow SASWE labmates for all the stimulating discussions and support during my study period. Last but not least, I would also like to thank my parents, elder brother, and elder sister for all their prayers. They were always supporting and encouraging me with their best wishes to keep me concentrated and motivated on my research work.

At the time of writing this dissertation, Chapters 2 and 5 have been published in *Journal of Hydrometeorology. Chapters 3 and 4 have been published in Journal of Hydrology and Journal of Renewable and Sustainable Energy,* respectively. These articles are:

Chapter 2:
Eldardiry, H., and Hossain, F. (2019). Understanding Reservoir Operating Rules in the Transboundary Nile River Basin Using Macroscale Hydrologic Modeling with Satellite Measurements. Journal of Hydrometeorology, 20(11), 2253-2269 (DOI: https://doi.org/10.1175/JHM-D-19-0058.1).

Chapter 3:
Eldardiry, H., and Hossain, F. (2021). Evaluating the Hydropower Potential of the Grand Ethiopian Renaissance Dam. Journal of Renewable and Sustainable Energy.

Chapter 4:
Eldardiry, H., and Hossain, F. (2020). A Blueprint for Adapting High Aswan Dam Operation in Egypt to Challenges of Filling and Operation of the Grand Ethiopian Renaissance Dam. Journal of Hydrology. 125708 (DOI: https://doi.org/10.1016/j.jhydrol.2020.125708).

Chapter 5:
Eldardiry, H., and Hossain, F. (2021). The Value of Long-term Streamflow Forecasts in Adaptive Reservoir Operation: The Case of High Aswan Dam in the Transboundary Nile River Basin. Journal of Hydrometeorology. (DOI: https://doi.org/10.1175/JHM-D-20-0241.1)

Chapter 1: Introduction

1.1 Transboundary Nile River Basin

The Nile River Basin (NRB) is a transboundary river basin that provides a crucial resource for the economy, politics, and the cultural life of eleven countries in the eastern and northeastern Africa. The NRB is currently home to more than 200 million people sharing its water resources for various purposes including agriculture, industry, municipal uses, and in-stream water for navigation and hydropower generation. However, a central water management issue for the NRB is maintaining a sustainable supply of water in the context of multiple stresses including intense population growth, recurring drought, climate change and increasing competition for water. The Nile region is characterized by high population growth and considerable development challenges (Awulachew et al. 2008). The population in the NRB is expected to double in the next twenty-five years. Such an increase will further deplete the region's already scarce water supplies with increasing food and energy demands.

A major challenge to the future governance of water in the NRB is the construction of new dams in the downstream riparian countries. The future hydropower dams inventory provided by Zarfl et al (2015) reveals an increasingly impounded Nile river for hydropower development in the NRB (Figure 1.1). Recently, challenges in managing and securing sustainable water for downstream countries in the NRB are increasing by the introduction of a new large-scale hydropower dam known as the Grand Ethiopian Renaissance Dam (GERD) to the Blue Nile River just upstream of the Ethiopian-Sudan border in Ethiopia. The GERD is one of the major efforts pursued by the Ethiopian government to develop hydropower generation within Ethiopia and thereby reduce poverty. The GERD is currently under-construction and is a gravity dam on the Blue Nile River in Ethiopia located close to the Ethiopia-Sudan border. It will be the largest

hydropower producing dam in Africa with 74 km^3 of reservoir storage and a nameplate generating capacity of 5150 MW (Mulat and Moges, 2014). However, these ambitious Ethiopian plans are expected to impose more stresses on water resources for downstream countries especially Egypt.

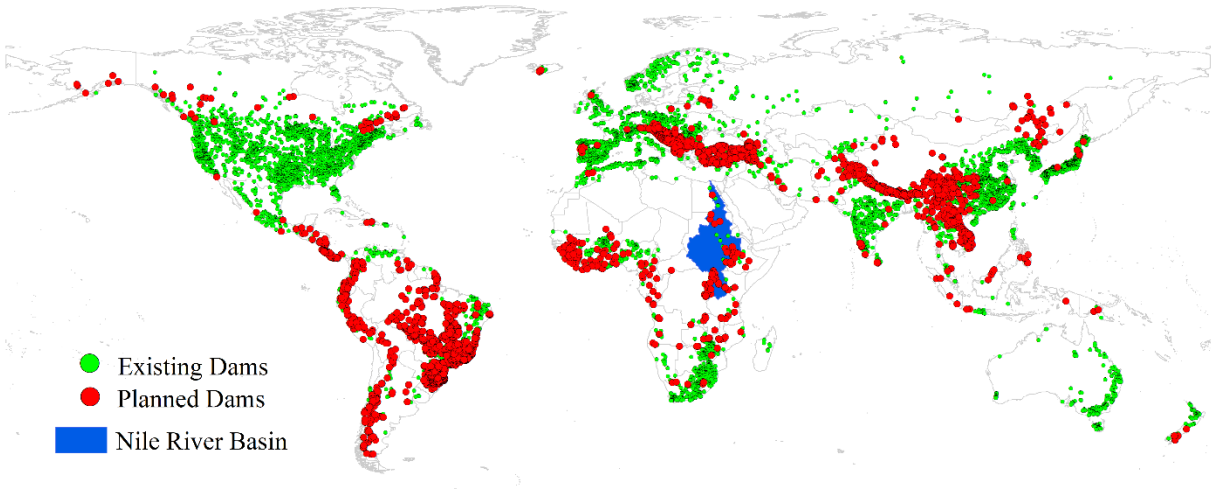

Figure 1.1. Global map of existing and planned dams as provided by the GRanD Database (Lehner et al. 2011) and Zarfl et al. (2015), respectively.

In addition to GERD, three dams (Shereik, Kajbar, and Dal dams) are planned in northern Sudan with a total hydropower capacity exceeding 2000 MW. If these dams become operational, water availability for Egypt, as the most a downstream country, will change dramatically. Therefore, a country like Egypt with its huge population, needs to understand what changes these dams will bring to its water security and agricultural production (agriculture accounts for more than 85% of water use in Egypt. Sudan, and Ethiopia; Figure 1.2). The Nile river flow is almost fully controlled by the High Aswan Dam (HAD) once it enters Egypt. Therefore, changes in future water supply will impact the HAD reservoir operation, which will need to adapt its operation to a new set of conditions.

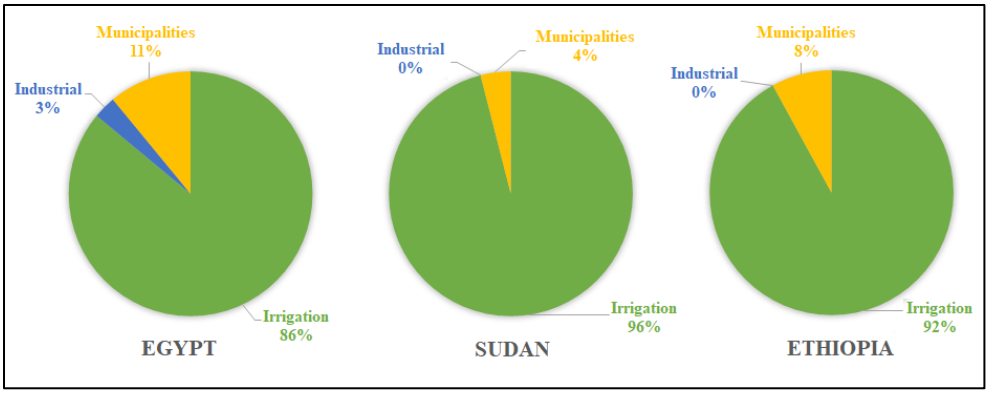

Figure 1.2. Percentage of water withdrawals by sector in the eastern NRB countries (FAO, 2016).

1.2 Adaptive Reservoir Operation

Reservoirs are important water storage infrastructures that are operated to ensure an adequate supply of water by storing water in times of surplus and releasing it in times of scarcity. In the past 60 years, more than 50,000 large dams (higher than 15 m) have been built in the past 60 years (Lehner et al. 2011; Berga et al. 2006). In addition to the need of the of the dam to better regulate the river flow, the global dam-building boom is also attributed to other factors including economic benefits, technocratic nature, and strong political dimensions (Schulz et al. 2018) The reservoir operation policies are usually defined in the form of rule curves, or guide curves to guide reservoir storage and release decisions based on long-term inflow data, downstream water demands, experiential judgment, and engineering standard (Wan et al. 2019). In practice, reservoir operating rules are generally determined at the planning stage. However, after a period of operation, the reservoir operating rule needs to be periodically reevaluated to adapt to changes introduced into the water system. Among the factors affecting reservoir operation in the post-planning stage: 1) increasing downstream water demands with population growth; 2) changes in reservoir storage characteristics due to sediment deposits; 3) irrigation

practices; 4) groundwater access in the area served by the reservoir; 5) climate change effects on the hydrological cycle.; and 6) introducing new hydraulic structures into the water distribution system. An efficient approach to respond to changes in system and deal with anticipated uncertainties is adaptive management (Huntjens et al. 2011). Bormann et al. (1994) defined adaptive management as "*learning to manage by managing to learn*".

Adaptive reservoir operation (ARO) aims to develop robust and flexible strategies such that the reservoir operation performs well under different possible futures and can be modified if necessary (Raadgever et al. 2008). ARO requires a systematic process of active learning by all stakeholders, and continuous improvement of management strategies by learning from the outcomes of implemented policies (Pahl-Wostl 2007). Previous studies have explored revisiting reservoir operating policies to deal with future changes in the water system (e.g., Ahmadi et al. 2014; Eum and Simonovic 2010). However, most of these studies failed to account for the impacts of future dams on the operation of existing dams. Therefore, ARO is an essential approach to respond to the challenges introduced by new upstream dams in transboundary river basins. Such challenges are particularly evident in the case of the GERD in the Nile river.

1.3 Research Objectives

Addressing challenges to manage and operate reservoirs in developing nations is hindered by lack of data (e.g., operating policy or storage plans) shared among neighboring nations. This dissertation will benefit from the availability of high spatial and temporal resolution satellite observations as a potential solution for limited data availability. *The overarching goal of this dissertation is to derive adaptive reservoir operating policy under the combined impacts from climate variability, population pressures and planned dams.* The specific questions addressed in this dissertation are:

1. Can satellite observations with hydrologic modeling be used to understand reservoir operation in the Nile River Basin?
2. Can Grand Ethiopian Renaissance Dam live up to its promise of hydropower?
3. How can the HAD adapt its operation to the filling and operation of the upstream transboundary GERD?
4. What is the value of long-term (seasonal) streamflow forecast in improving HAD operation?

To address such questions, this dissertation integrated a suite of satellite missions,e.g., Tropical Rainfall Measuring Mission (TRMM), Landsat, Moderate Resolution Imaging Spectroradiometer (MODIS) and forecast products with macroscale hydrological modeling to derive adaptive reservoir operation strategies in the transboundary NRB. This dissertation will particularly focus on the adaptation of HAD operation to GERD construction, which typifies one of the challenges facing dam operators and water managers in downstream Nile riparian countries. Recently, various studies have investigated the impacts of GERD on downstream countries with more focus on the GERD filling strategies (King and Block 2014; Mulat and Moges 2014; Zhang et al. 2015; Wheeler et al. 2016). However, crucial insights on how dam operators can adapt to potential impacts have not been capitalized in previous studies. In addition, the work presented in this dissertation is unique in its singular lack of dependency on real-time in-situ observations (that are often unavailable) to derive adaptive reservoir operation. Thus, taking advantage of satellite observation makes the approach presented in this dissertation easily transferable to other river basins (e.g., Mekong river with increasing dams).

1.4 Dissertation Outline

This dissertation is organized as follows: in the second chapter of this dissertation, a modeling framework was developed to simulate streamflow and understand reservoir operation in the NRB using satellite earth observations and macroscale hydrologic modeling. Building upon this satellite-based modeling, the third chapter evaluated the hydrological potential of the Upper Blue Nile (UBN) basin for meeting the declared hydropower production design from the GERD. The fourth chapter presented a blueprint for adapting HAD operation under the impacts of filling/operation of the GERD based on a Water Supply Stress Index (WaSSI). In the fifth chapter, a forecast-based adaptive reservoir operation is introduced to explore how HAD can improve its operation by using long-term streamflow forecasts. The last chapter provides concluding remarks and potential implications of the work presented in this dissertation.

Chapter 2: Understanding reservoir operating rules in the transboundary Nile River Basin using macroscale hydrologic modeling with satellite measurements

Note: This chapter has been published mostly in its current form in Journal of Hydrometeorology (Eldardiry and Hossain 2019);

Eldardiry, H., and Hossain, F. (2019). Understanding Reservoir Operating Rules in the Transboundary Nile River Basin Using Macroscale Hydrologic Modeling with Satellite Measurements. Journal of Hydrometeorology, 20(11), 2253-2269 (DOI: https://doi.org/10.1175/JHM-D-19-0058.1).

Abstract

Challenges to manage and secure sustainable water supply are expected to become more acute in Egypt as the lowermost riparian country of the Nile basin with the construction of new transboundary water infrastructures in Ethiopia and Sudan. To understand the impact of such transboundary water projects on Egypt, it is first necessary to develop a modeling tool that can simulate potential flow and reservoir scenarios inside Egypt without requiring in-situ hydrologic or transboundary dam data that is typically unavailable. This study presents the water management value of a modeling framework to predict the current and future reservoir operating rules in lower Nile basin using satellite earth observations and hydrologic models. The platform comprises the Variable Infiltration Capacity (VIC) hydrologic model driven by high spatial and temporal resolution of satellite observations. Reservoir storage change is estimated using altimeter and visible imagery of lake area for Lake Nasser and then applied to infer reservoir operation for High Aswan Dam (HAD). The modeling framework based on satellite observations yielded a simulated streamflow at the outlet for Blue Nile Basin (BNB) with a Nash-Sutcliffe efficiency of 0.68 with a correlation and RMSE of 0.94 and 1095 m^3/sec, respectively. Storage and outflow discharge of HAD were estimated for the period of 1998-2002 within 1.4 %

accuracy (0.076 km^3/month) when compared with published reports. Because BNB controls the lion share of the variability to HAD inflow inside Egypt, the proposed modeling framework is appropriate for policy makers to understand the implications of transboundary projects on future water security of Egypt.

2.1 Introduction

The Nile River basin is home to more than 200 million people sharing the water resources for agriculture, industry, municipal uses, in-stream navigation and hydropower generation. Maintaining a sustainable supply of water resources to meet these demands is a major water management issue for the Nile region due to increasing population, increasing water demand, recurring drought, and climate change. Nowhere is this issue more critical than in Egypt, the lowermost riparian country with more than 90 million that is singularly dependent on the Nile river. In addition to a rapidly growing population, the agricultural sector in Egypt depends primarily on Nile water with a percentage of water withdrawal of 86% (FAO 2016). Such challenges to manage and secure sustainable water are expected to become more acute (for Egypt) with the construction of a new large-scale hydropower dam in Ethiopia known as Grand Ethiopian Renaissance Dam (GERD) (Figure 2.1). The GERD will be the key driver of flow regime change as the largest hydropower dam in Africa with over 60 km^3 of active reservoir storage (e.g., 10 times Grand Coulee Dam in the US) and a 6000 MW hydropower capacity (King and Block 2014; Mulat and Moges 2014: Zhang et al. 2015).

In addition to the ongoing construction of the GERD dam, the future hydropower dams inventory provided by Zarfl et al (2015) reveals an increasingly impounded Nile river for hydropower development upstream of Egypt. For instance, Figure 2.1 shows three planned dams (Shereik, Kajbar, and Dal dams) in northern Sudan with a total hydropower capacity exceeding

2000 MW. If these dams become operational, the water availability for the three more powerful nations (Egypt, Sudan and Ethiopia) will change dramatically. Hence, downstream countries (in this case it is only Egypt) need to understand what changes the upstream transboundary dams will bring to water security and changes to the Nile flow regime on seasonal and inter-annual time scales.

Egypt is the most downstream country that primarily relies on Nile water inflow as the main source of water supply with an annual average flow of 55.5 km^3/year under the Nile Waters Agreement of 1959 between Egypt and Sudan. Eighty-four percent of the water entering Egypt at Lake Nasser originates from the Ethiopian highlands through the Blue Nile Basin (BNB) (57%), Sobat river (14%) and Atbara river (13%) (Shahin 1985). At the peak flow season (July through October), the BNB provides nearly 70% of all water reaching High Aswan Dam (HAD) in Egypt, while the remaining 30% is supplied by the White Nile and the Atbara river (Melesse et al. 2011; Taye et al. 2015). Alternative sources of water supply in Egypt include rainfall on the northern strip of the Mediterranean Sea and Sinai region, and groundwater (Allam and Allam 2007). The Nile river flow is almost fully controlled by the HAD once it enters Egypt. The HAD controls flow entering Lake Nasser to supply water required for irrigation and hydropower generation and to protect Egypt against floods in the Nile delta (Abu-Zeid and El-Shibini 1997).

While GERD completion is expected to improve the energy and food security for Ethiopia, its impact on HAD operation and water security in Egypt is currently unknown. Adapting the current policies for HAD operation (and without considering GERD), Mohie El Din and Moussa (2016) reported an expected water shortage of 26 km^3/year given population growth rate, expansion in industrial water withdrawals, and increase in agricultural areas. It is likely that a project like GERD will intensify such threats of water shortage and therefore result

in reduced reliability for energy and food production in Egypt (Mulat and Moges 2014). Mohie El Din and Moussa (2016) proposed different planning measures to offset the expected shortage in water supply including, planning alternatives to the irrigation canals, controlling pumping rates of deep groundwater, and applying sprinkler and drip irrigation systems in new agricultural lands.

The current construction of the GERD dam along the BNB in Ethiopia will make the HAD operation rules face considerable uncertainty. The question now is, how should the reservoir rules be readjusted to cope with the expected reduction in inflow from the BNB against an uncertain and closely-guarded transboundary dam operation by GERD? Transboundary dams in developing nations most often do not share reservoir operating policy or storage plans with neighboring nations (Balthrop and Hossain 2010; Gerlak et al. 2013). Since a major concern is how the filling of the GERD reservoir will impact water availability in Egypt, it is important to understand current operation of HAD as an important first step. The use of hydro-meteorological data is a key information for understanding reservoir operation. However, such data are frequently not readily available, particularly in transboundary river basins, either because of lack of in-situ measurements or due to lack of data sharing agreements among the riparian countries (Hossain et al. 2007; Plengsaeng et al. 2014). The limited ground-based observation network over the Nile river basin makes satellite products that are currently available at a wide range of spatial and temporal resolutions more appropriate.

The current study builds a modeling framework to understand the HAD reservoir operation using satellite observations. This satellite-based framework comprises two main components: 1) a macroscale hydrological model for the BNB; and 2) a satellite altimetry-based reservoir component combined with a hydrologic model to infer the operation of HAD reservoir.

Satellite remote sensing has been shown to play a fundamental role in predicting the hydrologic state of the developing nations situated in international river basins (Hossain and Katiyar 2006). The use of such satellite-driven approach in modeling hydrologic conditions has been successfully implemented in operational environments for transboundary basins like Mekong basin (Bonnema and Hossain 2017; Bonnema and Hossain 2019) and Ganges-Brahmaputra-Meghna (GBM) basin in Southeast Asia (Siddique-E-Akbor et al. 2014), Indus river basin (Iqbal et al. 2016; Iqbal et al. 2017). Over the Nile river basin, satellite observations have been applied for many applications, such as rainfall estimation (e.g., Dinku et al. 2011; Rientjes et al. 2011; Habib et al. 2012; Gebremichael et al. 2014), evapotranspiration modeling (e.g., Enku et al. 2011; Allam et al. 2016) and monitoring water storage using GRACE (Gravity Recovery and Climate Experiment) satellites (e.g., Longuevergne et al. 2013; Awange et al. 2014). Our study builds on the current availability of satellite-based observations of various water cycle variables, terrain and land cover at high temporal and spatial resolutions to set up a macroscale hydrological model for the BNB. Our first objective is to implement the Variable Infiltration Capacity (VIC) macroscale model for the BNB to develop the first component of the satellite-based framework.

The second objective of our study is to understand the reservoir operation for Lake Nasser impounded by the HAD. The introduction of satellite remote sensing provides a pragmatic way forward to monitor reservoir dynamics through imagery or data from various freely-available satellite sensors such as Landsat and MODIS sensors (Wulder et al. 2012). Measuring water level fluctuations in reservoirs is now well-established using satellite altimetry (Birkett 1998; Alsdorf et al. 2001; Calmant et al. 2008). For example, Keys and Scott (2018) used MODIS images and altimetry data over Lake Tana to estimate surface area and water level,

respectively. They found that in-situ data and satellite-based estimation for surface area and water level are in a high level of agreement with correlation coefficient of 0.88 and 0.97, respectively. In our study, the outputs from the hydrological model (mainly the routed streamflow) are combined with altimetry-based water levels and SRTM data to estimate the outflow from the HAD reservoir using a water balance approach. A similar approach has been applied by Bonnema and Hossain (2017) in the Mekong River and by Bonnema et al. (2016) in the Karnaphulli river. They reported the feasibility of satellite driven models in capturing the spatiotemporal variability of reservoir dynamics in terms of outflows and storage change. Given the limited data shared between Nile riparian countries, building a predictive framework based on the satellite information is fundamentally the only pathway towards understanding the impacts of ongoing and future transboundary water projects on surface water availability.

A central question addressed by our study is: can we benefit from satellite hydro-meteorologic observations and hydrologic modeling to build a skillful predictive framework that can efficiently reproduce the operation of the HAD? Building such satellite-based framework will contribute to the existing class of models available for the Nile basin, that have been primarily driven by in-situ data and requires retrieving such data from local water resource agencies in near real-time. RIBASIM (van der Krogt and Ogink, 2013), and RiverWare (Wheeler and Setzer, 2012) are two examples of hydrologic models which were developed as part of Eastern Nile Planning Models project in the Eastern Nile Technical Regional Office (ENTRO) of Nile Basin Initiative (NBI)). While the in-situ data for such models were made available by the ENTRO office, our satellite framework has the benefit of using globally free satellite images to understand reservoir operation independent of availability of in-situ data from multiple agencies. Furthermore, our predictive framework is intended to lay the background for subsequent

investigation of the impacts of future water projects on the management of water resources in eastern Nile basin riparian countries (Ethiopia, Sudan, and Egypt). Examples of such investigations that can be explored by our modeling framework include: 1) studying the impacts of GERD (during filling and operation phases) on the water reaching Sudan and Egypt; and 2) revisiting the HAD operation rules to account for water flow changes induced by upstream projects. The remainder of the paper is organized as follows: we introduce the study area in section 2, data sources and methods are summarized in section 3, results for the hydrological modeling and monitoring HAD reservoir operation are discussed in section 4, implications of the developed framework and concluding remarks are in sections 5 and 6, respectively.

2.2 Study Area

The Nile River Basin is a major transboundary river that passes through eleven countries in northeastern Africa (Figure 2.1): Burundi, Egypt, Eritrea, Ethiopia, Kenya, Rwanda, Sudan, South Sudan, Tanzania, Uganda and the Democratic Republic of the Congo (DRC). It comprises two major tributaries, the Blue Nile Basin and the White Nile. The White Nile originates from the Great Lakes region of central Africa, and flows north through Tanzania, Lake Victoria, Uganda and southern Sudan. The Blue Nile starts at Lake Tana in Ethiopia and is considered the primary tributary of the main Nile River (given its high contribution to total Nile river discharge). The confluence of the Blue Nile and the White Nile is at the Sudanese capital Khartoum. The river then flows north through Sudan and Egypt to drain into the Mediterranean Sea. Precipitation within the basin is highly seasonal, driven primarily by the northward and southward movement of the Inter Tropical Convergence Zone (ITCZ) and other large-scale oceanic-atmospheric drivers (Block and Rajagopalan 2007). Annual precipitation rates in the

Ethiopian highlands range from 800 to 2200 mm, with the majority falling during the main rainy season (from June to September) (Melesse et al. 2011).

The water management in the Nile River is challenging due to increasing population, climate change, and future plans on building new dams. Figure 2.1 shows the existing, planned, and under construction dams in the basin according to the Global Reservoir and Dam (GRanD) Database (Lehner et al. 2011) and the global inventory of hydropower dams produced by Zarfl et al. (2015). The major dams on the Nile are Roseires Dam (situated in BNB in Sudan), Sennar Dam (situated in BNB in Sudan), Merowe Dam (the main Nile in Sudan), High Aswan Dam (the main Nile in Egypt), and Owen Falls Dam (White Nile at Lake Victoria in Uganda). The purposes of the major dams are to produce hydroelectric power and provide water supply needed to meet irrigation demands. The most downstream dam is the HAD dam that was built to provide hydropower (2100 MW) and regulate the water releases for irrigation demands in the Nile Delta.

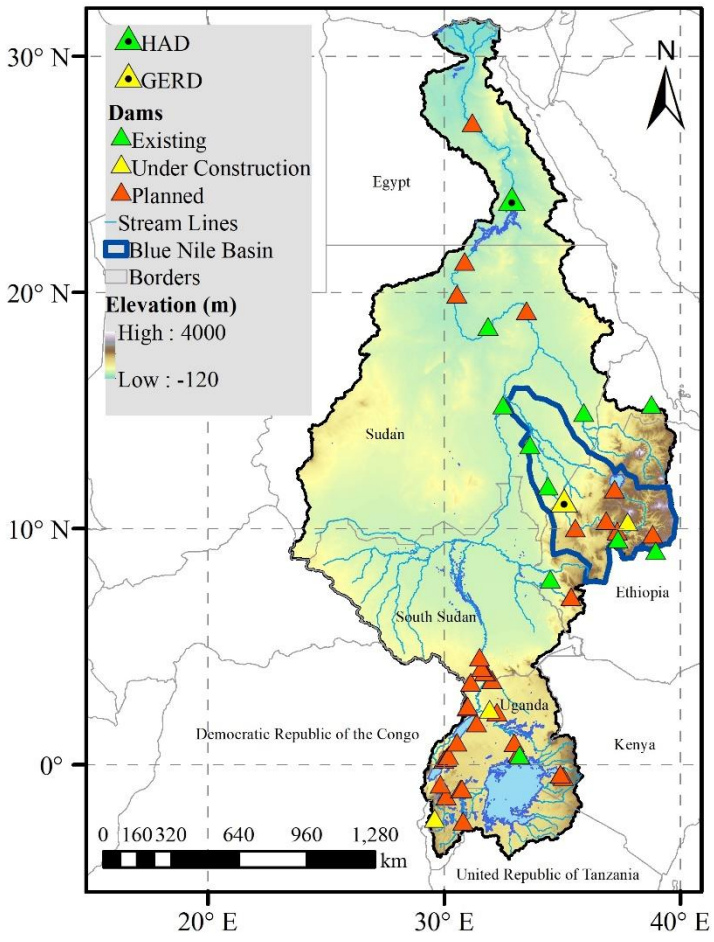

Figure 2.1. Map of Nile river basin with different stages of dams (existing, under construction, and planned) as provided by the GRanD Database (Lehner et al., 2011) and Zarfl et al. (2015).

The HAD storage reservoir is Lake Nasser which is one of the largest man-made lakes in the world and is key to Egypt's water security. The lake has a length of about 500 km and it is located in a very dry climate with an average annual evaporation of 2.1 m/year (about 8% of the average reservoir depth) and negligible rainfall (Ebaid and Ismail 2010). The operation rule of Lake Nasser reservoir is paramount to ensuring adequate water supply and the safety of the HAD. At the beginning of the water year (1st of August), the water level is kept at 175 m above mean sea level (AMSL) to fulfil high and low flow requirement (Muala et al. 2014). When the water level upstream exceeds 178 m, water is redirected to the Toshka Depression and, if

necessary, sluices emergency spillway are used to release the surplus flow (Bastawesy et al. 2008). The maximum retention at 180 m AMSL is obtained in November. As water is released from January to July, the reservoir levels decrease (El-Shafie et al. 2007). The regulation of the HAD reservoir and releases to fulfill downstream irrigation in Egypt have been decided on by the 1959 treaty between Egypt and Sudan (Waterbury 2008; Awulachew et al. 2011). This treaty, entitled "The Full Utilization of the Nile," allocated all the Nile flow between the two countries (55.5 km^3 for Egypt and 18.5 km^3 for Sudan) with no consideration of upstream riparian countries and their development plans. However, such situation is currently changing with ongoing development projects in the BNB (e.g., GERD dam) and hence, it becomes of utmost importance to re-evaluate the operation of the HAD dam.

2.3 Datasets and Methods

2.3.1 Macroscale Hydrologic Model

As mentioned earlier, the first objective of our study is to build and demonstrate predictive skill of a hydrological modeling framework for the BNB that can be used to assess reservoir operations in the Nile River. We used the Variable Infiltration Capacity (VIC) model. VIC is a macroscale hydrological model that represents surface and subsurface hydrologic processes on spatially distributed grid cells (Liang et al. 1994, 1996). The model parameterization includes the representation of subgrid-scale variability in vegetation coverage, topography, precipitation, and soil moisture storage capacity. The VIC model has been successfully used for a large number of hydrological studies in different climatic environments (see for example: Lohmann et al. 1998; Nijssen et al. 2001; Maurer et al. 2002; Liang and Guo 2003; Zhu and Lettenmaier 2007).

In our study, the VIC model was implemented at 0.1° (~10 km) spatial resolution for the BNB and using the water balance approach for each grid cell. Table 2.1 summarizes the types of data that are processed and analyzed for setting the BNB VIC model: 1) topographic data, 2) meteorological forcing data, 3) vegetation data, and 4) soil data. The VIC model primary forcing for running water balance mode are precipitation, maximum and minimum temperature, and daily average wind speed. The daily satellite-based precipitation was retrieved from the latest version of the Climate Hazards group Infrared Precipitation with Stations (CHIRPS v.2) dataset for 37-year period 1981-2017 (Funk et al. 2014, 2015). CHIRPS has been globally used as an useful rainfall dataset for trend analysis and seasonal drought monitoring (e.g., Bayissa et al. 2017; Paredes-Trejo et al. 2017; Gao et al. 2018), given its long time-series record (more than 30 years) and high spatial resolution (0.05°). For example, Bayissa et al. (2017) selected the CHIRPS rainfall product, due to its higher accuracy compared to other satellite-based precipitation estimates (e.g., PERSIANN and TRMM products), to assess the spatial and temporal variability of meteorological drought for the Upper BNB. They concluded that CHIRPS rainfall product can be used for developing grid-based drought monitoring tools for the basin. Daily temperature (minimum and maximum) and wind speed data were obtained from the Global Summary of the Day by National Climatic Data Center (GSOD/NCDC).

Table 2.1. Summary of the datasets used as inputs in the VIC modeling of the BNB.

Input	Dataset	Spatial Resolution
Precipitation	Climate Hazards group Infrared Precipitation with Stations (CHIRPS)	0.05°
Temperature	National Climatic Data Center (NCDC)	Gauges
Wind Speed	National Climatic Data Center (NCDC)	Gauges

Topography	Shuttle Radar Topographic Model (SRTM)	30 m
Soil type	Harmonized World Soil Database (HWSD)	30 arc-second
Land Cover	Global Land Cover Characterization (GLCC)	1 kilometer
Vegetation type	Moderate Resolution Imaging Spectroradiometer (MODIS)	500 meter

A digital elevation model (DEM) was created for the BNB by collecting elevation data from the Shuttle Radar Topographic Model (SRTM). The SRTM data was used to determine the stream network (flow direction data) in the BNB. Vegetation data such as monthly leaf area index and albedo were obtained from the Moderate Resolution Imaging Spectroradiometer (MODIS) mission. The MODIS data has been widely used to classify vegetation type over many river basins (see for example Teferi et al. (2015) and Allam et al. (2016) over the upper BNB). Land cover type was prepared using the Global Land Cover Characterization (GLCC) (Loveland et al. 2000), while soil type data was obtained from the Harmonized World Soil Database (HWSD) (Nachtergaele, 1999).

The aforementioned forcing datasets were processed over the BNB at a daily scale and re-gridded to the 0.1° spatial scale to drive the VIC model land surface simulations. The runoff (from the VIC outputs) over each grid cell was then routed separately using the routing model scheme of Lohmann et al. (1998). We calibrated the BNB model for daily and monthly streamflow at Khartoum station (outlet of the BNB) (Figure 2.1). The calibration and validation procedures were performed over five-year periods (1993-1997) and (1998-2002), respectively, during which streamflow observations are available. In-situ data were obtained for calibration and validation periods from reports published by the Ministry of Water Resources and Irrigation (MWRI) in Egypt. In addition to visual comparison of monthly simulated and observed

hydrographs, error statistics were used to assess the model performance. These metrics are relative bias (RBIAS), root-mean-squared error (RMSE), normalized root-mean-squared error (NRMSE), correlation coefficient, and Nash-Sutcliffe model efficiency coefficient (NSE).

2.3.2 Reservoir Modeling Approach

The reservoir modeling approach was built on the VIC modeling framework. Dam operating rules for Lake Nasser reservoir were inferred by calculating outflow discharges of HAD using a water balance approach. Figure 2.2 shows a schematic diagram for the different tributaries contributing to the inflow at HAD. Figure 2.3 shows the monthly streamflow along the tributaries feeding the Main Nile (Blue Nile, White Nile, and Atabara River). Because BNB represents the lionshare of the total flow in the main Nile in Egypt, the variability of inflow to Lake Nasser can be assumed to be primarily controlled by the BNB flow. Average monthly flow contributing from the White Nile and Atbara rivers were retrieved from Sutcliff and Perks (1999) at the two outlet stations: Mogren and Atbara, respectively. The estimation of reservoir releases were then computed through a three-step process as follows:

2.3.2.1 Deriving Area- Elevation Curve

A relationship between reservoir surface area and elevation was established for the reservoir under study (Lake Nasser in our case). This relationship is known as the area-elevation curve. For Lake Nasser, a 30 m resolution digital elevation model (DEM) provided by SRTM was classified into 1 m elevation bands over the reservoir and surrounding area. The surface area of each elevation band provides an estimate of the reservoir surface corresponding to the water elevation reached. Deriving area-elevation curve using satellite-based estimates has been widely employed in previous studies (see for example Wang et al. 2013 over the Three Gorges reservoir and Bonnema and Hossain (2017) over the Mekong River). To infer water elevation below the

level when SRTM overpassed the HAD reservoir, additional observations of water surface area from Landsat images were used. The classification of the Landsat image was performed using the normalized difference water index (NDWI) using the reflectance values in the green and near infrared wavelengths, respectively (for more details, see Bonnema and Hossain 2017). Figure 2.4 shows the derived relationship between water surface elevation and surface area over Lake Nasser.

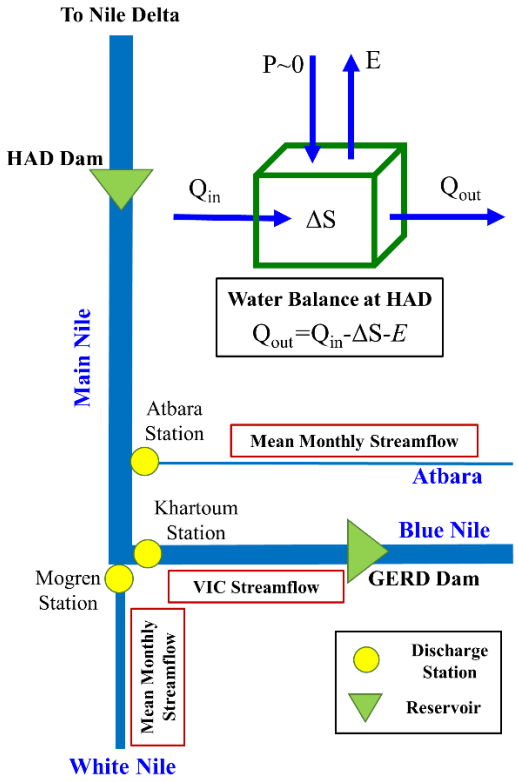

Figure 2.2. Schematic diagram of the streamflow from the Nile river tributaries that contribute to the total flow reaching the HAD dam in Egypt. The yellow dots represents the two stations

(Mogren and Atbara) at the outlets of the White Nile and Atbara River, respectively, where average monthly streamflow is considered.

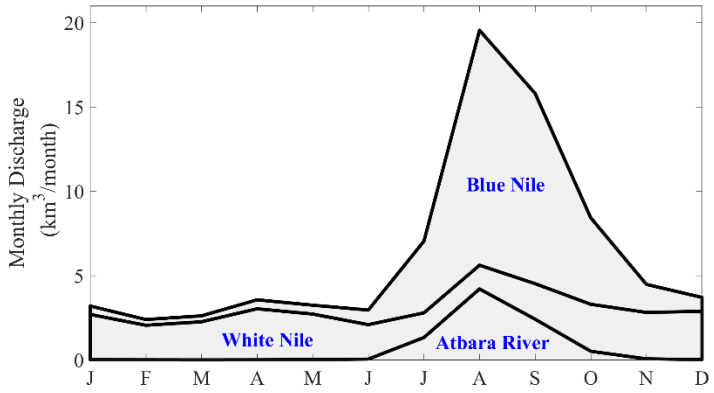

Figure 2.3. The contribution of Blue Nile, White Nile, and Atbara River tributaries to the monthly streamflow of the Main Nile (data source: Sutcliff and Parks (1999)).

2.3.2.2 Altimetry-Based Water Levels

The derived area-elevation curve was used to convert satellite measurements of water surface elevation into reservoir volume. The water levels over Lake Nasser were estimated using the radar altimetry-based water surface elevations that were acquired from the operational satellite altimetry Hydroweb database. This database involved five radar altimetry missions including T/P (Topex/Poseidon), Jason-1, Jason-2, GFO (Geosat Fellow On) and ENVISAT (ENVIronmental SATellite). The reader is referred to Crétaux et al. (2011) for a detailed description of the procedures used for processing water level in Hydroweb. To validate our results, in-situ water levels from a gaging station upstream of HAD were compared with satellite derived estimates. Figure 2.5 shows the altimetry water level for the period 1998-2002 in good agreement with observed water levels in terms of phase and amplitude. Correlation coefficient and RMSE of monthly data from Hydroweb against in situ water levels are 0.99 and 0.40m,

respectively. The RMSE represents about 0.22 % of the mean monthly water level ~178.49 m. Such metrics indicate very close agreement with measured levels and the skill of altimetry-based water levels for our water balance modeling. The Hydroweb was chosen over other preprocessed datasets because of its accuracy over Lake Nasser reservoir. For example, we observed that the mean absolute error of water level over lake Nasser from the Hydroweb dataset was 0.3 m compared to 0.7 m using the USDA Global Reservoir and Lake Monitoring (GRLM) database.

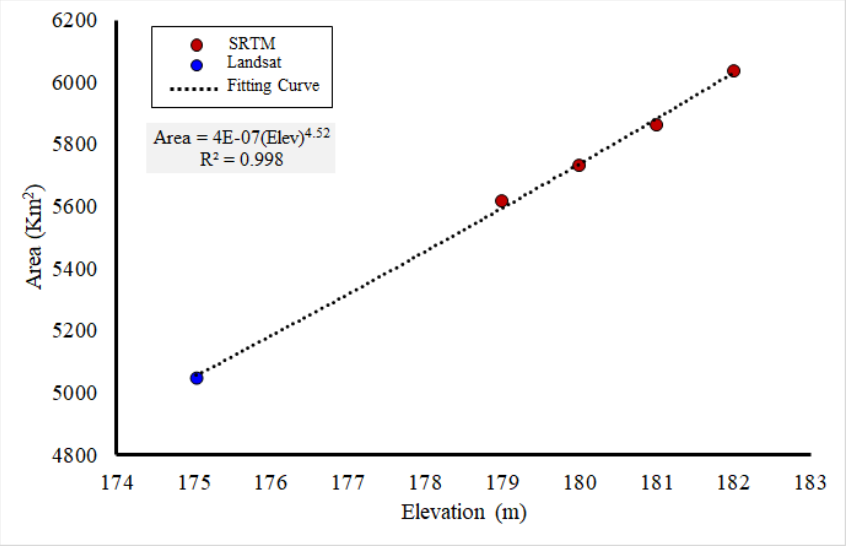

Figure 2.4. Deriving Elevation-Area curve for the HAD using SRTM (the lowest point is derived from Landsat Image and the corresponding altimetry-based water level).

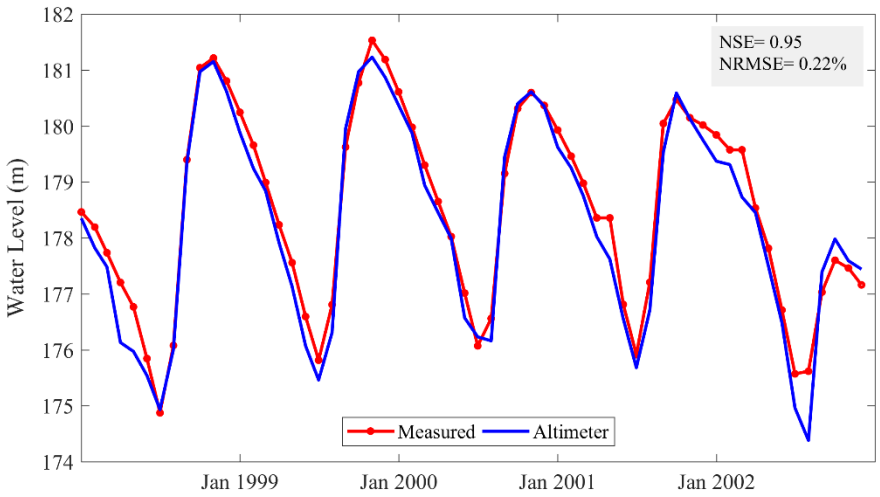

Figure 2.5. Altimetry-based water levels compared to gauge readings over Lake Nasser.

2.3.2.3 Water Balance Model

A water balance model (Equation 1) was used to compute the reservoir release, which was then applied to establish a monthly release curve for the HAD reservoir. The water balance equation (assuming negligible groundwater interactions) is:

$$Q_{out} = Q_{in} - \frac{dS}{dt} - E \quad \text{(Equation 1)}$$

where Q_{in} is the inflow in km^3/month, Q_{out} is the reservoir discharge downstream of the HAD in km^3/month, E is the open water evaporation in km^3/month, and dS/dt represents the change in storage volume with time in km^3/month. The monthly inflow to the reservoir (Q_{in}) was obtained from routing of the VIC modeled runoff at Khartoum station and adding the average monthly flow from the White Nile and Atbara River (see the schematic diagram in Figure 2.2). Considering only the Blue Nile variability in the streamflow reaching HAD is justified by the larger share of discharge from the BNB compared to Atbara river and the White Nile (Figure 2.3). In addition, we compared the variability introduced by the three rivers (Blue Nile, White

Nile, and Atbara river) to the flow in the Main Nile using the range of monthly discharge at the outlet of each river standardized by the mean monthly discharge upstream of HAD (range is calculated as the difference between the maximum and minimum monthly streamflow retrieved from gauges at the outlet of each river). We found that the variability from the Blue Nile is much higher than that introduced by the White Nile and Atbara river, especially during the rainy season (June to September), when the variability is more than 100% of the mean flow in the Main Nile (Figure not shown). The evaporation losses (E) were estimated using the standard energy balance method as described by Chow et al. (1988). Minimum and maximum temperature required for the energy balance method were obtained from the GSOD/NCDC dataset. Two constraints were added in the water balance model to control the HAD releases. First, the inflow to the HAD is reduced by a factor of 25% which corresponds to the average Sudan share of the Main Nile flow (18.5 km^3/year out of 84 km^3/year) according to the 1959 Nile Waters Agreement (Waterbury 2008). Second, the maximum HAD release is set to 8.1 km^3/month in order to maintain the water level in the HAD reservoir below 178 m. As noted earlier in section 2, any excess discharge above 178 m is always spilled into Toshka depression in the western desert of Egypt.

2.4 Results and Discussion

2.4.1 Model Calibration and Validation

As described in section 3.2, the VIC model for the BNB is forced by CHIRPS precipitation estimates, while temperature and wind speed are provided by NCDC gauges. We calibrated the soil parameters of VIC model to reflect hydrological response and adjust the runoff generation accordingly. Table 2.2 summarizes the soil parameters calibrated to simulate the streamflow at Khartoum station (outlet of the BNB). Figure 2.6 shows the daily and monthly

time series of simulated streamflow and compared with measured discharge at Khartoum station. Figure 2.6a and Figure 2.6b show high correlation between the modeled and measured streamflow at daily and monthly. The correlation coefficient and NSE for daily (and monthly) streamflow are 0.85 (0.49) and 0.94 (0.68), respectively (Table 2.3). The model simulations show also better fit with monthly flows as indicated by lower values of RBIAS and RMSE (e.g., 751 m3/sec for monthly streamflow of the calibration period 1993-1997 compared to 1280 m3/sec from daily simulations for the same period). In general, the VIC simulations reproduced the observed long-term monthly mean hydrograph and also captured inter-annual and intra-annual flow variations. The skillful predictability of the VIC model at the Khartoum station is confirmed during the validation period of 1998-2002 where a correlation coefficient of 0.96 between monthly simulated and measured streamflow is observed.

Table 2.2. Soil parameters calibrated for VIC modeling of the BNB.

Parameter	Definition	Typical Range	Calibrated Value for the BNB	
			US Eldiem Station	DS Eldiem Station
binf	Shape parameter of the infiltration curve	>0~0.4	0.2	0.01
d	Soil depth	>0.1~1.5	0.7	1.3
Ds	The fraction of maximum velocity of baseflow	>0~1	0.1	0.002
Ws	The fraction of the maximum soil moisture	>0~1	0.9	0.9

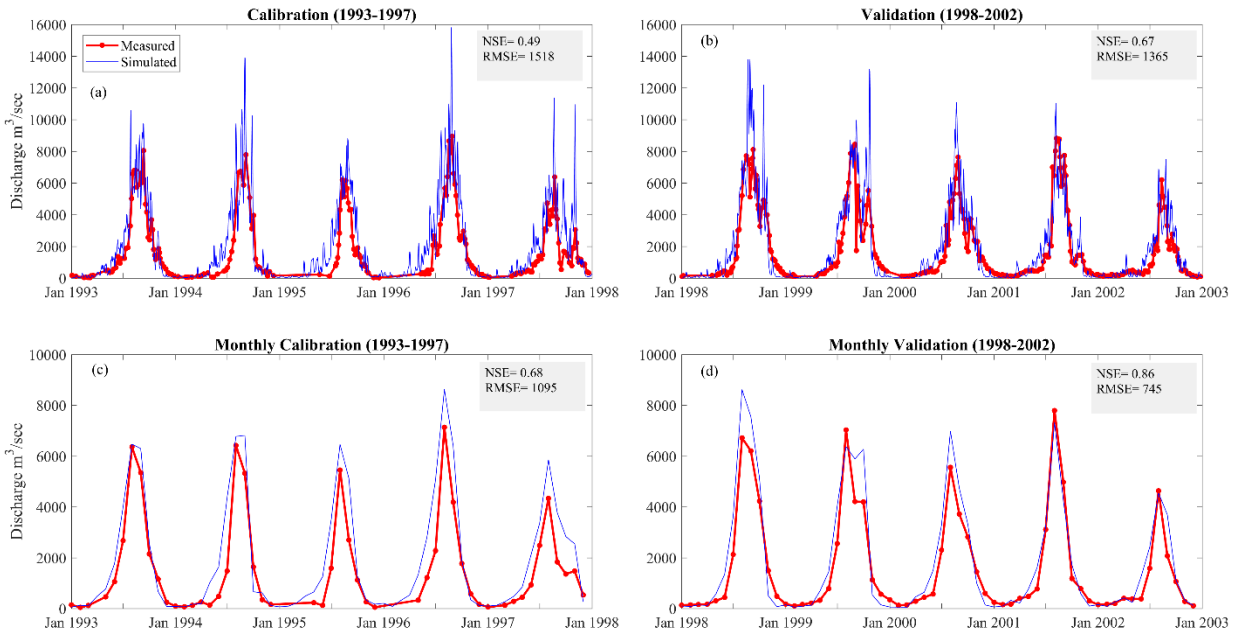

Figure 2.6. Model calibration (left panels) and validation (right panels) for the BNB at Khartoum Station for the periods (1993-1997) and (1998-2002), respectively. The model performance assessment at daily (a-b) and monthly (c-d) scales is shown using Nash Sutcliff Efficiency (NSE) coefficient, and normalized root mean square error (NRMSE).

Furthermore, we tested the model performance for the Blue Nile upstream of Eldiem station, where the GERD is currently being constructed. The ability of the model to simulate the flow upstream of Eldiem station is critical to the success of the modeling framework in exploring future impacts of planned dams in the BNB (e.g., GERD dam). Monthly simulated streamflow was compared with discharge at Eldiem station for the calibration (1993-1997) and validation (1998-2002) periods. The simulated flow showed an overestimation in three years (1993, 1995, and 1997) of the calibration period at the peak flows (in August) (Figure 2.7a). Conversely, streamflow was underestimated at peak flows of the five validation years with an average absolute bias of 889 m3/s (compared to 1226 m3/s for the calibration period) (Figure 2.7b). However, the model generally showed a close agreement between the simulated and observed

monthly streamflow with a NSE and correlation coefficient of 0.92 and 0.97, respectively during the validation period (NSE=0.81 and correlation coefficient = 0.93 for the calibration period). According to the watershed modeling evaluation guidelines established by Moriasi et al. (2007), hydrological modeling of streamflow with such NSE greater than 0.50 is considered to be very satisfactory for simulating streamflow at a monthly time step. Overall, the performance results of the calibrated VIC model are reasonable for our proposed investigations, especially with its skill in capturing the peak and variability of the streamflow.

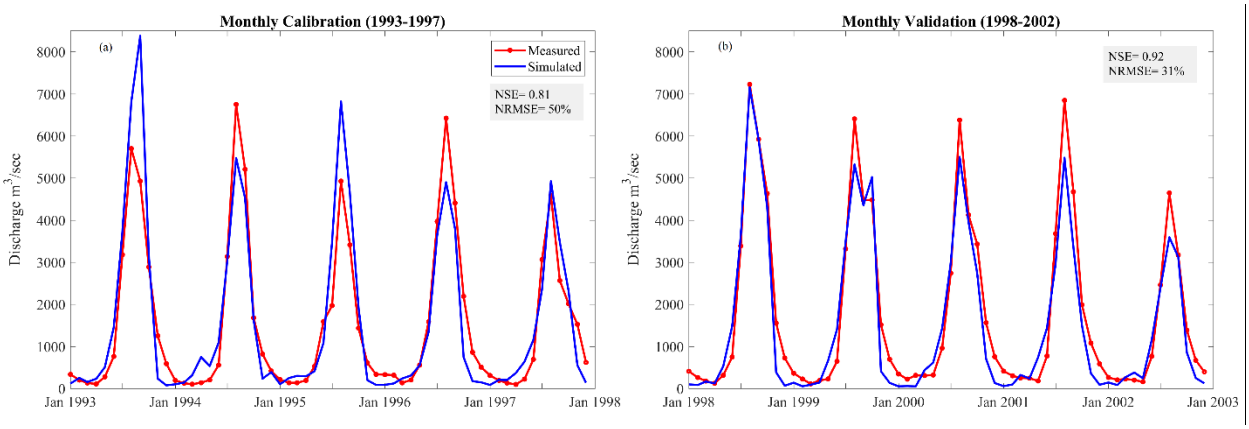

Figure 2.7. Model calibration and validation of monthly streamflow at Eldiem station (the location of the GERD dam at the boundary between Ethiopia and Sudan) for the periods (1993-1997) and (1998-2002), respectively.

Table 2.3. Performance statistics for the calibration and validation of the streamflow at Khartoum and Eldiem stations.

Station	Simulation	NSE	Correlation Coefficient	RBIAS	RMSE (m^3/s)	NRMSE
			Calibration (1993-1997)			
Khartoum	Daily	0.49	0.85	37 %	1518	78 %

	Monthly	0.68	0.94	43 %	1095	69 %
Eldiem	Monthly	0.81	0.93	3%	772	50 %
			Validation (1998-2002)			
Khartoum	Daily	0.67	0.88	17 %	1365	68 %
	Monthly	0.86	0.96	18 %	745	47 %
Eldiem	Monthly	0.92	0.97	-11 %	540	31 %

2.4.2 Hydrologic Characterization of the Blue Nile

The BNB modeling framework developed in our study was used to understand long-term trends and climatology of various hydrologic variables in the BNB including precipitation, evaporation, runoff, and streamflow. Such hydrologic characterization is essential for future investigations of new dams operating policy, which consequently impacts the downstream water structures. For instance, it is important to demonstrate the predictability of our VIC model in characterizing the evaporation over the BNB (especially at GERD location). Evaporation at GERD impounding lake is a key variable in subsequent studies that consider GERD impacts, given the claims by the Ethiopian side that GERD will increase the water flows downstream by reducing evaporation from Lake Nasser (Yihdego et al. 2017; Taye et al. 2016). Additionally, we provided a characterization of the streamflow reaching the GERD which is a critical information for exploring future scenarios of filling/post-filing of GERD and the consequences on HAD operation.

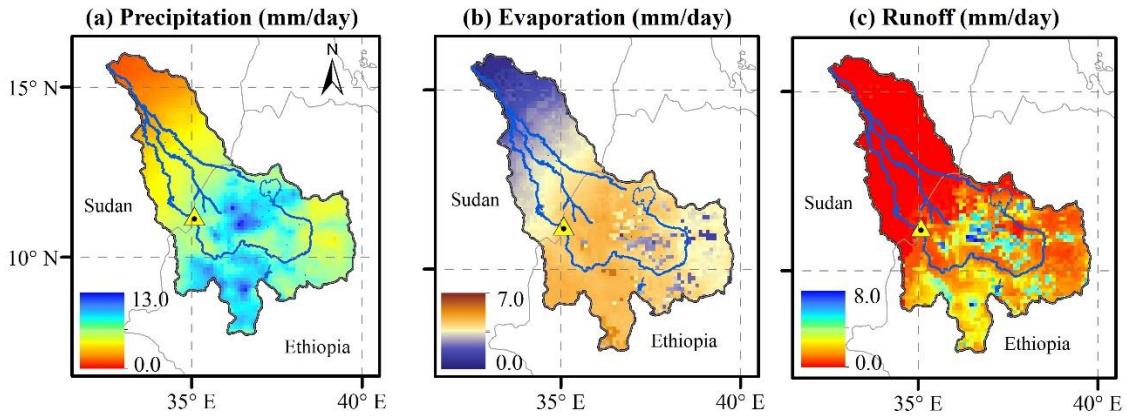

Figure 2.8. Average daily climatology of a) precipitation, b) evaporation, and c) runoff for the BNB in the JJAS (June-July-August-September) season over the period of analysis (1981-2017). The yellow triangle represents the location of the GERD dam (Eldiem station) at the boundary between Ethiopia and Sudan.

Figure 2.8 shows the climatological daily average of precipitation (from CHIRPS dataset), evaporation, and runoff (retrieved from the VIC model outputs) in the rainy season (JJAS: June, July, August, and September) for the study period 1981-2017 over the entire BNB. Most of the basin precipitation is produced in the upper BNB in Ethiopia (Lake Tana eastern of the basin in the Ethiopian plateau). The spatially averaged monthly rainfall over the upper BNB ranges from 9 mm (standard deviation=6 mm) in December to a high of 290 mm (standard deviation=19 mm) in July. The rainy season during the summer (June to August) is shown by the seasonal cycle of the monthly average precipitation in Figure 2.9. The wet season is defined from June through September (October is the transition month from the wet season to the dry season), while the dry season starts from November through April (May is the transition month from the dry season to the wet season). As indicated by the error bars in Figure 2.9, the inter-annual variability in precipitation is relatively high for the transition months with October having the highest standard deviation of 23 mm. Figure 2.8b shows the spatial variation of evaporation rates

over the entire BNB. This was calculated by summing the canopy evaporation, transpiration, and bare soil evaporation from the VIC model and then averaged over each grid cell. Higher evaporation rates are seen in upstream regions of the BNB with an average monthly evaporation of 82 mm. The overall characterization of the hydrologic variables from the BNB VIC modeling are in close agreement with previous studies that described the BNB hydrology (e.g., Melesse et al. 2011; Elshamy et al. 2009).

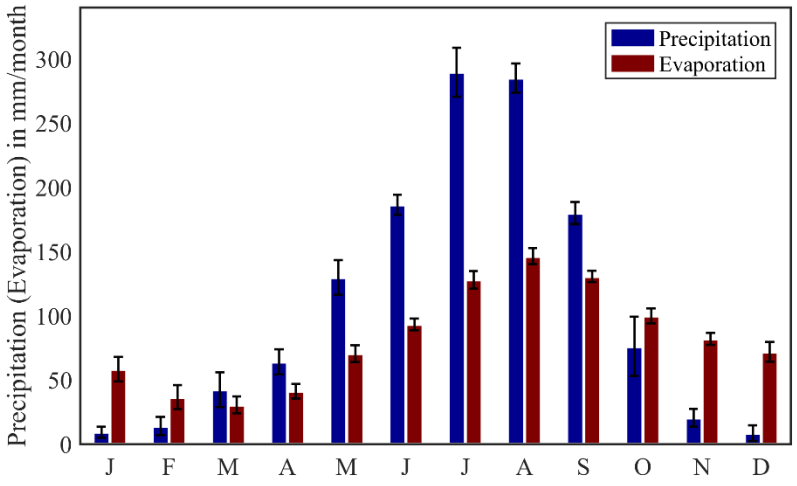

Figure 2.9. Average monthly precipitation (from CHIPRS in mm/month) and evaporation (from VIC output in mm/month) over the upper BNB basin (upstream Eldiem station) during the period 1981-2017 (error bars indicate the standard deviation).

Figure 2.10a shows the cumulative distribution of the annual streamflow at Eldiem station, i.e., inflow to GERD dam. The median annual streamflow is about 47.5 km^3/year which represents about two third of the expected storage in the GERD reservoir (74 km^3). The inter-annual and intra-annual variability of the streamflow are indicated by the interquartile range of the box plot and the month by month changes shown in Figure 2.10b. Higher streamflow is produced during the wet season months (JJAS) where heavier precipitation fall on the upper Blue

Nile basin. Examples of wet years with the highest monthly streamflow at Eldiem station are: September 1993 (21.7 km^3/month) and August 2011 (20 km^3/month). The streamflow at Eldiem station lags rainfall by about one month with peak discharge in August. The average monthly discharge in August (for the 1981-2017 period) is 13.4 km^3/month with interquartile range of 3 km^3/month. The highest intra-annual variability of streamflow is observed in September with interquartile range of 3.9 km^3/month. Such variability in the streamflow reaching Eldiem station is controlled by the effect of timing and sequence of El Niño and La Niña in the upper BNB. For instance, Zaroug et al. (2014) found that 80 % of the drought cases in the upper BNB are associated with El Niño events. The predictive skill of the VIC model to characterize the streamflow climatology upstream of the GERD is crucial for exploring impacts on water management in Egypt due to the eastern (Blue) Nile region.

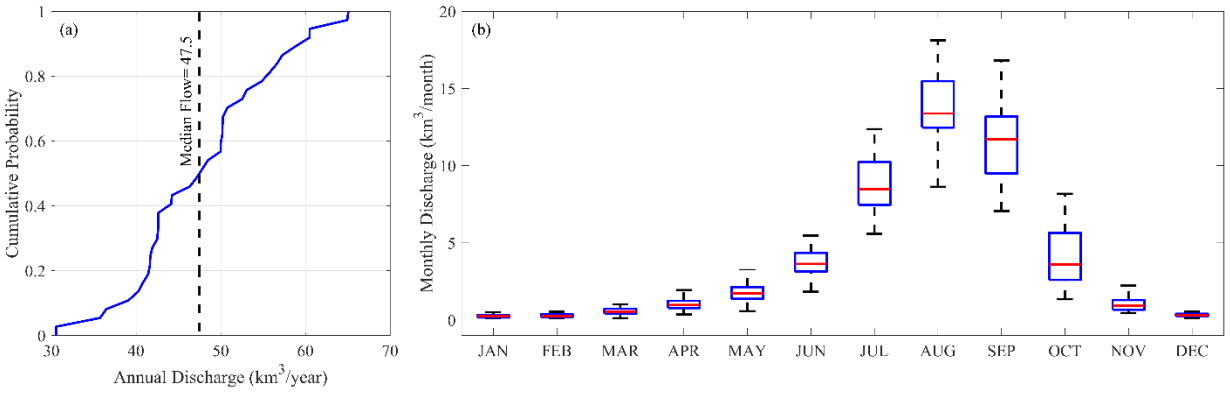

Figure 2.10. a) Cumulative probability of annual flow reaching Eldiem (inflow of GERD). b) Monthly distribution of the monthly streamflow for the historical record (1981-2017). On each box, the central mark indicates the median depth, and the bottom and top edges of the box indicate the 25th and 75th percentiles (or interquartile range), respectively. The whiskers of the box extend to the most extreme data points not considered outliers.

2.4.3 Water Balance of HAD Reservoir

The outflow discharges of High Aswan Dam (HAD) were computed following the water balance described in section (3.2.3). Figure 2.11a shows the comparison of the outflow using the water balance model based on altimetry satellite water levels and the measured discharge at the HAD sluice gates. The modeled outflows show higher variations between the monthly discharges with some spikes of overestimation especially in the dry season. However, there is good agreement between the streamflow at months of peak flow. The water balance model resulted in a NSE of 0.20 and a correlation coefficient of 0.67. Figure 2.11b shows the HAD operating curve for each month (averaged over the period 1998-2002) as compared to the measured releases. The water balance approach captures the overall HAD operating curve with higher releases in the summer season compared to the rest of the year. The simulated HAD releases match more closely with measured discharge during summer (June through August), with less than 10% NRMSE (Table 2.4) and slight overestimation (relative bias = 7%). Conversely, the performance of the simulated HAD outflow is less accurate for the fall season (September through November) with considerable underestimation in the reservoir releases (relative bias= 27% and NRMSE= 47%). This trend can be also seen in the hydrograph in Figure 2.11b.

The differences between observed and modeled streamflow may be due to several sources of uncertainties in the water balance equation. The inflow simulated by the VIC model, for example, is one factor that affects the inflow term of the water balance equation. For instance, the water balance performance is lower in years impacted by the differences between the measured discharge and the streamflow simulated by the VIC model at Khartoum station (for example the simulated peak discharge in 1998 and 2000 are overestimated compared to the

measured discharge; Figure 2.6d). When only considering the year 2002, which has very comparable simulated and measured discharge, the performance of the reservoir model was significantly improved with higher NSE (0.87) and correlation coefficient (0.94) (see dashed lines in Figure 2.11b). In addition, tracking down some points (having larger magnitude of error) in HAD outflow curve, we found that overestimation or underestimation of altimetry water levels can impact significantly the water balance equation. For example, one meter of overestimation in altimetry water level in April 1998 resulted in higher HAD simulated outflow (8.1 km^3 compared to only 4.5 km^3 measured downstream of the HAD). Testing the sensitivity of the water balance approach to the HAD inflow and the water level (Figure not shown), we noticed that improvement in NSE is more sensitive to the water level estimates (NSE increased from 0.20 to 0.36 when using measured water level at HAD reservoir, while keeping the other components of the water balance equation the same). Furthermore, as indicated by Muala et al. (2014), the large residence time of Lake Nasser (large reservoir size compared to inflow) can increase the uncertainty in computed reservoir releases as the water balance approach assumes a plug flow reservoir.

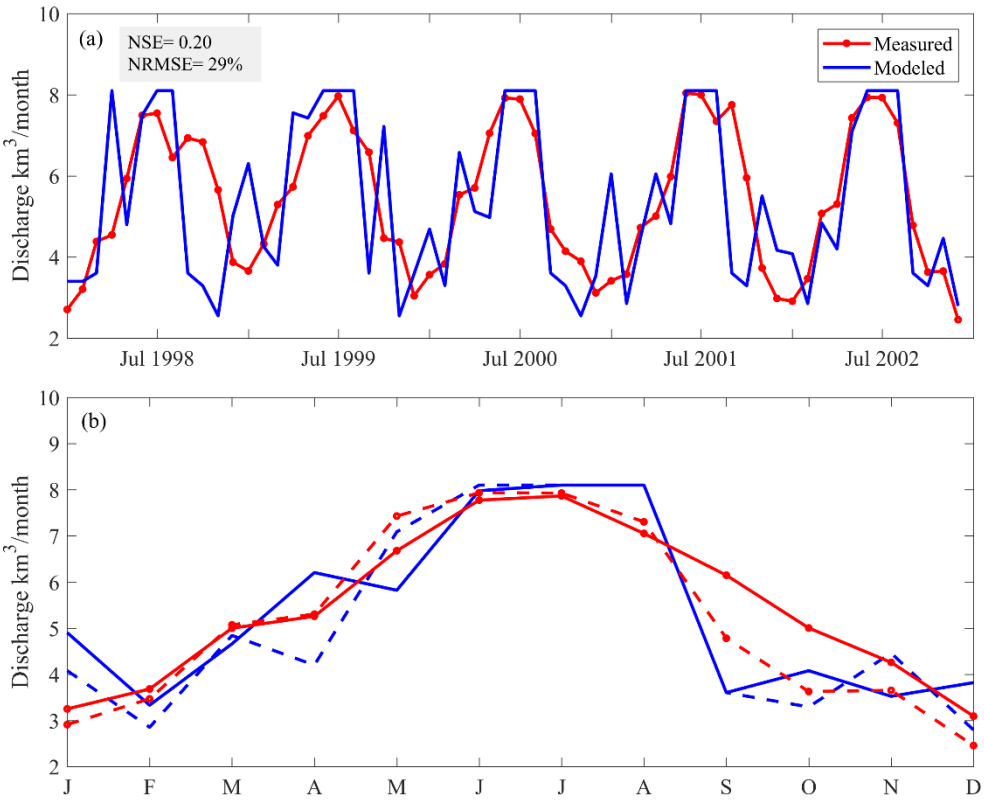

Figure 2.11. Monthly outflow (a) and derived operating curve (b) for HAD dam based on water balance model and compared to measured discharge at HAD sluice gates (solid lines in (b) are monthly discharge averaged over the period 1998-2002 and dashed lines indicate monthly discharge for only 2002).

While our primary objective is to build a satellite-based model that is capable of inferring the operation of reservoirs with more focus on large reservoirs (like HAD and GERD), one of the limitation of our current framework is the exclusion of the relatively smaller dams (e.g., Merowe dam in Sudan with storage capacity of 12.5 km^3 compared to 132 and 74 km^3 for HAD and GERD, respectively). This limitation can be justified by such large difference in the storage capacity; however, if the reservoir model is to be applied in Sudan, for instance, including Merowe will be very important since it is the largest hydropower facility in Sudan and the

storage at its reservoir impacts the upstream dams, e.g., Sennar and Roseires (Satti et al., 2015). It is worth noting that the results of our study, i.e., the performance the water balance model in simulating HAD outflow, are not impacted by the Merowe dam (since its operation started in 2009 while our model validation is for the period 1998-2002). However, given the potential implications of our modeling framework to include the impacts of GERD on downstream countries, future studies are encouraged to employ the same water balance approach on other dams upstream of HAD to estimate the dam releases (in a similar manner as applied for HAD). For example, one can perform the water balance equation at Merowe dam first to estimate reservoir outflow which can be then directed to HAD as monthly inflow (i.e., multi-reservoir water balance approach). Given such limitations in our modeling framework, further improvement of the simulation of HAD reservoir releases will require more accurate representation on other components of the water balance equation including: evaporation, water diversion to Toshka spillway, seepage (that is neglected in our formula), and other constraints or decisions that can be taken by the reservoir operators to meet downstream demands. Nonetheless, the overall performance of the reservoir modeling approach is considered adequate for water management to conduct a scenario assessment of the HAD operation under future challenges (e.g., GERD operation and climate change).

Table 2.4. Performance Statistics for modeling the HAD releases using the water balance approach during the period (1998-2002)

Season*	RBIAS	RMSE	NRMSE	NSE
Winter (DJF)	-20 %	1.20	36 %	-5.40
Spring (MAM)	-1.5 %	1.40	25 %	-1.53

Summer (JJA)	7 %	0.68	9 %	-1.36
Fall (SON)	-27 %	2.40	47 %	-2.28
Overall	-1.4	1.56	28.64	0.20

* Statistics are broken down by season (DJF: December-January-February, MAM: March-April-May, JJA: June-July-August, SON: September-October-November,).

2.4.4 HAD Operation during Dry vs Wet Episodes

The HAD releases change during dry and wet episodes of discharges especially with the prevalence of extended droughts during the recent decades (Meze-Hausken 2004). The water balance approach at the HAD dam can provide more insights into how the HAD dam is operated under different climatic conditions. Figure 2.12 shows the use of the water balance approach based on satellite observations to derive the HAD operating curve during dry vs wet years. The dry and wet years are defined at Eldiem station by setting a threshold for the total discharge anomalies of the JJAS season for the full analysis period (1981-2017) (Figure 2.12a). The threshold is set equal to half of the discharge anomaly standard deviation: any discharge anomaly above 3.64 km^3 is considered as flooding condition (wet year), and any discharge anomaly below 3.64 km^3 as drought condition (dry year). We then selected a three year episode of dry (and wet) conditions to understand how HAD was operated under such conditions. The dry and wet episodes selected are the years (2005-2006-2007) and (2011-2012-2013), respectively.

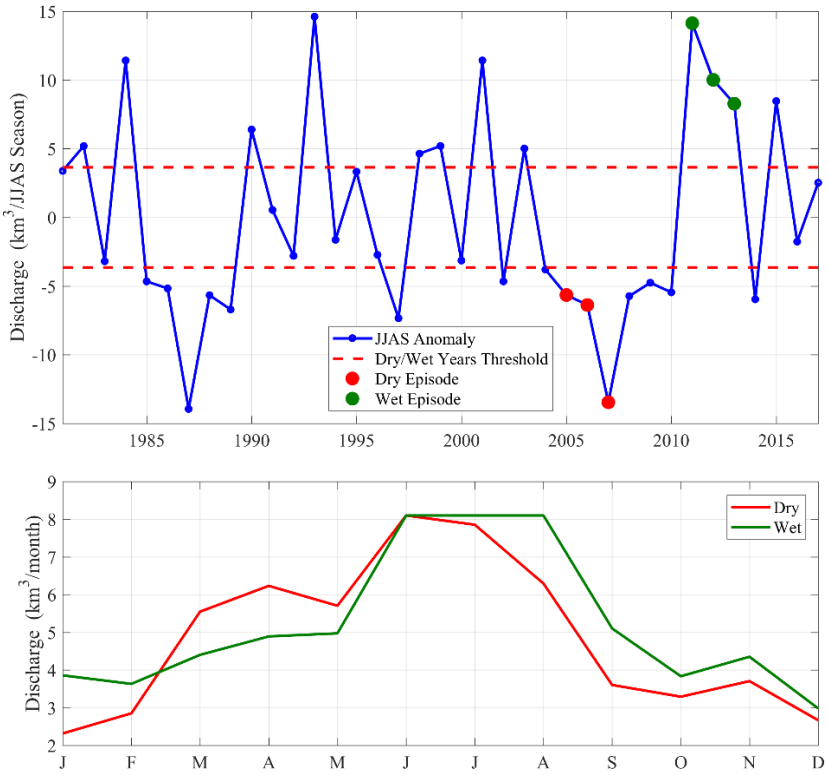

Figure 2.12. a) The discharge anomalies at Eldiem station averaged over the rainy season JJAS (June-July-August-September) during the period (1981–2017), the red dashed line represents the threshold for the dry vs wet year identification at half of the standard deviation of the JJAS total discharge. b) Operating curve of HAD for wet vs drought episodes using the water balance approach.

Figure 2.12b shows the releases (averaged over the three year episode) for each month of the dry (and wet) years using the water balance approach. As expected, lower discharge is released during dry conditions in most of the months (with exception of the spring season: March to May). A higher release during those months could be due to greater irrigation or water supply demand in the downstream dictated by a dry year. The largest difference between the releases in dry and wet years is noticed in August with 1.8 km^3/month more discharge released in wet years. We expect that inferring reservoir operating patterns under such extreme climatic conditions will

make it easier for Egypt to make decisions such as storing or spilling water to prepare for drought or flooding conditions exacerbated by GERD regulation.

The streamflow variability and hydrologic droughts and floods impact the agricultural sector land use. Figure 2.13 shows an example how the agricultural area over the Nile Delta in Egypt changed during the period (1999-2017). The percentage of agricultural area is calculated using the annual Normalized Difference Vegetation Index (NDVI) generated from the Near-Infrared (NIR) and Red (R) bands of Landsat 7 scenes. This percentage is calculated as the ratio between the number of pixels with NDVI greater than 0.50 and the total pixels in the delta region. The NDVI greater than 0.5 is used as an indication of dense vegetation areas with the crops at peak growth stage (Jeevalakshmi et al. 2016). A significant shift in the agricultural area is noticed during two periods: period (1) considers the time between 2006-2010 that shows declining trend in the agricultural area; and period (2) between 2011-2014 when the agricultural area changed from 10% to more than 30%. Such variation in the agricultural area can be attributed to the streamflow variability during dry (2006-2010) vs wet years (2011-2014). The different trends in the agricultural area for the two periods reflect the importance of considering the operation of dams under flow variability. Such variability is notable in annual Nile river flows as reported in previous studies (Eltahir 1996; Siam and Eltahir 2017) and it is more likely to increase in future with climate change (Conway 2005). In addition to streamflow variability, changes in agricultural areas can also be associated with variations in non-climatic factors, e.g., development decisions, changes in government policies, and marginal changes in market conditions (Epule et al. 2018; Kassem et al. 2019). The impacts of non-climatic factors are noticed when comparing the agricultural land use dynamics in some years where an increase (or decreases) in agricultural areas are not associated with wet (or dry) years (for example reduction

in agricultural area from 2014 to 2015 (Figure 2.13) corresponds to a wetter year in 2015 (Figure 2.12)).

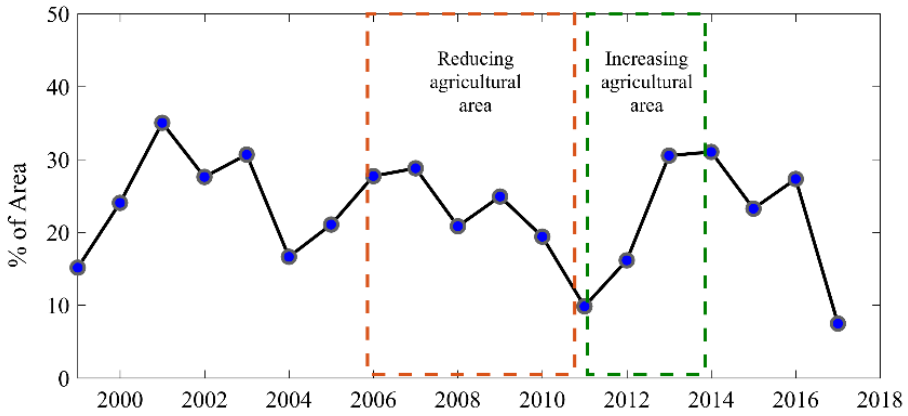

Figure 2.13. Annual percentage of agricultural area in the Nile Delta region (calculated using NDVI greater than 0.50).

2.5 Conclusion

Our study presents the development of a modeling platform to predict the current and future reservoir operating rules in lower Nile River basin using satellite hydrometeorologic observations and macroscale hydrologic model. Our main findings are as follows:

1. The hydrological modeling of the BNB shows high accuracy in simulating streamflow along the BNB (validated at Khartoum and Eldiem stations). Such a modeling framework is a practical step to circumventing real-world data sharing issues in transboundary basins via the use of satellite observations.
2. The characterization of the streamflow climatology at Eldiem station lags rainfall by one month with peak discharge in August. The highest intra-annual variability of the streamflow is noticed in August and September. The ability of the VIC model to characterize the streamflow climatology upstream of the GERD is important for future

assessment GERD filling and operation scenarios and their impacts on HAD inflow. Understanding such impacts is also crucial to re-evaluating the current operating rule for HAD to meet the downstream water demands in the context of emerging water management challenges.

3. Our results for the monthly HAD releases using satellite altimeter show good agreement with measured discharge downstream of the dam. The ability to estimate reservoir outflow using satellite remote sensing has wide implications in transboundary water management. For instance, policy makers can be supplied with better information of the HAD (and GERD) operations, which subsequently help making more informed decisions about a wide array of water management issues.

The BNB modeling framework presented in our study has various implications in the management of water resources in the downstream countries of the Nile River. Building upon our model framework, long-term sustainability of the Food Energy Water (FEW) security in the Eastern Nile basin can be explored in a nexus approach. Such a FEW nexus can highlight the interdependence of the three critical resources and therefore provide an effective way to control the releases from the basin dams. For example, any imposed changes to future flow reaching the HAD will impact the hydropower generated (Energy domain) at the dam and the water released for irrigation in the Nile delta (Food domain). Such changes in the FEW system are more pronounced in the Eastern Nile basin due increasing pressures on water resources from multiple stresses including human-induced land use changes and high population growth, rising demand for natural resources, and external factors such as climate change and variability (Al-Saidi et al. 2017).

Building a well-established satellite-based modeling framework for monitoring or predicting reservoir operations can benefit water managers and various stakeholders. For a country like Egypt, our developed framework can be operationalized in a Decision Support System (DSS) to monitor basin's transboundary reservoir operations, water storage and release patterns by other and upstream riparian countries. Although the in-situ data needed by such DSS systems is unavailable in the developing countries (Giupponi and Sgobbi 2013), especially in the case of transboundary basins, our framework shows the skill of satellite hydrometeorologic observations to drive hydrological modeling and infer the dam operations. Furthermore, the developed BNB model can benefit from the application of numerical weather prediction (NWP) forecast models, e.g., NCEP Global Forecast System (GFS) to forecast short-term river flow. Flow forecasting is particularly important for adaptive management of water resources and development of reservoir regulation policies. The monitoring of upstream reservoirs and the prediction of impact on water availability downstream can help decision makers identify realistic measures to overcome water shortage problem in the short and long-terms. Before embarking on a detailed investigation of revised operating policy, we first explore the 'energy' aspect of the NRB. In particular, the next chapter, Chapter Three of this dissertation, demonstrates the benefits of the modeling framework developed in this chapter to evaluate the hydrological potential of the upper Blue Nile basin for meeting the declared hydropower production design from the GERD. A thorough assessment of the hydropower potential and feasibility of an upstream dam like the GERD is critical for the HAD before exploring revised operating policy as GERD has been billed primarily as a source for additional energy for the region.

Chapter 3: Evaluating the Hydropower Potential of the Grand Ethiopian Renaissance Dam

Eldardiry, H., and Hossain, F. (2021). Evaluating the Hydropower Potential of the Grand Ethiopian Renaissance Dam. Journal of Renewable and Sustainable Energy.

Abstract

One of the largest hydropower projects in Africa is the Grand Ethiopian Renaissance Dam (GERD), which is currently under construction in the Upper Blue Nile (UBN) basin in Ethiopia. The GERD has been billed as a hydropower project that will significantly improve electricity supply in Ethiopia and neighboring countries with a total capacity of 5150 MW. This paper evaluates the hydrological potential of the UBN basin for meeting the declared hydropower production design from the GERD. Our investigation indicated that the hydrology of the UBN can only sustain the inflow to GERD that would produce 13,629 GWh per annum (capacity factor=0.30). Our study also demonstrated that initial plans to upgrade the GERD capacity (from 5250MW to 6000MW to 6450 MW) have not been beneficial to improving the dam's hydropower production potential.

3.1 Introduction

Africa faces frequent shortages in electricity and in some regions it is a severe crisis (Karekezi and Kimani 2002; Wolde-Rufael 2006). Apart from North Africa, e.g., Egypt and Algeria, where electrification rate exceeds 95%, only 25.9% of the population in Sub-Saharan Africa has access to electricity (Suberu et al. 2013). Thus, hydropower, as a renewable source of

energy, can be viewed as an important contributor to the future energy security of Africa. With only 3% of its water used for hydropower generation, Africa is currently an "under dammed" continent (compared to 52% in South Asia) with a high potential of hydropower exploitation (Mataen 2012). The global boom in the construction of hydropower dams is now spreading to Africa with more than 160 planned hydropower dams (Zarfl et al. 2015). The Grand Ethiopian Renaissance Dam (GERD), which is currently under construction in Ethiopia, is one such mega hydropower project with installed turbine capacity of about 5150 MW (Basheer et al. 2020; Eldardiry and Hossain 2020). This is more than two times that installed in the next major hydropower dam – the High Aswan Dam in Egypt commissioned 50 years ago.

GERD is part of an ambitious energy development strategy by Ethiopia to benefit from hydropower generation potential as a renewable energy source (Block and Strzepek 2012). However, Ethiopian plans in unlocking this hydropower energy potential faces challenges including climate variability, socio-economic impacts, and the geo-political situations of the region (Degefu et al. 2015; Nasr and Neef 2016; Van der Zwaan et al. 2018; Annys et al. 2019). For instance, in developing countries like Ethiopia, hydropower developments are mainly resisted by the public due to possible displacement of local communities from their original dwelling place. The GERD project has regional and continental dimensions as the largest hydropower dam in Africa and is an important component of future electrification of Africa (Kumagai 2016). With about 83% of Ethiopia's population currently lacking access to electricity, GERD aims to expand rural electrification, reduce poverty and stimulate economic growth in Ethiopia (Barnes et al. 2016). In addition, Ethiopia is expected to be a major electricity exporter in the future by trading 15% of its yearly electricity generation in the Eastern African Power Pool (EAPP) (Sridharan et al. 2019). Thus, GERD, as a main component of Ethiopia hydropower

development, will benefit EAPP countries including Rwanda, Djibouti, Tanzania, Kenya, Burundi, Uganda, Sudan, and Egypt. Furthermore, GERD is of interest to countries beyond African and Nile nations. Regional stakeholders such as Saudi Arabia, Kuwait and the United Arab Emirates can be major importers of agricultural production from Ethiopia enabled by GERD operations (Whittington et al. 2014).

Construction of GERD poses a challenge for downstream countries, especially Egypt. While Egypt has been historically afforded a position of hegemony in the Nile basin (Whittington 2004; Cascão 2009), the building of GERD dam will gradually tip the balance of regional power in Ethiopia's favor (Cascão and Nicol 2016; Yihdego et al., 2016). Recently, studies have focused on exploring the impacts of GERD on downstream countries (King and Block 2014; Mulat and Moges 2014; Zhang et al. 2015; Wheeler et al. 2016; Eldardiry and Hossain 2020). These studies concluded an expected reduction in downstream streamflow during the filling phase of the GERD. However, studies on the impact of GERD operation and its ability to meet the designed hydropower production goals have not yet been reported in literature. The operation of GERD will regulate the flow in the Blue Nile and therefore mitigate the increase in the intra-annual variability of Nile flow due to climate change (Siam and Eltahir 2017).

Recently, criticism has been expressed on the potential over-sizing of the GERD's installed hydropower capacity. Beyene (2013) and Abtew and Dessu (2019) questioned GERD's ability to operate at the design capacity of 5250 MW, which was the initial design capacity before upgrading the turbines to a capacity of 6450 MW (EEPCo 2019) and followed by a recent change to 5150 MW (Basheer et al. 2020). This concern about the GERD's ability to fulfil its promise of hydropower is legitimate when one compares the total storage volume (74 km^3) and installed turbines capacity (5150 MW) of GERD with similar counterparts in Africa (see Table

1). For instance, the High Aswan Dam (the largest existing hydropower dam in Africa), features a total storage volume of 162 km^3 with only 2100 MW installed turbine capacity. In this study, we investigate the exploited GERD's hydropower capacity from the hydrologic perspective of the Upper Blue Nile (UBN), where GERD is located. *Our study builds upon a hydrological modeling of the UBN integrated with reservoir optimization scheme to evaluate the hydropower potential of GERD*. The remainder of the paper is organized as follows. First, we describe the study area and the specifications of the GERD in section 2. Data sources and methods are introduced in section 3. Results for the GERD operation and its hydropower production under various scenarios are discussed in section 4, and finally concluding remarks and future implications of the work are summarized in section 5.

Table 3.1. Comparison of GERD with examples of major hydropower dams in Africa.

Dam	River	Country	Storage Volume (km^3)	Average Annual Flow (km^3/year)	Maximum Head (m)	Installed Capacity (MW)
GERD	Blue Nile	Ethiopia	74	49	133	5150
High Aswan Dam	Nile	Egypt	162	84	74	2100
Akosombo	Volta	Ghana	148	31	68.8	1038
Kariba	Zambezi	Zambia and Zimbabwe	180	60	92	1626
Cahora Bassa	Zambezi	Mozambique	63	77.7	157	2075
Merowe	Nile	Sudan	12.5	84	51	1250

3.2 Upper Blue Nile and Grand Ethiopian Renaissance Dam

The Grand Ethiopian Renaissance Dam (GERD) is located at the outlet of the Upper Blue Nile basin (UBN) in Ethiopia (Figure 3.1). The UBN extends from Lake Tana in the Ethiopian highlands to the Sudanese border at Eldiem with a drainage area of 176,000 km^2 (more than half of the Blue Nile basin's area). The climate of UBN climatology varies from humid to semiarid. The annual precipitation increases from northeast to southwest and ranges from 1200 to 1600 mm (Conway 2000). The mean annual temperature and potential evapotranspiration in UBN are estimated to be about 18.5°C and 1100 mm, respectively (Kim et al. 2007). The UBN provides more than 90% of the total flow in the Blue Nile basin at the Sudanese capital Khartoum, where the confluence of the Blue Nile and the White Nile is located. The steep topography in the Blue Nile gorge provides two particular features for perfect dam locations: 1) high heads for hydropower generation; and 2) low surface-to-volume ratios (Whittington et al. 2014). In 1964, the US Bureau of Reclamation (USBR) conducted a comprehensive study to explore viable sites for potential development projects in the Blue Nile Basin. The study proposed multiple locations of hydropower dams along the UBN. The current GERD location is the same site proposed by USBR for a smaller dam called the Border Dam near the Ethiopian–Sudanese border.

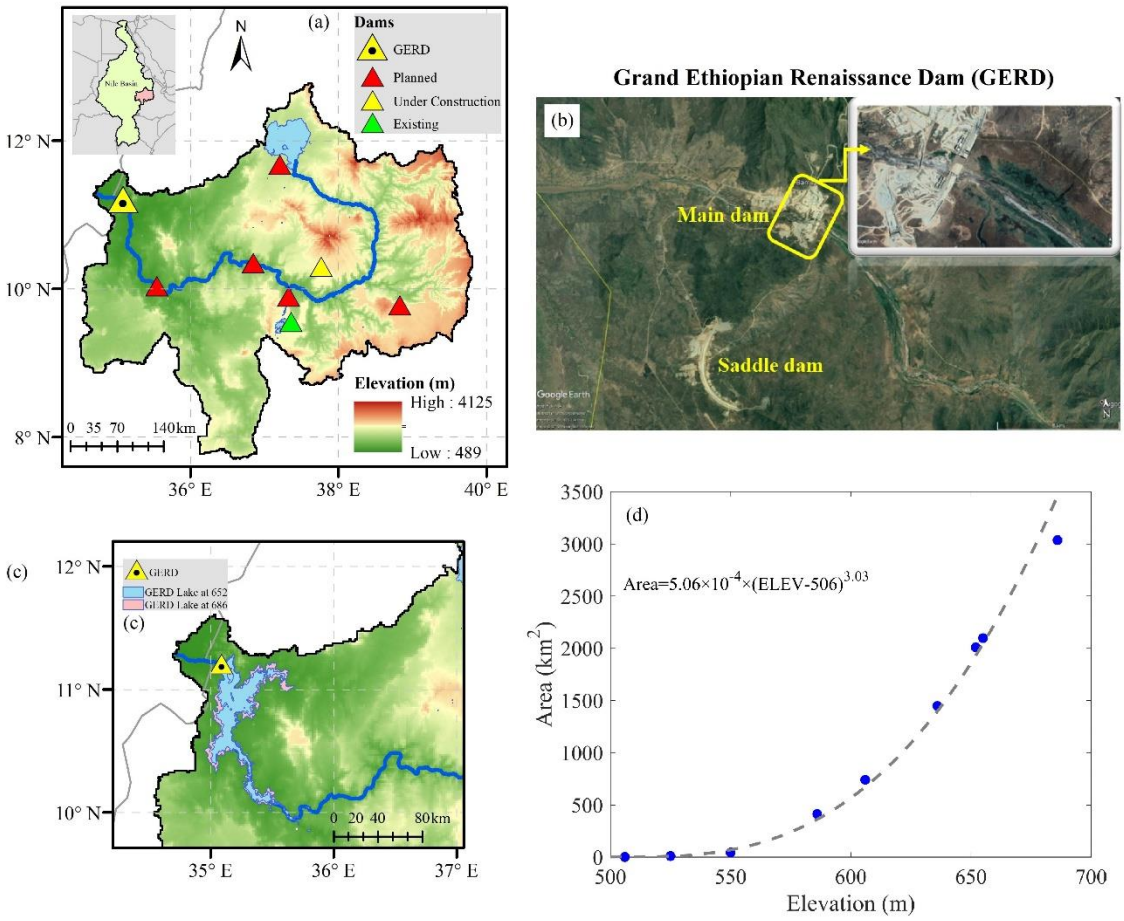

Figure 3.1. Map of the Upper Blue Nile with the location of the existing, planned, and under construction dams (Lehner et al. 2011; Zarfl et al. 2015). The location of the GERD dam is highlighted near the Ethiopian-Sudanese border. (b) Satellite image of the current construction stage for the GERD dam and the accompanied saddle dam (Retrieved from Google Earth on November 20, 2019). (c) Delineation of the inundation extent of the GERD at elevations of 652 m (blue only) and 686 m (pink and blue) above mean sea level. (d) Area-Elevation Curve (AEC) derived for the reservoir lake of the Grand Ethiopian Renaissance Dam using satellite observations of land elevation from Shuttle Radar Topography Mission (SRTM).

The construction of the GERD started in 2011 and is currently more than 70% completed (see for example Figure 3.1b for a recent satellite image retrieved from Google Earth on

November 2019). The construction site of the main dam is at a ground level of 506 m AMSL (Above Mean Sea Level) and can only store water with a maximum depth of 100 m (606 m AMSL). The water above 606 m will spill downstream into the Blue Nile (ElBastawesy, 2014). For this reason, the main dam is supported by a saddle dam (to the west of the GERD) to avoid spilling of water above 606 m AMSL through the tributary at the saddle dam location. The GERD dam will have three spillways: 1) a main gated spillway located to the left of the main dam at a base elevation of 624.9 m AMSL, and 84 m wide at the outflow gates; 2) an ungated spillway, or auxiliary spillway, located at the center of the main dam with a base-level at 640 m (the full supply level of the reservoir); and, 3) an emergency spillway located to the right of the curved saddle dam, with a base level at 642 m. The dam crest is 15 m above the main gated spillway (crest level=655 m AMSL) (Figure 3.2).

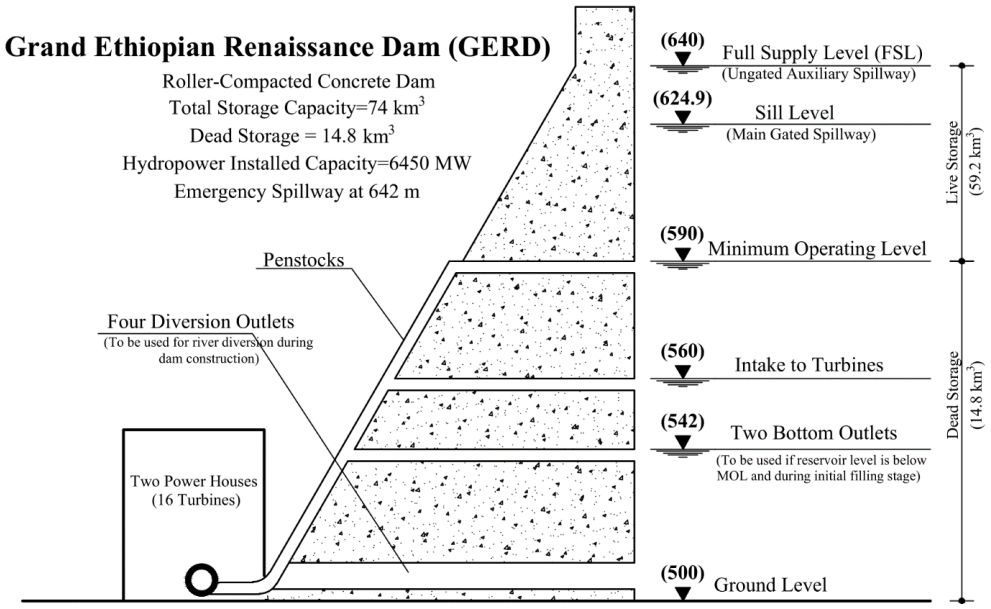

Figure 3.2. Cross-section of the Grand Ethiopian Renaissance Dam with assumed hydraulic capacities. All elevations are above mean sea level [Source: MIT (2014); Wheeler et al. (2016); Abtew and Dessu (2019)].

With its current design of turbines (5150 MW), the GERD will become the largest hydropower dam in Africa in terms of generation capacity. Such a design capacity is expected to greatly improve electricity supply in Ethiopia and neighboring African countries that have rapidly growing populations (see Figure 3.3a for comparison of eastern Nile countries population). In addition, GERD is expected to significantly improve the hydropower production in Ethiopia. Currently, hydropower contributes to more than 95% of the country's total electricity generation (compared to about 8% in Egypt; Figure 3.3b).

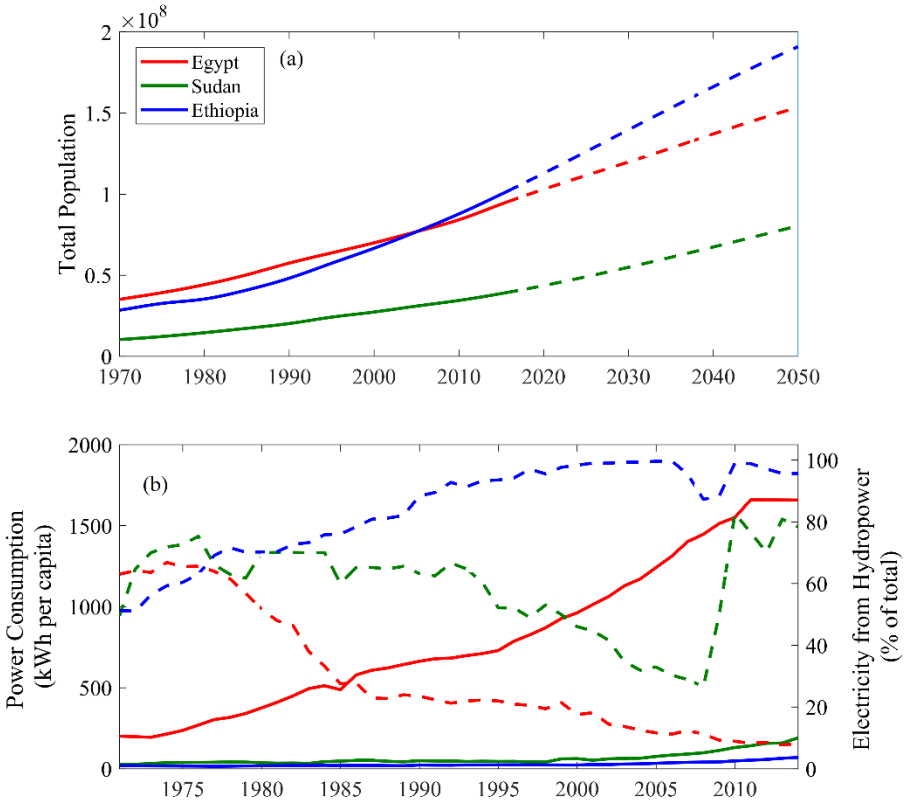

Figure 3.3. (a) Annual population change in the eastern NRB countries (dashed lines indicates projected population). (b) solid and dashed lines indicate power consumption per capita (left y-axis) and the percentage of hydropower generation from the total electricity production (right y-axis), respectively [Data Source: World Bank Database].

3.3 Data and Methods

3.3.1 Modeling UBN Hydrology

Accurate representation of the UBN hydrology is critical to modeling the GERD reservoir inflow and subsequently for inferring its operation and power production. In our study, we used a macroscale hydrological model developed by Eldardiry and Hossain (2019) over the Blue Nile Basin (BNB) using the Variable Infiltration Capacity (VIC). The VIC model was implemented at 0.1° (∼10 km) spatial resolution for the BNB and driven by high spatial and temporal resolution of satellite observations, e.g., SRTM, CHIRPS, and MODIS. The satellite-based forcing were processed over the BNB at a daily scale and re-gridded to the 0.1° spatial scale to drive the VIC model land surface simulations. The runoff (from the VIC outputs) over each grid cell was then routed separately using the routing model scheme of Lohmann et al. (1998). The simulation runs were performed for 37 years spanning the period from 1981 to 2017. The reader is referred to Eldardiry and Hossain (2019) for more details on the VIC modeling framework over the BNB. The satellite-driven VIC model for the BNB is used in our study to characterize the hydrology of the UBN and the streamflow climatology upstream of the GERD location.

3.3.2 Area-Elevation Curve

An area-elevation curve (AEC) is required to calculate the lake area and therefore water volume stored in the reservoir. We established the AEC for the GERD using a 30 m resolution

digital elevation model (DEM) provided by the Shuttle Radar and Topography Mission (SRTM). SRTM image was classified into 1 m elevation bands over the reservoir and surrounding area. The surface area of each band provides an estimate of the reservoir surface when water reaches that elevation Deriving area-elevation curve using satellite-based estimates has been widely employed in previous studies (see for example Wang et al., 2013 over the Three Gorges reservoir). Since GERD is still under construction, the reservoir had not been formed when SRTM overpassed in 2000. Thus, scenarios of different heights for the dam and the resulting reservoir levels are modeled in order to estimate the corresponding lake area. The exact locations of the GERD Dam and its saddle dam were retrieved from recent satellite images and modeled as barriers on the SRTM DEM with various elevation scenarios (Figure 3.1b). Figure 3.1c shows two examples of the GERD lake formed when assuming a crest level of dam at 652 m and 686 m (maximum possible dam height). At a crest level of 652 m (i.e., GERD stands 146 m height), the GERD has a total storage of 80.8 km^3 (area=2008 km^2). The derived area elevation curve (Figure 3.1d) is very close to what has been published by the Ethiopian Electric Power Corporation (EEPCo 2019). In addition, Eldardiry and Hossain (2020) showed the reasonable skill of satellite-based AEC of GERD when compared with those published in previous studies (Abtew and Dessu 2019 and Basheer et al. 2020 for GERD).

3.3.3 Reservoir Operation

The GERD has been reviewed by an International Panel of Experts (IPoE) from Egypt, Sudan, and Ethiopia. One key finding acknowledged by this panel was the unavailability of complete design documents and test data to critically review the project design (Abtew and Dessu 2019). Such data sharing is a common hurdle in transboundary basins and complicates technical feasibility or review studies for hydro projects through international cooperation. Thus,

it is important to simulate how GERD is likely to operate by deriving its reservoir rule curve. For deriving the rule curve, we adopted an optimization scheme that is based on deterministic dynamic programming (DDP) approach. The approach is developed by Karamouz and Houck (1982) to determine a safe range of releases that would avert flooding downstream of the dam (very high releases) or drought conditions (low releases). The problem under consideration is then how to operate GERD reservoir for T time periods (months or years) in order to minimize the total losses or damages that would incur in case the releases are beyond the safe range. A discrete, finite horizon dynamic program was established to solve the optimization problem. The decision of the optimal release was therefore decided based on a piecewise exponential form of the penalty function (P(Rt)) as follows:

$$P(R_t) = \begin{cases} A\left[exp\left(\frac{R_t}{R_{max}}\right) - exp\,(1)\right] & R_t \geq R_{max} \\ 0 & R_{min} \leq R_t \leq R_{max} \\ B\left[exp\left(-\frac{R_t}{R_{min}}\right) - exp\,(-1)\right] & R_t \leq R_{min} \end{cases} \qquad \text{(Equation 1)}$$

where Rt is the dam release at a time step (t), Rmax is the maximum dam release or the upper limit of the safe zone (assumed equal to 120% of the mean annual flow), Rmin, is the minimum dam release or the lower limit of the safe zone (assumed equal to 80% of the mean annual flow), and (A and B) are two constants that are defined based on how much damage will occur downstream the dam when the release is outside the safe zone. Due to lack of information on the damage predictions downstream of the GERD, we adopted the same values used by Karamouz and Houck (1982) (A=3.88×105 and B=1.58×106) such that the penalty function would result in losses equal to 106 units when the release is zero or twice the mean annual flow. This assumption implies that the operation is penalized similarly when there is no release (drought condition) or there is a flooding condition (defined as cases when release is twice the mean

inflow). The reservoir operation was then derived such that the total losses over a time horizon (T) are minimized. It is worth noting that GERD is assumed to be operated primarily for hydropower production, given its location at the Ethiopian-Sudanese border. The DDP optimization scheme is employed using a set of discrete water levels (or storage volumes) to optimize the GERD release such that the hydropower generation is maximized. The stages of the DDP approach are time periods (monthly in our case), and the states are reservoir water levels (with 0.01 m increments). The AEC for GERD (Figure 3.1d) was used to derive the reservoir storage corresponding to the water level state. A water balance equation was then applied to compute the GERD reservoir release (Rt) as follows (assuming negligible groundwater interactions):

$$R_t = Q_{in} - \frac{dS}{dt} + P - E \qquad \text{(Equation 2)}$$

where Q_{in} is the GERD inflow in km^3/month, R_t is the reservoir discharge downstream of the GERD in km^3/month, P is the precipitation over the GERD lake, E is the open water evaporation modeled by the VIC model in km^3/month, and dS/dt represents the change in storage volume with time in km^3/month. The monthly inflow to the reservoir (Q_{in}) was obtained from routing of the VIC modeled runoff at Eldiem station (location of GERD dam; Eldardiry and Hossain, 2019). The optimal GERD release ($R_t|opt$) is then derived as the storage level corresponding to the minimum loss ($P(R_t)$).

The hydropower generation from GERD was calculated based on the optimized release (and corresponding storage level) derived from the DDP program using the following equation:

$$HP = R_{turbine} * \eta\gamma h \qquad \text{(Equation 3)}$$

Here HP is the hydropower production (watt), η is the power plant efficiency, γ (N/m^3) is the specific weight of water, and h (m) is the effective head of water (m). $R_{turbine}$ (in m^3/sec) is the turbine flow of GERD. The turbine flow is set equal to the optimal GERD release ($R_t|opt$). If the power produced exceeds the GERD turbine capacity, then the turbine flow is calculated using the maximum HP (based on the installed capacity) and the excess flow is diverged through the dam spillway.

The assessment of GERD hydropower potential was based on running the reservoir operation model the variability in the streamflow resulted from the modeling of hydrologic conditions in the UBN for 37 years (1981-2017). The variability in the streamflow plays a paramount role in studying the hydropower generation as it significantly impacts the operation of the dam at inter-annual (from year to year) and intra-annual (monthly or seasonal) scales. Considering such variability using a long record of historical streamflow helps identify the hydrologic controls on hydropower generation under diverse climatic conditions including dry and wet years.

3.4 Results

3.4.1 Characterization of UBN Hydrology

The UBN is characterized by a wet rainy season (locally called kiremt season) from June through September, while the dry season starts from November through April (October and May are transition months between wet and dry seasons) (Conway 2000). Figure 3.4 shows the average precipitation and evaporation in the rainy season of the UBN (June through September). These are key variables to understand the inputs of the GERD reservoir, e.g., inflow and lake evaporation. The average monthly precipitation in the rainy season is 236 mm (standard deviation=11.4 mm) compared to only 24.5 mm (standard deviation=7.8 mm) in the dry season

months. Similar variations are also noticed for evaporation with higher rates in rainy season months (maximum and minimum monthly evaporation are in August=130 mm and March=31 mm, respectively). As depicted in Figure 3.4a and Figure 3.4b, lower elevation areas downstream of Lake Tana have higher precipitation and evaporation rates. Figure 3.4c shows the resultant monthly precipitation and evaporation over the GERD lake (delineated in Figure 3.1c). The months from April through September experience higher precipitation than evaporation with maximum difference in June (92.6 mm). Conversely, the dry season months have higher evaporation rates with maximum difference between precipitation and evaporation in November (-81.5 mm).

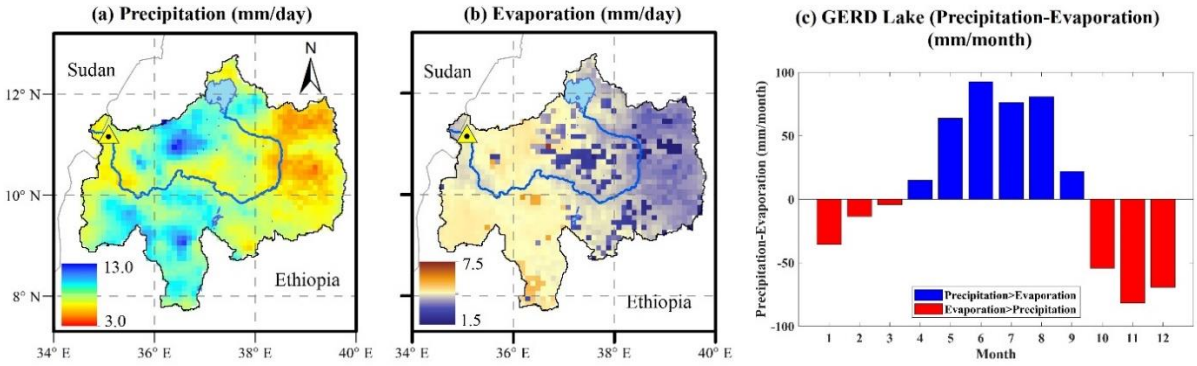

Figure 3.4. Hydrologic characterization of the Upper Blue Nile (UBN). Average (a) precipitation and (b) evaporation during the rainy season (June through September) of the UBN. (c) Difference between monthly precipitation and evaporation over GERD lake (delineated in Figure 3.1c).

Figure 3.5 shows the comparison of the VIC modeling of streamflow with the observed discharge at Eldiem station for a 12-year period (1993-2005). The model generally showed close agreement between the simulated and observed monthly streamflow with a correlation coefficient of 0.90. According to Moriasi et al. (2007), a model performance is considered to be satisfactory

when meeting three criteria: NSE>0.50, percent bias (PBIAS) ±25%, and ratio of the root mean square error to the standard deviation of measured data (RSR) ≤0.70. In case of Eldiem station, the three statistics meet the satisfactory criteria with NSE=0.79, PBIAS=2.5, and RSR=0.46. . On average, the annual simulated streamflow is in good agreement with the observed discharge with a slight overestimation of 1.25 km^3 (mostly in the wet season months) (Figure 3.5b). Figure 3.5c shows a climatological time series of annual simulated streamflow, or GERD inflow, during 37-year simulation period (1981-2017). The streamflow in the UBN varies from one year to another because of the effect of timing and sequence of El Niño and La Niña in the UBN (Zaroug et al. 2014). The annual streamflow reaching GERD has an average of 48 km^3 and ranges from 65 km^3 in 1993 (wet year) and 30.6 km^3 in 2007 (dry year).

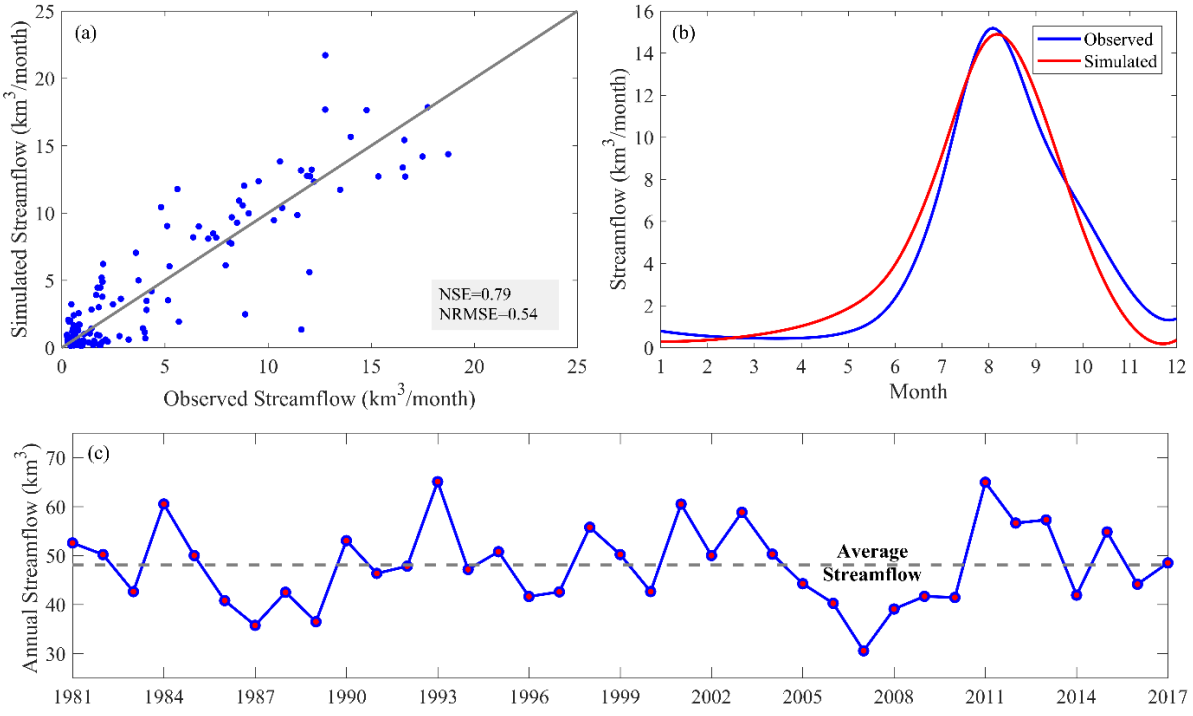

Figure 3.5. (a) Scatter plot of observed and simulated streamflow at Eldiem station (location of GERD dam and outlet of the Upper Blue Nile (UBN)). (b) Monthly streamflow (observed vs

simulated) averaged over 12-year period (1993-2005). (c) Annual simulated streamflow (GERD inflow) for the 37-year simulation period (1981-2017) at Eldiem station.

3.4.2 Deriving GERD Operating Rule

We derived the GERD operating rule using the DDP optimization approach explained in section (3.3) with the objective of hydropower maximization. The results in this section are only shown for the baseline scenario of GERD operation, i.e., installed capacity of 5150 MW. Figure 3.6a shows the range of monthly storage water level during the operation of the GERD dam. The dam is expected to operate at higher storage levels later in the rainy season (September and October), while lowering its storage early in the summer to prepare for the coming flood. For instance, GERD has an average storage level of 637.0 m (ranges between 631m and 640 m) and 622.1 m (ranges between 622 m and 623.1 m) in September and June, respectively. GERD releases an average monthly discharge of 4 km^3/month with higher releases in September (peak discharge=5.56 km^3/month). The inter-annual variability in the GERD releases varies significantly in September when the inflow reaches its peak (Figure 3.6b). The reason for that is the failure of the dam to store enough of the inflow in September (due to limiting its storage to a presumed level of 640 m), and therefore, resulted in wider range of releases. When operating the dam with a higher full supply level of 650m, the dam is able to store the excess flow in September and therefore the releases become less variable as compared to FSL=640 m scenario (dashed lines in Figure 3.6).

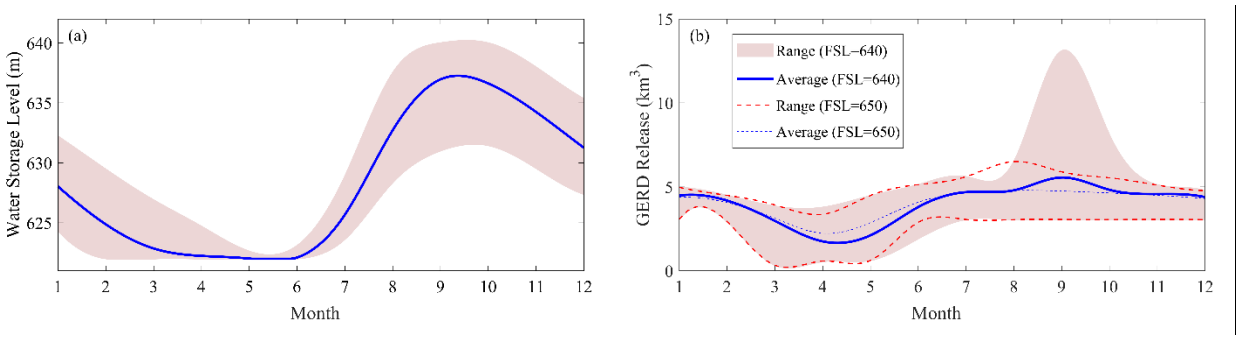

Figure 3.6. GERD operation based on 37-year historical climatology of streamflow (1981-2017) and installed capacity of 5150 MW (baseline scenario). (a) GERD storage level, (b) GERD release (summation of turbine and spillway release), The blue line indicates the average operation, while shaded area represents the range of operation (minimum and maximum) due to streamflow variability.

3.4.3 GERD Hydropower Potential

Figure 3.7 shows the range of monthly hydropower production from the GERD under a baseline scenario that assumes the current design criteria of GERD operation, i.e., nameplate installed capacity of 5150 MW. On average, the GERD can yield an annual hydropower production of 13,629 GWh with a peak production in September (1630 GWh). The monthly production changes significantly with the streamflow variability with an average monthly interquartile range of 366 GWh (about 32% of the average monthly hydropower production). The maximum interquartile range is noticed in April (797 GWh) and September (487GWh). These months have the GERD storage level at its minimum operating level (622 m) with low GERD inflow (less than 3 km^3/month) and therefore less dam releases.

On average, the baseline scenario can exploit between 456 MW (9% of installed capacity) and 2264 MW (44% of installed capacity) in April and September, respectively. The baseline scenario with an installed capacity of 5150 MW demonstrated that GERD can generate electricity

with an annual average of 13629 GWh. Changing the installed capacity doesn't impact the annual production which means that this cap in the electricity produced is primarily driven by the hydrology of the basin rather than the power plant configuration.

Changing the design levels of the GERD, e.g., minimum operating level (MOL) and full supply level (FSL) does not have significant effect on maximizing the use of installed turbine capacity (Figure not shown). For example, with an increase in the dam FSL to 650 m AMSL resulted in an average percentage of exploited capacity equals to 28.4% in September. The increase in dam height will allow for more storage of the flow in the dam (as can be indicated from Figure 3.6) and therefore less dam releases. Such reduction in releases will counter the effect of increase in FSL and resulted in less percentage of exploited capacity. Hence, any future plan to raise the dam crest level is unlikely to increase hydropower production, because the hydrology of the UBN does not sustain enough streamflow to exploit the turbine capacity installed.

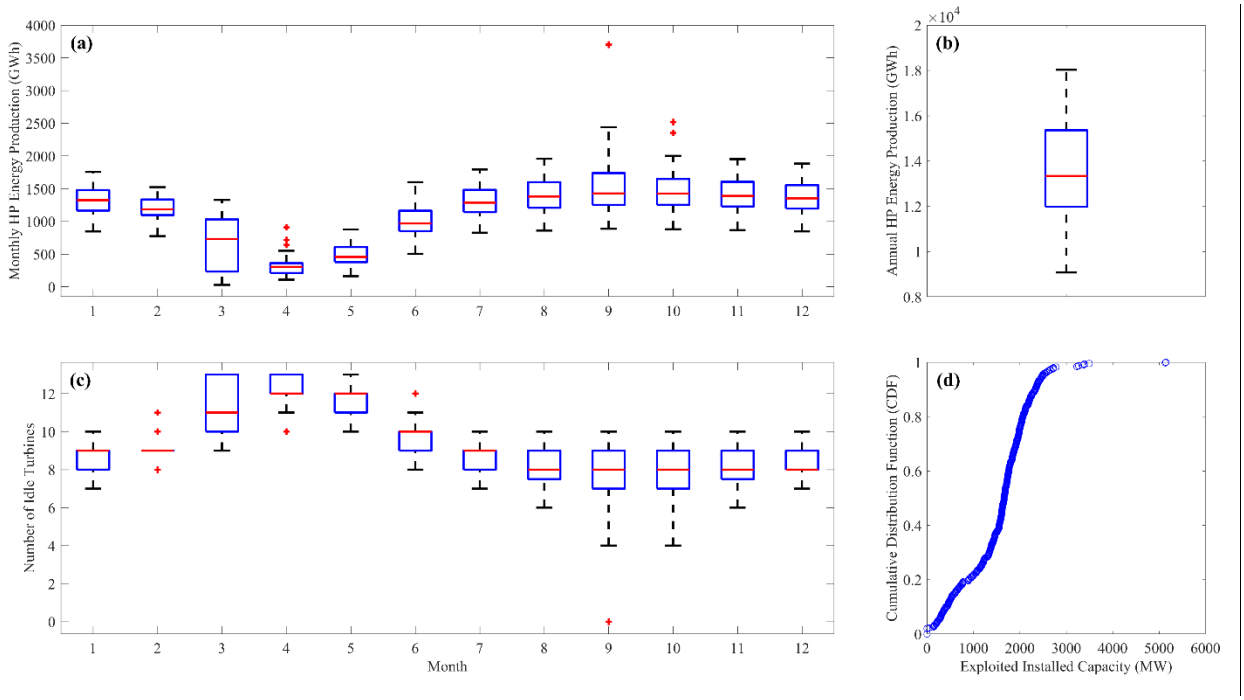

Figure 3.7. Box plot of the (a) monthly, (b) annual hydropower production of GERD, and (c) number of idle turbines during the monthly GERD operation at the baseline scenario with installed capacity of 5150 MW. (d) The empirical cumulative probability of the monthly exploited installed capacity based on 37 years of GERD operation.

Figure 3.7c depicts the number of idle turbines during monthly GERD operation. The number of idle turbines is calculated as the number of turbines, which are completely not used in each month. The median number of idle turbines ranges between 8 turbines (in the months following the flooding season; September through December) and 12 turbines (in April and May). The median exploited capacity (corresponding to 50% probability) is 1660 MW (Figure 7d). When considering climate variability with wet and dry years, the number of idle turbines can range between 4 (wet years) turbines and 10 (dry years) turbines in September and October. This analysis shows the importance of considering the number of turbines as a factor to evaluate the GERD hydropower efficiency.

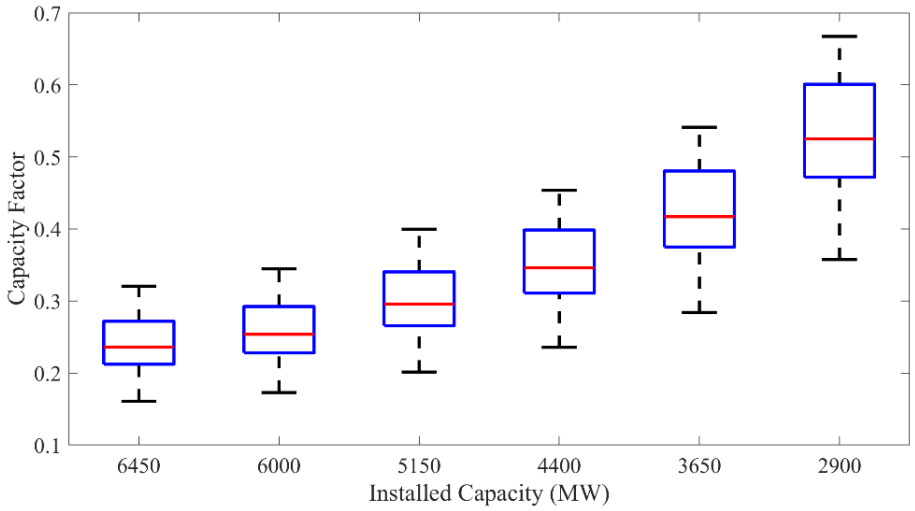

Figure 3.8. The range of capacity factor (CF) as a function of the GERD installed capacity.

Figure 3.8 shows the capacity factor of the GERD under different scenarios of installed capacity (ranging from 16 turbines of 6450 MW to 8 turbines of 2900 MW). Capacity factor indicates the percentage of hydropower generation in a period of time relative to the theoretical maximum possible generation if all the turbines worked at full capacity without interruption. The capacity factor for specific hydropower plant varies due to different factors including basin hydrology, plant age, mode of operation as well as relative contribution of hydropower to the overall energy portfolio of an electric grid. For example, the three Gorges Dam in China has the largest hydropower capacity in the world (22500 MW) and operates at a capacity factor of 46.7% (Qin et al. 2020). In US, the median hydropower capacity factor has been 38.1% in recent years (Uria-Martinez et al. 2018) with values as low as 25% and as high as 75%. For the GERD, the baseline scenario (with 5150 MW installed capacity) resulted in an average capacity factor of 30%. On the contrary, when assuming lower turbine capacity of 2900 MW, the electricity produced can attain 53% of the full capacity of the plant (Figure 3.8).

3.5 Conclusion

Our study evaluated hydropower production potential of GERD that is supported by the hydrology of the Upper Blue Nile (UBN). Historical characterization of the GERD inflow using a 37-year simulation of the UBN hydrology indicated a median flow of 48 km^3/year, which can produce about 13,629 GWh annual production (capacity factor=0.30). The hydrology of the UBN limited the hydropower potential of GERD and thus the initial plans to upgrade the GERD capacity (from 5250MW to 6000MW to 6450 MW) have not been beneficial to improving the dam's hydropower production. Therefore, the recent lowering of installed capacity (to 5150 MW) is more reasonable to offset the hydrologic constraints of the UBN. While operating a hydropower dam to satisfy the peak or base power load is a more realistic scenario, the analysis

presented in our study for the maximum production might be favored in the GERD case since the dam is billed to export much of the produced electricity to the neighboring countries.

While the current study assessed the GERD hydropower potential under the current hydrological conditions of the UBN, future hydropower production may even be reduced by climate change impacts, e.g., expected modification in hydrology and reservoir sedimentation (Schaefli 2015). As climate change is a key driver of future basin hydrology, any change in streamflow regime may jeopardize the hydropower potential of the dam. In addition to alterations in streamflow, sedimentation rate in reservoirs, which is currently estimated to cause an annual loss of about 0.8-1% of reservoir capacity, may also increase (Gaudard and Romerio 2014). As installed hydropower capacity continues to grow globally, considering such risks associated with basin hydrology and climate change is important to analyze the life cycle of planned hydropower projects and find out the optimum power plant design that is economically efficient and can live up to the declared promise of energy security.

Chapter 4: A Blueprint for Adapting High Aswan Dam Operation in Egypt to Challenges of Filling and Operation of the Grand Ethiopian Renaissance Dam

Note: This chapter has been published mostly in its current form in Journal of Hydrology (Eldardiry and Hossain 2020); **© Elsevier. Used with permission.**

Eldardiry, H., and Hossain, F. (2020). A Blueprint for Adapting High Aswan Dam Operation in Egypt to Challenges of Filling and Operation of the Grand Ethiopian Renaissance Dam. Journal of Hydrology. 125708 (DOI: https://doi.org/10.1016/j.jhydrol.2020.125708).

Abstract

Increasing hydropower development by upstream nations of the Nile River Basin indicates the need to adapt the operation of existing dams. In this study, we present a satellite-based blueprint to test scenarios of High Aswan Dam (HAD) operation under the impacts of filling and operation of the Grand Ethiopian Renaissance Dam (GERD) based on a Water Supply Stress Index (WaSSI). Our results show that the status quo conditions of the agricultural-based stress ($WaSSI_{AG}$) downstream of the HAD are subject to lower stresses in the summer months ($WaSSI_{AG}$<0.6 in May through August) when HAD empties its storage to prepare for the Blue Nile rainy season. To adapt to a faster GERD filling scenario (e.g., 3-year filling), HAD needs to modify its operation in summer months by elevating the downstream stress level (store more and release less), e.g., $WaSSI_{AG}$=0.70. Such adaptation can also help HAD recover its normal operating level in 4 years after GERD is completely filled compared to 7 years with no adaptation scenario. Additionally, maintaining HAD storage at higher levels prior to GERD filling can significantly reduce the HAD recovery period to only 2 years. Because GERD is already under construction, our blueprint provides a tangible way forward for HAD to adapt its operation to a real-world transboundary challenge and maintain water security for Egypt.

4.1 Introduction

Many river basins world-wide are experiencing increasing pressure on water resources, due to accelerated economic growth, rising population, increasing food demand, and climate change (Wada and Bierkens 2014; Munia et al. 2016). Such challenges are more evident in transboundary basins, e.g., the Nile basin (Paisley and Henshaw 2013; Rahman 2013), Euphrates-Tigris (Kibaroglu and Gürsoy 2015), or the Mekong basin (Grumbine and Xu 2011). These rivers are under intense development pressure, with multiple upstream dams planned or under construction that would dramatically alter a wide range of hydrological, agricultural, and ecological systems. In addition to dam development, climate variability is a significant factor when assessing water system sustainability (Vörösmarty et al. 2000; Kummu et al. 2014). The growing regional and global concerns about these adverse impacts of large-scale dam construction and climate variability have led to increasing interests to revisit the operation of existing dams (Grumbine et al. 2012; Digna et al. 2018).

Considering the growing number of dams under construction (more than 600 dams globally according to Zarfl et al. 2015), it is now timely to re-assess the impact of these emerging and upstream dams on downstream regions, particularly on existing reservoirs that are the mainstay of water security for those countries. The Nile River Basin (NRB) presents a classic and timely case for such a re-assessment with eleven transboundary countries that are continuously competing for scarce water resources to support a growing population and economic development challenges (Molden et al. 2009). Furthermore, upstream riparian countries in the NRB prioritize their national development aspirations against the backdrop of on-going agricultural practices and livelihood of downstream countries. For instance, Ethiopia and Sudan are now moving towards building new hydropower dams, which are expected to

provide the primary source of electricity. Building such dams can significantly alter downstream water availability for Egypt, especially during the filling phase of the dam's reservoir. With irrigation and hydropower as key drivers of economic and social development in the NRB, any development by upstream countries would lead to considerable friction and tensions on the use of the water among the riparian nations.

The announcement of the construction of Grand Ethiopian Renaissance Dam (GERD) in 2011 and the disagreements that ensued between Egypt and Ethiopia exemplifies a transboundary water challenge. The GERD project challenges Egypt's historical hegemonic position on the Nile basin and aspires to project the power of Ethiopia on Nile water sharing (Whittington et al. 2014; Cascão and Nicol 2016). As ongoing dam projects expand in the upstream portion of the NRB, water resources managers will need to advocate for the sustainable use of available water resources while ensuring the development goals for all countries. In the case of transboundary basins, employing adaptive management is currently best-suited to confront impending challenges and mitigate the impacts downstream of the basin (Pahl-Wostl 2007; Zeitoun et al. 2013). Thus, it is crucial to adapt the operation of existing reservoirs in NRB, e.g., High Aswan Dam (HAD) in Egypt, to upstream planned dams that are already under construction, e.g., GERD. An adaptive reservoir operation includes learning from the status quo downstream management practices to adapt better to future challenges (Georgakakos et al. 2012; Zhang et al. 2017).

The High Aswan Dam (HAD) forms the largest storage dam in the Nile basin (total storage capacity of 162 km^3) and is considered as the faucet that controls the water flowing downstream in Egypt. HAD operation is based on the Nile Waters Agreement of 1959 between Egypt and Sudan (assuming an annual average inflow of 55.5 km^3 allocated to Egypt) and under

the assumption that most of the Blue Nile flow will contribute as unregulated inflow to HAD. The upper Blue Nile, i.e., upstream of the GERD location, provides about 53% of the annual flow reaching downstream to Egypt. Therefore, introducing a large-scale dam like GERD into the Blue Nile will inevitably impact the flow reaching HAD during filling and later during operations of GERD. Such impacts, for example, include changes in the total annual flow volume reaching downstream (primarily during the GERD filling) and the seasonal timing of flow (primarily during the GERD post-filling phase). In addition, Egypt's water sustainability downstream, particularly for agricultural uses, is threatened as HAD currently lacks provision to adapt to GERD filling and operations. Therefore, it is important for a downstream country like Egypt with its growing population, to understand what changes GERD will bring to its water security and how HAD needs to adapt its operation to such imminent challenges.

Understanding impacts on reservoir operation is difficult in transboundary basins due to the historical lack of shared in-situ information on reservoir operation and water management practices (Hossain et al. 2007; Balthrop and Hossain 2010). However, such information is now becoming available from satellite remote sensing. Satellite data can provide estimates of different components of hydrological cycle including precipitation, evaporation, water level, water area, and soil moisture, which can then be used to predict the state of a reservoir (Famiglietti et al. 2015; Lettenmaier et al. 2015; Sheffield et al. 2018). Recently, satellite measurements have been successfully incorporated in reservoir models to understand the operation of dams in transboundary basins. For example, Eldardiry and Hossain (2019) have developed a satellite-based framework to derive the operating rules of High Aswan Dam (HAD) in the Nile basin. The centerpiece of this framework is the hydrological model that exploited the global availability of satellite observations at high spatial and temporal resolution as forcing

inputs. Our study builds upon this tested satellite-based modeling framework (Eldardiry and Hossain 2019) to address the following key question: *How can a downstream and pre-existing dam such as the HAD, adapt its operation to inflow alterations during the filling and operation phases of a newer dam in the upstream, such as the GERD?*

The adaptation of HAD operation to GERD construction typifies one of the challenges facing dam operators and water managers in downstream Nile riparian countries. Recently, various studies have investigated the impacts of GERD on downstream countries with more focus on the GERD filling strategies (King and Block 2014; Mulat and Moges 2014; Zhang et al. 2015; Wheeler et al. 2016). However, crucial insights on how dam operators can adapt to potential impacts have not been capitalized in previous studies. For example, Zhang et al. (2015) concluded reduction in downstream streamflow due to various factors including filling policy of GERD, climate variability, and projected climate change scenario. Wheeler et al. (2016) and (2018) introduced some HAD operation scenarios, drought (or no drought) management policy, based on GERD agreed annual release (cooperative approach). However, Wheeler at al. (2016) and (2018) focused only on the total annual shortages in HAD inflow without insights into the potential changes in HAD operation based on downstream agricultural adaptations. Our study proposes a physical blueprint that employs water scarcity indices to infer modified reservoir operation to adapt to expected streamflow alterations while maintaining the supply for downstream water use. Reinventing the operating curves for existing dams will provide an inclusive understanding of the potential adaptation alternatives to future challenges associated with planned dams and streamflow variability. The remainder of the paper is organized as follows. We describe the study area and the selected dams in section 2, data sources and methods are introduced in section 3, results for the HAD reservoir operation under GERD filling and

operation scenarios are discussed in section 4, discussion of results and concluding remarks are summarized in sections 5 and 6, respectively.

4.2 Study Area and Dams

The Nile River Basin (NRB) is a major transboundary river that passes through eleven countries in northeastern Africa (Figure 4.1). The NRB comprises two major tributaries, the Blue Nile (originates from the Ethiopian plateau) and the White Nile (originates from Lake Victoria in Jinja, Uganda). The Blue Nile is the primary tributary of the main Nile River, providing about 62% of the flow reaching Aswan (Melesse et al. 2011). The NRB is currently undergoing hydropolitical changes through the construction of large scale dams and the expansion of irrigation projects (Aljefri et al 2019). Figure 4.1 shows the existing, planned, and under construction dams along the Nile river according to the Global Reservoir and Dam (GRanD) database (Lehner et al. 2011), the GlObal geOreferenced Database of Dams (GOODD) (Mulligan et al. 2020), and Zarfl et al. (2015). The purposes of the major dams in the NRB (e.g., High Aswan Dam in Egypt, Roseires and Merowe dams in Sudan, and Nalubaale Power Station in Uganda) are to produce hydroelectric power and provide water supply needed to meet irrigation demands. The future hydropower dams inventory produced by Zarfl et al. (2015) reveals an increasingly impounded Nile river for hydropower development in NRB with more than 35 dams planned for construction. The current study focuses on the impacts of the Grand Ethiopian Renaissance Dam (GERD), currently under construction on the Blue Nile, on the operation of the downstream High Aswan Dam (HAD) in Egypt (Figure 4.1). The area-elevation curve was established for the two reservoirs (i.e., lakes of HAD and GERD) using a 30 m resolution digital elevation model (DEM) provided by the Shuttle Radar and Topography Mission (SRTM) (for more details on deriving area-elevation curves of HAD and GERD using

SRTM, the reader is referred to Eldardiry and Hossain (2019) and ElBastawesy (2014), respectively). The satellite-driven curves (both Area-Elevation and Volume-Elevation curves) were compared with those published in previous studies (Abtew and Dessu 2019 and Basheer et al. 2020 for GERD) and (Hurst et al. 1966 and Moussa 2018 for HAD). Our comparison shows a reasonable skill to infer the reservoir volume at different elevations for GERD and HAD with a mean percentage error of 7% (compared to Basheer et al. 2020) and 9% (compared to Hurst et al. 1966), respectively. Thus, satellite-driven curves can be very useful in inferring reservoir characteristics, e.g., storage level and volume, especially in transboundary basins, where bathymetric surveys are usually not available. The specifications of the HAD and GERD are summarized in Table 4.1 and explained as follows.

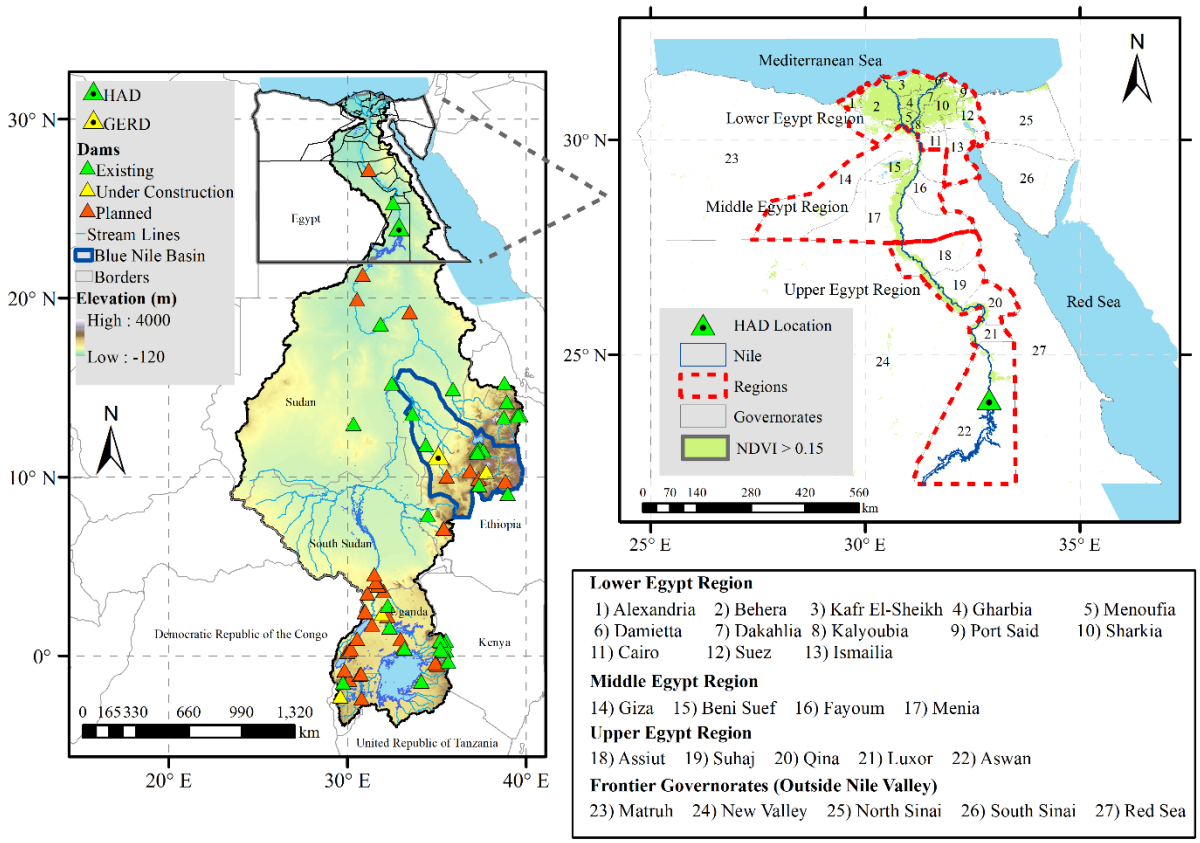

Figure 4.1. The Nile River basin (NRB) with the existing, planned, and under construction dams as provided by the GRanD database (Lehner et al. 2011), GOODD database (Mulligan et al. 2020), and Zarfl et al. (2015). The right panel highlights the location of the HAD dam and the downstream agricultural area in the Nile Delta and along the Nile valley.

4.2.1 High Aswan Dam (HAD)

The High Aswan Dam (HAD) is an embankment dam built across the Main Nile in Aswan, Egypt between 1960 and 1970 to provide long-term protection against drought and flood (Abd-El Monsef et al. 2015). HAD regulates the inflow primarily to meet the downstream water supply for irrigation demands in Nile Delta and along the Nile Valley (Figure 4.1), where 96% of Egypt's population is located. The HAD also serves hydropower generation, and water supply for industries and municipalities. The HAD reservoir, Lake Nasser, started impounding in 1964 and reached an operating level (175 m above mean sea level-AMSL) in 1975 (El-Shabrawy 2009; Moussa 2018). The operation rules of Lake Nasser reservoir are designed to ensure adequate water supply and safety of the HAD. The HAD reservoir has a total storage of 162 km^3 with minimum and maximum operating levels of 147 m and 182 m AMSL, respectively. At the beginning of the water year (1^{st} of August), the water level is kept at 175 m AMSL (Full Supply Level) to store incoming high flows (Moussa 2018). The storage increases gradually in the summer and, subsequently, the reservoir levels decrease from January to July as water is released. The HAD is equipped with six pairs of turbines, each having a capacity of 175 MW, and the power station has total capacity of 2100 MW (Table 4.1). One pair of turbines is assumed inoperative at any time because of maintenance problems, and another turbine is left idle to provide spinning reserve (Thomas and Revelle 1966; Moussa et al. 2018). The maximum annual hydropower production at the dam is therefore considered to be 1134 GWH per month

(assuming the full operation of 9 turbines during the month). In our study, we assumed a more conservative approach to the estimation of hydropower production capacity by applying a 50% load factor to the maximum production, yielding a value of 567 GWH/month (or 6804 GWH/year).

4.2.2 Grand Ethiopian Renaissance Dam (GERD)

The Grand Ethiopian Renaissance Dam (GERD) location was first identified in a study conducted by the US Bureau of Reclamation to explore the potential hydropower dam sites in the Blue Nile Basin (USBR 1964). The construction site of the main dam is at a ground level of 500 m above mean sea level (AMSL) and can only store water with a maximum level of 606 m AMSL (ElBastawesy 2014). The current design of GERD is to supply a storage at an elevation of 640 m (Full Supply Level) with a corresponding capacity of 74 km^3. The main dam is supported by a rock-fill saddle dam (to the west of the GERD) to provide the storage between 606 m and 640 m (Abtew and Dessu 2019). The GERD is planned to have 16 turbines with a total capacity of 5150 MW, making it the largest hydropower dam in Africa and it is likely to bring significant improvements to the electricity access for the entire Nile (MIT 2014).

Table 4.1. The specifications of the existing downstream dam (HAD) and planned upstream dam (GERD).

Specification	HAD	GERD
Ground and Crest Levels	85-196 m	500-655 m
Minimum Operating Level	147 m	590 m
Full Supply Level (AMSL)	175 m	640 m
Emergency Spillway Level	178 m (Toshka spillway)	642 m

Storage (km^3)	162 km^3 (Dead=32 km^3 - Live=90 km^3 - Emergency=40 km^3)	74 km^3 (Dead=14.8 km^3 and Live=59.2 km^3)
Hydropower Capacity (Turbines)	2100 MW (12 Turbines)	5150 MW (16 Turbines)

4.3 Methods and Data

This study presents an integration of models with satellite observations to re-evaluate the operation of HAD (the pre-existing downstream dam) under the impacts of GERD (the upstream dam currently under construction). Revisiting the operation of the HAD during the filling and operation phases of GERD followed a modeling blueprint that integrates satellite observations into hydrological and reservoir modeling as illustrated in Figure 4.2. The adaptation of HAD operation to GERD filling/operation phases is then assessed by building different scenarios of HAD operation under the impacts of different factors including: GERD filling period, initial storage level at HAD, and the downstream supply stress levels (Table 4.2). The proposed blueprint comprises four main components that are described in the next sections.

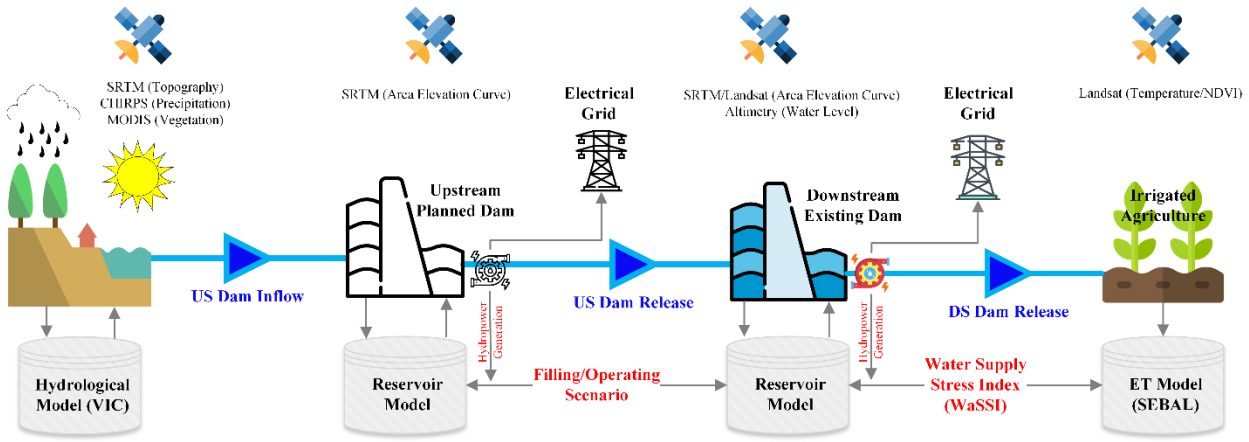

Figure 4.2. Schematic diagram of the blueprint proposed in our study to re-evaluate the operation of existing dam under the filling/operation of an upstream planned dam.

Table 4.2. Decision factors considered in the assessment of HAD operation under the filling/operation of GERD (upstream dam).

Decision Factor	Scenario
Upstream dam (GERD)	Filling vs operation phase
GERD filling period	2 to 12 years
HAD and GERD inflow	Dry vs normal vs wet years
HAD initial storage level	Low vs high
Downstream stress level	Status quo stress vs predefined stress level

4.3.1 Reservoir Inflow Scenarios

To understand the filling and operation scenarios of a planned dam, hydrologic information on the watershed upstream of the dam is required. Such information includes precipitation, lake evaporation, and reservoir inflow. In our study, we used the Variable Infiltration Capacity (VIC) model to simulate the hydrologic conditions over the upper Blue Nile Basin (BNB). The VIC model was implemented at 0.1° (~10 km) spatial resolution for the BNB and driven by high spatial and temporal resolution of satellite observations, e.g., SRTM, CHIRPS, and MODIS. The previous study by Eldardiry and Hossain (2019) has demonstrated the fidelity of the VIC model with satellite observations for simulating streamflow along the BNB (validated at Khartoum and Eldiem stations with a Nash Sutucliff Efficiency of 0.68 and 0.92, respectively). For further details, the reader is referred to Eldardiry and Hossain (2019) for understanding the VIC modeling framework over the BNB. The satellite-driven VIC model for the BNB is used in this study to characterize the streamflow climatology upstream of the GERD (inflow at Eldiem station) for 37 years (1981-2017). The use of 37-year streamflow climatology allowed the assessment of GERD filling/operation scenarios under expected inter-annual and intra-annual variability of streamflow. Such variability is significant in the annual Nile river

flows (Siam and Eltahir 2017) and is expected to increase in future with climate change (Conway 2017).

In our study, we followed a GERD filling approach that assumes monthly filling of the dam in a pattern identical to its inflow, i.e., higher storage in summer months during a number of filling years that satisfies the total dam storage capacity (74 km^3). In each filling year, we assumed the volume stored in the reservoir is proportional to the total dam inflow. Thus, the storage volume (S_i) for each year of filling is calculated as follows:

$$S_i = S_{max} * \frac{Q_i}{\sum_{i=1}^{N} Q_i} \qquad \text{(Equation 1)}$$

Where Q_i is the total annual flow volume for year (i) of filling, N is the total number of filling years, S_{max} is the storage capacity of the dam (74 km^3 for GERD). We used the historical inflow (1981-2017) simulated by the hydrological model (streamflow outputs of VIC routing model) at Eldiem station to calculate the possible range of GERD releases assuming different scenarios of GERD filling (ranging from 2- to 12-year filling scenarios). To account for the streamflow variability and possible filling years with dry or wet hydrologic conditions, we filled the dam during a moving time window of N years for each N-year filling scenario. For example, for a 3-year filling scenario, we produced 35 possible climatological conditions to fill the dam in 3 years (the first window is between 1981 and 1983 and the last window is between 2015 and 2017). Similarly, for a 12-year filling scenario, the first window includes the inflow for years between 1981 and 1992 and the last window assumes filling years between 2006-2017.

We assumed the filling of GERD will start in August, when the flow in the upper BNB is at its peak. The monthly inflow to the HAD reservoir was obtained by routing the GERD outflow in the BNB to Khartoum station and adding the monthly flow from the White Nile and Atbara

River. To include the interannual variability in the flow from the White Nile and Atbara river, we considered three scenarios that reflect normal (average flow), dry (average - standard deviation), and wet (average + standard deviation) flow conditions (Figure 4.3a). These conditions resulted in additional annual flow to the HAD that ranges from 26 km^3 (dry conditions in White Nile and Atbara river) to 48 km^3 (wet conditions in White Nile and Atbara river). When GERD starts filling, we assumed the initial level of the HAD to be at low (169.32 m AMSL) or high (178.37 m AMSL) storage conditions based on HAD operation in the recent years (2011-2020) (Figure 4.3b). The HAD levels are estimated based on radar altimetry-based water surface elevations that were acquired from the operational satellite altimetry Hydroweb database (Crétaux et al., 2011).

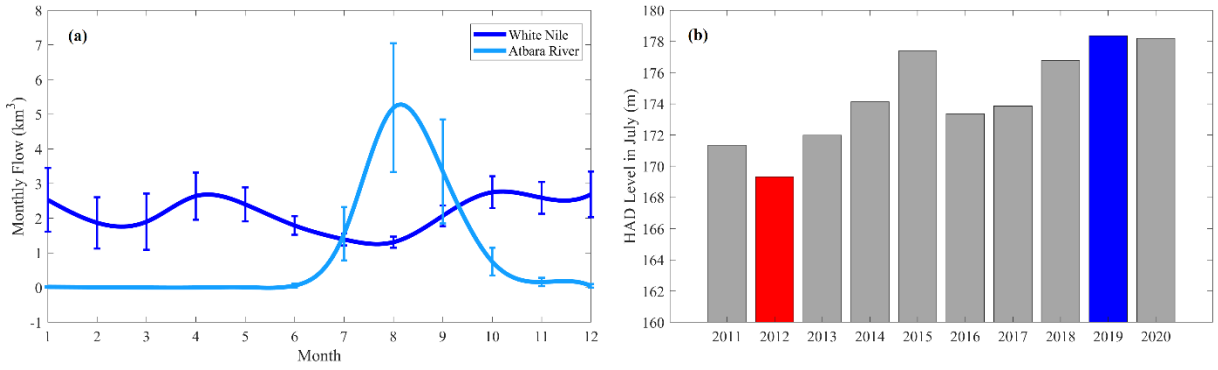

Figure 4.3. a) The average monthly flow at the outlet of White Nile and Atbara rivers (error bars indicate the standard deviation) [Data Source: Global Runoff Data Centre (GRDC)]. b) The HAD level in July in the recent years (2011-2020). The red and blue bars indicate the lowest and highest water level that are used as initial storage HAD level when GERD starts filling [Data Source: Hydroweb database].

4.3.2 Irrigation Water Use

Agriculture is the dominant water use in the eastern Nile countries. In Egypt, 86% of the HAD releases are consumed by the agricultural sector, while the remaining 14% are shared

between municipalities and industrial sectors (FAO 2016). Hence, the expected changes in the HAD inflow, as a result of GERD filling and/or operation, will inevitably impact agricultural consumption downstream of HAD. Adapting the current operation of HAD to upstream changes requires a thorough understanding of the crop patterns in Egypt and subsequently the water requirements for irrigation. A common approach to represent the irrigation demand by a specific crop is to use the evapotranspiration as a proxy of the water consumptive use. Evapotranspiration (ET_c) is a key component of the hydrologic cycle and its accurate estimation is of vital importance for hydrologic water balance, irrigation system design and management, and water resources planning and management (Fisher et al. 2017).

To address ET_c variability in regions with limited ground-based measurements, as is the case in the NRB, satellite images are an excellent means for determining and mapping the spatial and temporal structure of ET_c (Allen et al. 2007). Various satellite-based methods have been suggested in literature (Liou and Kark 2014), e.g., SEBAL (Surface Energy Balance Algorithm for Land) and METRIC (Mapping Evapotranspiration at High Resolution and with Internalized Calibration). Such remote sensing approaches can provide accurate and more frequent monitoring of the crop water requirements in regions where in-situ data are not readily available. In our study, we employed the Surface Energy Balance Algorithm for Land (SEBAL) algorithm (Bastiaanssen et al. 1998, 2005). SEBAL has been successfully implemented in previous studies to estimate ET using satellite images (e.g., Senay et al. 2016; Elnmer et al. 2019). In the SEBAL model, ET is computed from satellite images and weather data using the surface energy balance. Since the satellite image provides information for the overpass time only, SEBAL computes an instantaneous ET flux for the image time. SEBAL calculates ET through a series of computations that generate: net surface radiation, soil heat flux, and sensible heat flux to the air.

A residual energy flux is then calculated by subtracting the soil heat flux and sensible heat flux from the net radiation at the surface. This residual energy is used to convert the liquid water into water vapor (or latent heat flux), i.e., evapotranspiration. Therefore, the ET flux is calculated for each pixel of the image as a residual of the surface energy budget equation:

$$\lambda ET = R_n - G - H \qquad \text{(Equation 2)}$$

where; λET is the latent heat flux (W/m^2), R_n is the net radiation flux at the surface (W/m^2), G is the soil heat flux (W/m^2), and H is the sensible heat flux to the air (W/m^2).

In our study, the SEBAL was applied on freely available Landsat-8 satellite images to estimate total ET_c over different governorates (administrative boundaries in Egypt) located downstream of the HAD reservoir (see Figure 4.1). The monthly SEBAL-based ET_c was estimated for the period between January 2014 and December 2017 (the most recent years of our VIC simulations). The SEBAL model also requires the meteorological data of land surface, such as wind speed, surface pressure, and air temperature as inputs for the surface energy balance calculations. The meteorological data of land surface were obtained from the outputs of the Global Land Data Assimilation System (GLDAS) (Rodell et al. 2004). GLDAS outputs have been evaluated globally with high accuracy in northern Africa when compared with gauge-based counterparts (see for example Decker et al. (2012) and Ji et al. (2015)). To avoid the misclassification of non-vegetation areas, we modified the SEBAL algorithm by adding random forest classification scheme to mask all areas that are not considered as potential agricultural area. The SEBAL parameters, e.g., hot and cold pixel selection, are calibrated using the irrigation water use data retrieved from the annual bulletin of water resources and irrigation, issued by the Central Agency for Public Mobilization and Statistics (CAPMAS) in Egypt , which is provided for each governorate downstream of the HAD (CAPMAS 2014).

4.3.3 Water Scarcity Index

To understand water stresses downstream of the HAD, we adopted the water supply stress index (WaSSI) approach (Falkenmark 1989; Sun et al. 2008; Eldardiry et al. 2016; Borrok et al. 2018). The WaSSI index is expressed as a ratio of water demand to water supply. Thus, the higher the WaSSI value, the more stress the water system faces. Similar indices have been used in global assessment of water scarcity (see for example Munia et al. 2016; Wada et al 2011). In our GERD/HAD assessment, we include two sectoral-based WaSSI indices to address the stresses due to agricultural water use and hydropower generation as follows:

$$WaSSI_{AG} = \frac{WC_{AG}}{WS_{SW}} = \frac{ET_c}{R_{dam}} \qquad \text{(Equation 3)}$$

$$WaSSI_{HP} = \frac{R_{turbine|HP}}{R_{dam}} \qquad \text{(Equation 4)}$$

Here WC_{AG} is the irrigation water consumption calculated using the SEBAL model (ET_c) as explained in the (3.2), WS_{SW} is the surface water supply which is set equal to the total reservoir release (R_{dam}) (i.e., summation of both turbine and spillway discharges, while accounting for downstream environmental flow). $R_{turbine}$ is the turbine flow required for hydropower production (HP) based on downstream electricity demand. $R_{turbine}$ (in m^3/sec) is calculated using the following equation:

$$R_{turbine} = \frac{HP}{\eta \gamma h} \qquad \text{(Equation 5)}$$

where HP is the hydropower production (watt), η is the power plant efficiency, γ (N/m^3) is the specific weight of water, and h (m) is the effective head of water (m) calculated as the height between open water surface elevation and turbine elevation.

4.3.4 WaSSI-Based Optimal Reservoir Operation

To infer an optimal operating policy of the reservoirs under study (GERD and HAD), a deterministic dynamic programming (DDP) approach is followed. The DDP approach was originally developed by Karamouz and Houck (1982) and modified here to optimize the dam operation using the WaSSI index. A penalty function is first assumed to decide the range of acceptable dam releases (or the safe zone). Beyond this range, an increase in release may result in flooding downstream of the dam, while reduction in release will cause drought conditions with water shortage for downstream demands (Figure 4.4). Similar to Karamouz and Houck (1982), a piecewise exponential form of the penalty function ($P(R_t)$) is used as follows:

$$P(R_t) = \begin{cases} A\left[exp\left(\frac{R_t}{R_{max}}\right) - exp\,(1)\right] & R_t \geq R_{max} \\ 0 & R_{min} \leq R_t \leq R_{max} \\ B\left[exp\left(-\frac{R_t}{R_{min}}\right) - exp\,(-1)\right] & R_t \leq R_{min} \end{cases} \qquad \text{(Equation 6)}$$

where R_t is the dam release at a time step (t), R_{max} is the maximum dam release or the upper limit of the safe zone, and R_{min}, is the minimum dam release or the lower limit of the safe zone. A and B are two constants that are defined based on how much damage will occur downstream the dam when the release is outside the safe zone. We here applied the same values used by Karamouz and Houck (1982) ($A=3.88\times10^5$ and $B=1.58\times10^6$) such that the penalty function would result in losses equal to 10^6 units when the release is zero or twice the mean annual flow (when assuming R_{max} is 120% of the mean annual flow). Applying DDP optimization approach, we used a set of discrete finite horizon of water levels (or storage volumes) with 0.01 m increments to derive monthly dam releases and the corresponding losses (from equation 6). The safe range of water levels is defined as the zone with any release within the minimum and maximum dam release, i.e., zero penalty function (Figure 4.4). The minimum and maximum HAD releases are set to 1.8

and 8.1 km^3/month, respectively based on the historical dam operation (Moussa et al. 2018). The optimal reservoir operation is then derived such that the total losses over a time horizon (T=37 years of simulation) are minimized within the safe zone. An additional constraint is also added to find the release inside the safe zone that would ensure same or less than a defined WaSSI level. Figure 4.4 shows a schematic of the penalty function integrated with the WaSSI stress to find the optimal reservoir release. The agriculture-based stress ($WaSSI_{AG}$) is prioritized in our optimization since the hydropower can be a by-product of the dam release for irrigation (i.e., $WaSSI_{HP} \leq 1$). In case when the dam release is not enough to produce the target hydropower (i.e., $WaSSI_{HP} > 1$), the DDP method keeps searching for release in the safe zone that would fulfill the hydropower demand (which in turn reduces the downstream $WaSSI_{AG}$).

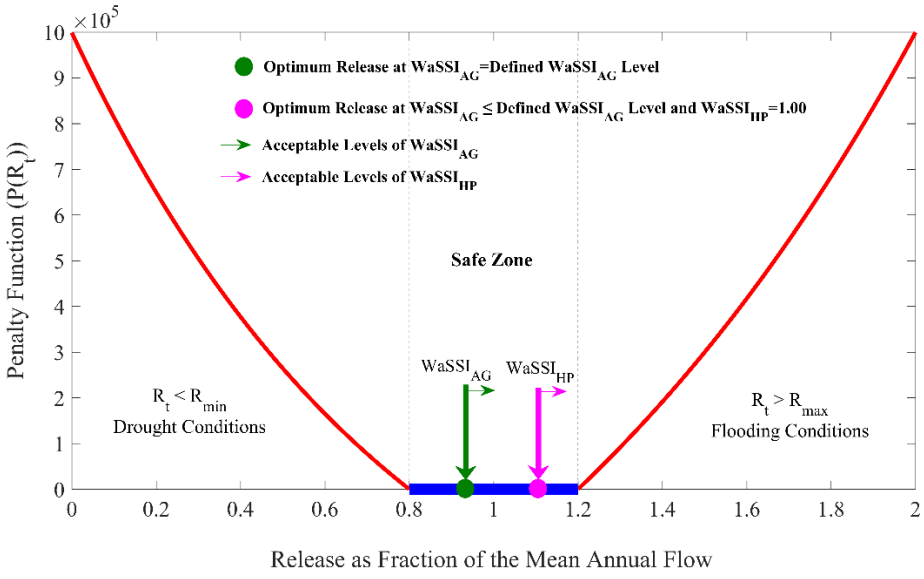

Figure 4.4. Illustration of the Discrete Dynamic Programming (DDP) method based on the WaSSI stress index.

4.4 Results

4.4.1 Status Quo Stresses Downstream of HAD

Understanding the status quo stresses on the water system downstream of HAD is a key step to further explore the impacts of upstream dams on HAD operation. The stresses include the use by different demand sectors, e.g., irrigation, industrial, and municipal sectors. However, since agriculture represents 86% of the water use downstream HAD, we focused our stress analysis on consumptive water use for irrigation. The irrigation water use in Egypt varies during three crop seasons: 1) the winter season starts from October to December and ends between April and June (main crops are wheat, clover, barley); 2) the summer crops from March to June and harvested from August to November (main crops are cotton, rice, maize, and sorghum); and 3) Nili season which is a delayed summer season between July and August (main crops are rice, and sorghum). Table 4.3 shows the cropped area of the agricultural seasons over three regions downstream of the HAD (upper, middle, and lower Egypt) as provided by the statistics released by the Ministry of Agriculture and Land Reclamation (MALR 2014). High density of cropped areas are located in the Nile Delta in northern Egypt, where most of the water intensive crops are grown (e.g., rice and wheat). The percentage of cropped area in the Nile delta ranges between 62% in the winter to 65% in the summer to 46% in the Nili season. The HAD releases serve a total cropped areas of 26,898 km^2 and 26,538 km^2 in the winter and summer seasons, respectively. Only 5% of the cropped area in Egypt are outside the Nile valley in the frontier governorates, which are mainly irrigated by groundwater from the Nubian Sandstone Aquifer System, e.g., Matruh and New valley or rainfall, e.g., Sinai. The Nili crops cover smaller areas mostly in Middle Egypt (783 km^2), and dominated by growing of Maize.

Table 4.3. Cropping areas* (km^2) and the most dominant crops in the three regions (upper, middle, and lower Egypt) downstream of the High Aswan Dam (the three regions are delineated in Figure 4.1).

Season	Lower Egypt (Nile Delta)	Middle Egypt	Upper Egypt
Winter	17,630 (Wheat-Clover)	5445 (Wheat-Clover)	3823 (Wheat-Clover)
Summer	17,566 (Rice-Maize)	4524 (Maize-Sorgham)	4448 (Maize-Sugarcane)
Nili	896 (Maize-Corn)	783 (Maize-Vegetables)	118 (Maize-Corn)

*Data are available at the Ministry of Agriculture and Land Reclamation database (MALR 2014).

The characterization of the cropping pattern downstream of the HAD is crucial to understanding the seasonal and spatial variations in crop water requirements. Figure 4.5a shows the monthly evapotranspiration, as estimated by SEBAL, downstream of the HAD (calculated as the summation of ET_c over the governorates in upper, middle, and lower Egypt). The total annual water use of irrigation in Egypt ranges between 36.5 km^3 in 2015 and 43.4 km^3 in 2014 (average ET_c over the 4 years 2014-2017= 40.3 km^3). The ET_c in Egypt features a bimodal pattern with two peaks in March and August with an average of 4.2 km^3 and 4.5 km^3, respectively. In terms of spatial variations (Figure not shown), the Nile Delta (lower Egypt region) has the highest annual water use, due to the growing of highly water intensive crops, e.g., wheat in winter and rice in summer (Table 4.3). For example, the annual water consumption by irrigation in Behera governorate is 5.4 km^3 which constitutes about 13.5% of the total irrigation water in Egypt.

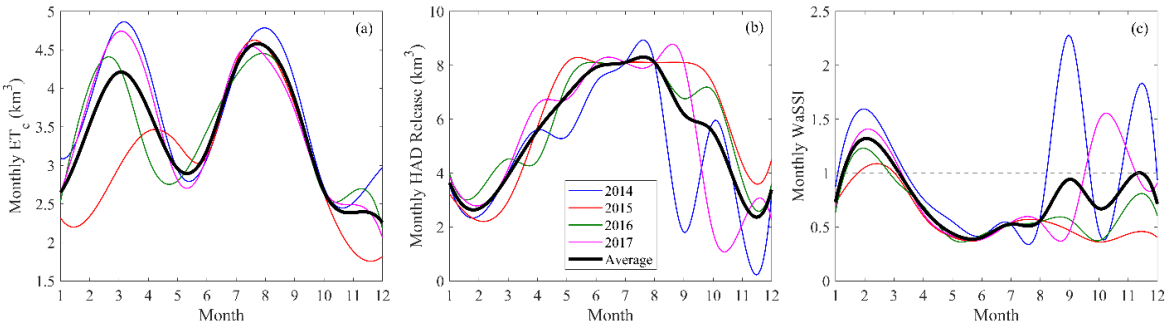

Figure 4.5. Satellite-based estimates of the monthly evapotranspiration (SEBAL), HAD releases (Eldardiry and Hossain 2019), and water stress index WaSSI downstream of the HAD dam for the most recent years of the simulation period (2014-2017).

The HAD releases for the recent years (2014-2017) are derived based on the satellite-based framework developed by Eldardiry and Hossain (2019) to monitor the HAD operation (Figure 4.5b). The operation of HAD for irrigation purposes is determined based on seasonal plan (prepared by the MALR) of downstream irrigation requirements (Gouda 2016). Most of the water released from HAD are directed downstream to Nile Delta where most of the cropped lands are located (with an average total annual release of 65 km^3). Combining the information on water use (from SEBAL ETc) and water supply (from HAD releases), we calculated the annual and monthly stress index ($WaSSI_{AG}$) downstream of the HAD. The annual stresses indicate stress levels less than one (i.e., HAD releases are sufficient to meet downstream agricultural demands), with an average stress of 0.63 (the highest $WaSSI_{AG}$ =0.76 in 2014). Looking closer at monthly scale (Figure 4.5c) portrays a better understanding of the seasonal variations in the stress. While the stresses are exacerbated in the winter months with average stresses exceeding one in February (average $WaSSI_{AG}$=1.32), lower stress levels are noticed in the summer months (e.g., average $WaSSI_{AG}$=0.40 in June). The seasonal discrepancy in the monthly stresses is attributed to the low (or high) flows released in the winter (or summer) months (Figure 4.5b). During the

winter months, insufficient supply of HAD releases is encountered by relying on rainfall, as the case in northern regions (e.g., Alexandria, Behera, and Kafr El-Sheikh governorates), or by pumping groundwater. In addition, the stress variation across months highlights the opportunities to derive better operating rules for HAD by managing the downstream stresses, especially in years when inflow is expected to be reduced by GERD filling.

4.4.2 HAD under Filling Scenarios of GERD

The GERD reservoir is considered completely filled when the reservoir storage reaches its maximum capacity of 74 km^3. Not surprisingly, as the number of filling years increases, the GERD release becomes less sensitive to the filling duration (Figure 4.6). For instance, the difference in the median GERD release between the 7- and 6- year filling scenario is 1.5 km^3 compared to 6.5 km^3 difference between the 3- and 4- year filling scenarios. The results agree to great extent with Wheeler et al. (2016) who followed a more cooperative scenario that assumes an agreed annual release for filling the GERD. For example, if the downstream countries agreed to an annual release of 35 km^3, Wheeler et al. (2016) found that it would take an average of 6 years to fill the dam. Similar results can be inferred from Figure 4.6 for a 6-year scenario that corresponds to a median GERD release of 35.32 km^3. The annual assessment of GERD filling indicates that downstream flow can be highly affected by short filling periods with more than 30% of reduction in Blue Nile inflow with filling scenarios of less than six years. With longer periods of filling (> 6 years), smaller differences are noticed between the GERD release and thus lesser impacts on downstream flow.

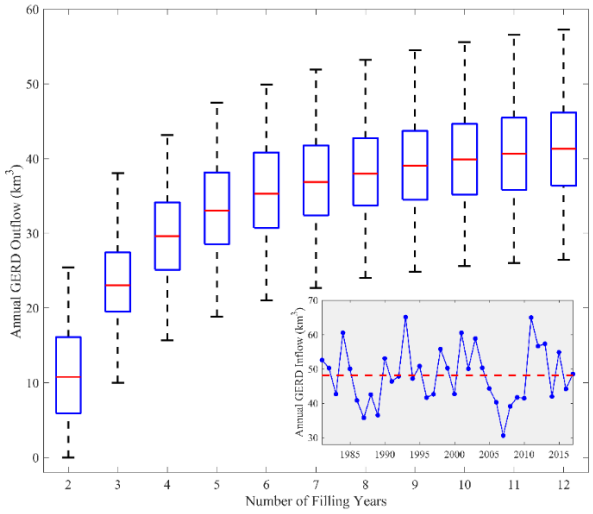

Figure 4.6. The annual GERD outflow during different scenarios of GERD filling (2- through 12- year filling scenarios). The inset shows the historical (1981-2017) annual GERD inflow, i.e., naturalized flow (the red dashed line indicates the median streamflow).

The GERD releases during the filling scenarios are routed downstream to Khartoum station and then added to the flow from the White Nile and Atbara river to form the total inflow into HAD. Figure 4.7 shows the changes in HAD water level when considering the 3- and 7-year GERD filling scenarios, which represent two examples of fast- and slow-paced filling proposals, respectively. The HAD water level is calculated under two different scenarios of downstream $WaSSI_{AG}$ stress level; first, we consider the status-quo conditions that resulted from our analysis in section (4.1). Second, we assumed a predefined constant $WaSSI_{AG}$ levels throughout the year (only $WaSSI_{AG}$ =0.70 is shown in Figure 4.7). The predefined $WaSSI_{AG}$ level represent an adaptation scenario by HAD operators to the impacts of GERD filling. For example, the stress level of 0.70 will result in lower stresses in the winter months, which means either less cropping areas or finding alternative resources like groundwater or precipitation. Conversely, the stress will be elevated in the summer season (e.g., $WaSSI_{AG}$ in June will change from 0.40 to 0.70),

which means storing more water in the HAD reservoir. The irrigation demand downstream of HAD is assumed the same during the filling period using the monthly average of SEBAL ET estimates shown in Figure 4.5a. The changes in HAD operation under different scenarios are explained using the slope of a linear regression fitting to the water level signals during the filling period.

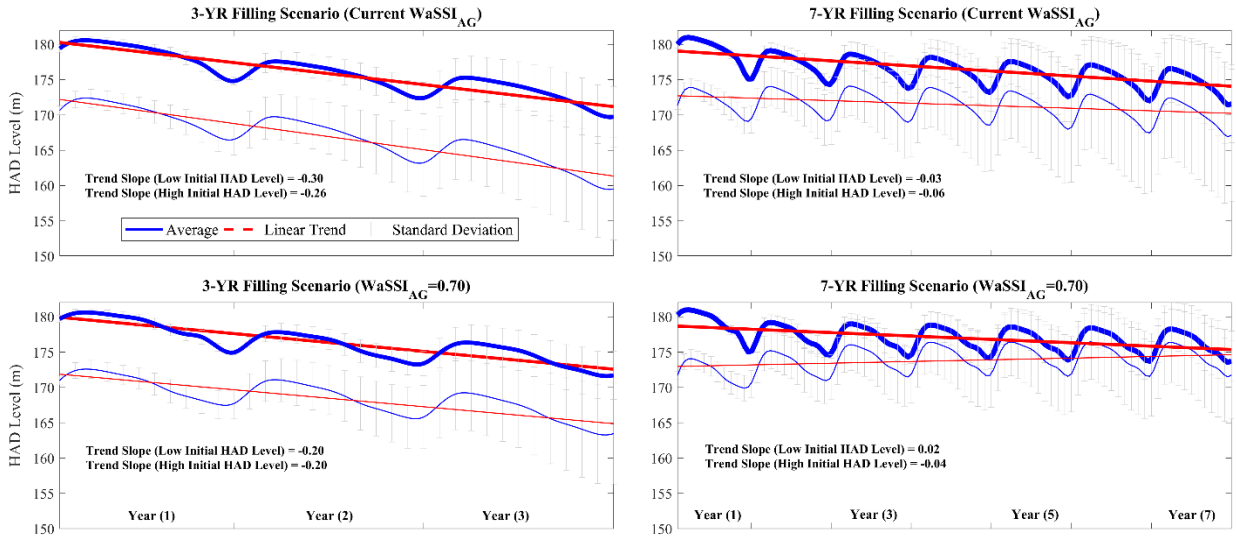

Figure 4.7. The HAD water level (m) under the 3- and 7- year GERD filling scenarios with different levels of stress index WaSSI (current stress levels vs predefined stress level= 0.70). The thick and thin lines indicate the high and low initial HAD storage levels, respectively.

Figure 4.7 shows a significant drop in the HAD level when assuming a 3-year filling scenario, with more reduction in HAD storage if Egypt adopts the current stresses downstream of HAD (compared to a predefined $WaSSI_{AG}$=0.70). A linear decreasing trend of (-0.30 m/month) is noticed in HAD level when employing the current $WaSSI_{AG}$ levels and assuming a scenario of low starting level at HAD reservoir. This trend can be alleviated by about 33% (slope=-0.20) if considering HAD will release less water to maintain a constant $WaSSI_{AG}$ level of 0.70. Similarly, a smaller decreasing trend (-0.14) is noticed when elevating the stress level to 0.70 for only

months with $WaSSI_{AG}$<0.6 (May through August), while keeping the other months at the current levels (Figure not shown).

A flatter pattern is noticed for 7-year filling scenario with negligible trends (trend slope = -0.03 and 0.02 for current stresses and $WaSSI_{AG}$ =0.70, respectively). Figure 4.7 also shows how HAD can operate if GERD filling starts when HAD is at high storage conditions, i.e., above the normal operation level (175 m), as the case noticed recently in July 2018 (HAD level is at 176.77 m) and 2019 (HAD level is at 178.37 m). While the trend slope is still negative when assuming high initial HAD level scenario, the impacts on HAD operation are reduced with relatively high storage levels during GERD filling years. The HAD level at the end of the GERD filling period can be elevated by considering higher downstream stresses and/or longer GERD filling period (e.g., HAD level will reach 173.76 m with $WaSSI_{AG}$=0.70 and 7-year filling period). Table 4.4 summarizes the scenarios in Figure 4.7 and the corresponding changes in trend slope and HAD level (at the end of the filling period).

Table 4.4. Summary of the trend slope and HAD level (at the end of filling period) under different scenarios of GERD filling, initial HAD storage level, and downstream stress condition.

GERD Filling	Downstream Stress Conditions	Initial HAD Storage Level	Trend Slope	HAD Level* (m)
3-Year Filling Scenario	Non-Adaptive Approach (Current $WaSSI_{AG}$)	Low	-0.30	159.52 (±7.23)
		High	-0.26	169.73 (±4.31)
	Adaptive Approach ($WaSSI_{AG}$=0.70)	Low	-0.20	163.47 (±7.15)
		High	-0.20	171.73 (±3.42)
7-Year Filling Scenario	Non-Adaptive Approach (Current $WaSSI_{AG}$)	Low	-0.03	167.13 (±9.36)
		High	-0.06	171.57 (±5.51)
	Adaptive Approach ($WaSSI_{AG}$=0.70)	Low	0.02	171.75 (±6.22)
		High	-0.04	173.76 (±2.90)

* Average (± standard deviation) HAD level at the end of GERD filling period

The improvement in the HAD storage levels when adapting its downstream stress is primarily attributed to the increase in the stress level during the rainy season in the BNB (June to September). While the current HAD operation indicates higher releases during this rainy season, coping with future challenges requires revisiting the operating curve. For instance, our stress-based analysis suggests elevating the stress during the summer months, i.e., store more and release less. This approach will secure enough water during the low flow months while preserving the power generation production of the dam. The effect of streamflow variability is indicated with the standard deviation bars in Figure 4.7. The higher variability was noticed in later years due to the use of a fixed initial HAD water level, i.e., 169.32 (178.37m) for low (high) storage conditions, which resulted in narrower HAD storage options in the safe zone of DDP optimization (Figure 4.4). As the filling progresses, the safe zone of optimization becomes wider and therefore the HAD level becomes more sensitive to inflow variability.

The combined effects of the GERD filling scenarios, HAD initial storage level, and downstream $WaSSI_{AG}$ stress condition on HAD operation is summarized by plotting the HAD level at the end of the filling period under different stress conditions vs years of GERD filling (Figure not shown). The current average HAD level in July (174.47 m; averaged for the 10 years 2011-2020) can be reached when setting downstream stress level to 0.80 and assuming GERD to be filled in more than 8 years. When considering GERD filling scenario with high initial HAD level and $WaSSI_{AG}$ of 0.80, the HAD can reach its target operating level if GERD follows a filling scenario of more than 5 years. As the stress level is relieved to smaller levels (e.g., current stress conditions or $WaSSI_{AG}$=0.60), longer periods (more than 12 years) will be required to secure the target HAD operation.

To further explain the impacts of streamflow variability (i.e., dry and wet years) on the HAD level, Figure 4.8 shows the cumulative probability of the HAD level at the end of the 3- and 7-year filling scenarios. Lower HAD levels are noticed under the current $WaSSI_{AG}$ levels or when setting $WaSSI_{AG}$=0.70 with the chance of reaching the minimum operating level of 147 m. For example, the HAD level has a probability of 1% to reach 147 m in case of 3-year GERD filling scenario and applying the current stress levels downstream of HAD (Figure 4.8a). Below this elevation (147 m AMSL) is the HAD dead storage and therefore, HAD cannot operate to meet downstream water demand. Wheeler et al. (2016) concluded a similar probability range (1~2 %) when drought management policy was implemented at HAD. Assuming a low initial HAD storage when GERD starts filling, the median HAD level varies across the different scenarios from 168.14 m (for 3-year filling and current stress levels) to 174.72 m (for 7-year filling and $WaSSI_{AG}$=0.70). A more optimistic picture of the HAD levels can be demonstrated by the maximum HAD levels that can go up to more than 175 m AMSL (HAD normal operating level) when assuming a high initial storage HAD levels at different filling scenarios (Figure 4.8b). The range of HAD levels shows the importance of considering the streamflow variability when assessing the operation of HAD during the filling of upstream dams.

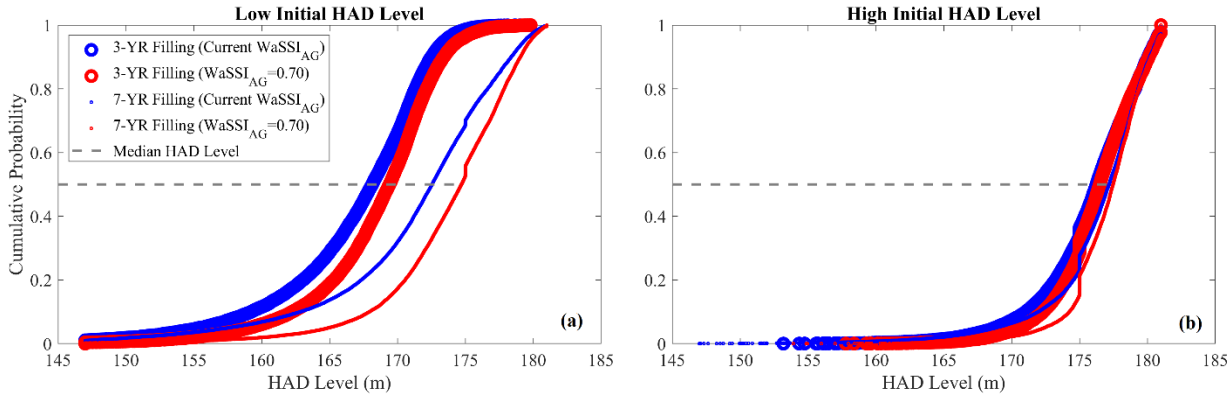

Figure 4.8. The cumulative probability of HAD water level under different GERD filling scenarios and stress levels ($WaSSI_{AG}$) (pooling all monthly water levels during GERD filling scenario into one sample).

It is important to adapt HAD operation to expected reduction in inflow (during GERD filling) . The approach we followed in our paper is to tweak the downstream stress so that the water system becomes more stressed during the summer months instead of the status quo low stress conditions. As the stress is elevated, HAD has to be operated in a way that stores more water compared to current conditions (Figure 4.9a). For example, in a 3-year GERD filling scenario, a stress level of 0.70 will store 7.9 km^3 in August (release=6.5 km^3) compared to 6.4 km^3 (release=8.08 km^3) when adopting the current stress levels. Despite assuming the same downstream $WaSSI_{AG}$, differences in the HAD releases between 3-year and 7-year filling is due to the effect of hydropower optimization ($WaSSI_{HP}$). As a result, the release is more controlled by hydropower production in some months (e.g., October through January) and therefore lower HAD levels will require releasing more water in case of 3-year filling. Similarly for a 7-year filling scenario, as HAD level is higher (compared to 3-year filling), less water will be released to attain the same hydropower stress $WaSSI_{HP}$.

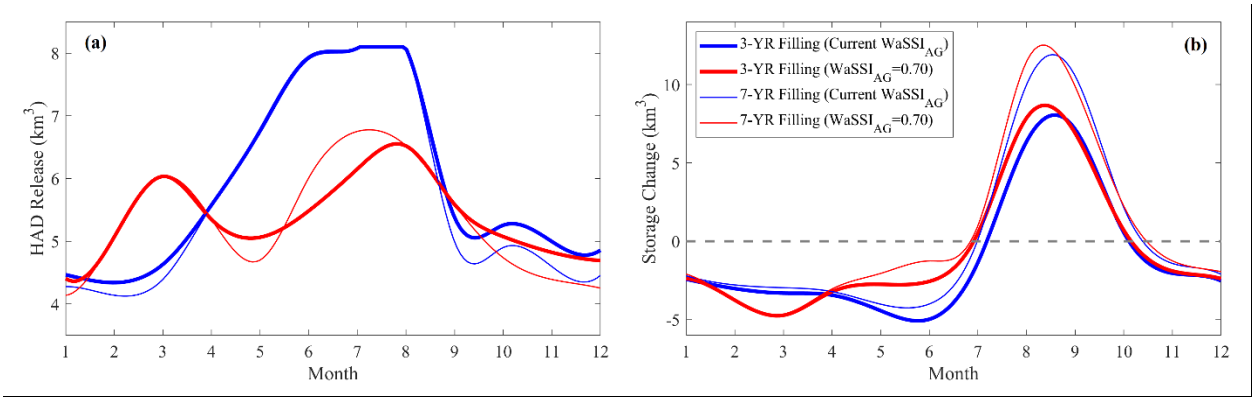

Figure 4.9. HAD releases (a) and storage change (b) during the 3- and 7-year GERD filling scenarios (showing only the average of the hydrological sequences developed for each filling scenario and assuming an initial HAD storage at low level).

4.4.3 GERD Operation (Post-filling Phase)

GERD dam is primarily constructed to produce hydropower electricity for Ethiopia and neighboring African countries. However, the operating rule for the GERD dam is not published and it is under a high level of negotiations between the three countries: Egypt, Sudan, and Ethiopia. A non-cooperative operation scenario (from the Ethiopian perspective) would only consider the optimization of the reservoir operation to maximize hydropower generation (given the dam location at the Ethiopian-Sudanese border). Following the optimization scheme explained in section (3.4.2), GERD operation was derived to maximize hydropower generation. Additional constraints were added to the DDP problem by setting limits on storage capacity (or GERD levels), and minimum and maximum outflows, i.e., R_{min} and R_{max} in equation 6 (assumed to be equal to 0.80 and 1.20 of the mean annual inflow, respectively). Different hydrologic variables of the GERD reservoir operation are shown in Figure 4.10. As expected, the derived GERD water levels are minimum in May before the rainy season (June through September) when the reservoir is being emptied (negative storage change in Figure 4.9d) to be able to store the flow in the rainy season (Figure 4.10a). The GERD reaches its maximum level in September (at the end of the rainy season) with an average equals to 636.96 m and standard deviation of 2.64 m. The average annual GERD outflow is about 48 km^3 with the highest releases (5.56 km^3) and storage change (9.17 km^3) in September and August, respectively.

As indicated in Figure 4.10a, the GERD will significantly regulate the downstream flow, with higher regulation during the non-rainy season, when the regulated flow is much higher than

the naturalized flow. To quantify the regulation in the GERD outflow, we used a regulation factor (RF) to evaluate the change in the naturalized flow (GERD inflow) after GERD operation. The RF is calculated as follows (Zhou et al. 2018):

$$RF = \frac{CV_{nat}}{CV_{reg}} \qquad \text{(Equation 7)}$$

Here CV_{nat} and CV_{reg} are the coefficients of variation (i.e., ratio of the standard deviation to the mean) of the monthly natural and regulated flow in the operation period, respectively. Three months (April, May, and September) have RF less than one, which indicates that regulation by reservoir has limited impact on reducing the monthly variations in natural flow of the Blue Nile (downstream of GERD). The highest regulation of streamflow is noticed from November through February with regulation factor ranges from 6.6 (in November) and 4.03 (in January), respectively. While the downstream flow is expected to reduce in the summer months (rainy season), the higher regulation in winter months balances such reduction by increasing GERD releases. These results agree with the percentage of GERD release estimated by Mulat and Moges (2014) who concluded that the minimum percentage released from GERD is within the wet months (July through October).

In terms of monthly streamflow variability, the months from June through November, which include mostly the rainy season in the BNB, experience reduction in monthly standard deviation with the largest decrease in August (69%) followed by October (58%). On the contrary, the months from December through May have significant increase in the monthly standard deviation of downstream flow (the largest increase is in January with percentage change of 338%). The high variability in the GERD release in September is attributed to the assumption of the dam being operated at Full Supply Level (FSL) of 640 m (e.g., Mulat and Moges 2014;

MIT 2014; Wheeler et al. 2016). The FSL of 640 m does not yield enough storage capacity for the dam (i.e., 74 km^3), especially during wet years when higher flows come in August and September. The GERD storage change peaks in August (average storage change=9.17 km^3); however, the dam fails to store enough of the inflow in September, and therefore, resulted in wider range of releases. This excess flow in wet years can also be released through the dam spillways, which would result in lower variations in September. The GERD operation was also tested for a higher FSL of 650 m (Figure not shown) and it yields a consistent variability throughout the year. For instance, the average monthly standard deviation dropped from 0.87 km^3 to 0.73 km^3 when changing the FSL from 640 to 650 m (compared to 1.14 km^3 for the naturalized GERD inflow, i.e., without imposing the dam effect). The change in variability is affected by more regulation in the reservoir releases when assuming a FSL of 650 m. A higher FSL allows more outflows in the spring (months before the rainy season) and therefore the reservoir has a buffer to store more water in September. For example, the mean GERD release in September changes from 5.56±2.39 km^3/month (FSL=640 m) to 4.74±0.75 km^3/month (FSL=650 m).

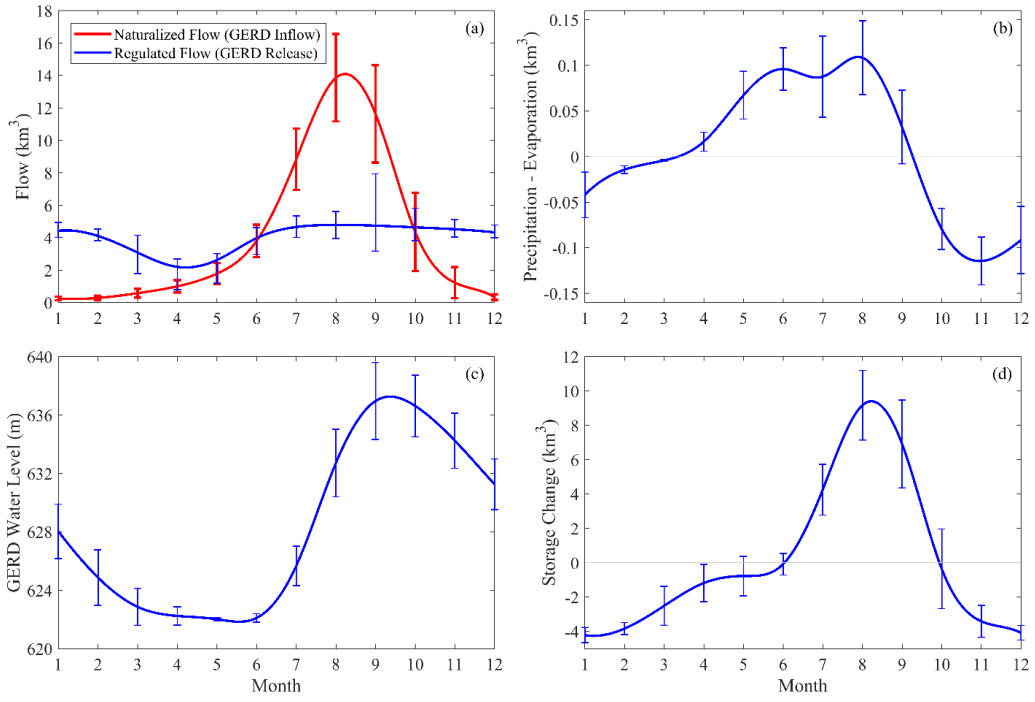

Figure 4.10. Different hydrologic variables (inflow, precipitation-evaporation, water level, and storage change) during the GERD operation phase (FSL=640 m AMSL).

4.4.4 HAD during GERD Operation

The HAD level at the end of the GERD filling period will drop down in most of the filling scenarios, e.g., the average HAD level at the end of the 3-year filling scenario is 159.52 m (169.72 m) when assuming low (high) HAD initial level scenario and adopting the current downstream stresses (Figure 4.7). Thereby, there will be a recovery period for HAD to get back to its normal operation levels. Figure 4.11 shows an illustrative example of how long it would take the HAD after the GERD filling to operate normally. Here, we considered HAD reaches its normal operation in the year when HAD level in September reaches at least 175 m (HAD normal operating level). In addition to the effect of HAD starting level, we accounted for streamflow variability and the possibility of the filling period to end in wet or dry years by considering: 1) the HAD level at the end of the GERD filling at normal, dry, and wet conditions (defined as

average HAD level ± Standard deviation) and 2) considering the GERD starting year of operation in different climatic conditions using a sliding window of one year in a 10-year period from 1981 through 1990 (these 10 years are selected as they include both wet (1984) and dry years (1986 to 1989)). Figure 4.12 summarizes the range of HAD recovery years under different GERD filling scenarios and considering the impacts of streamflow variability on GERD/HAD operation. When applying the current levels of downstream stresses and after a 3-year filling scenario, the HAD will, on average, recover after 7 years (assuming a low initial storage level at HAD; Figure 4.12a). If the water level at HAD is at a higher level (e.g., as the case of 2019 when HAD level reaches 178.37 m in July) when GERD starts filling (3-year filling scenario), the recovery period can be shortened significantly to only 3 years (Figure 4.12c).

Similar to considering adaptation to downstream stress, recovery years also decrease when extending the filling period. For example, if considering a downstream $WaSSI_{AG}$ of 0.70 with a 7-year filling scenario, the recovery period can drop down to 2 years (compared to 3 years when assuming current stress levels downstream with a low initial level at HAD). Additionally, if HAD operators prepare in advance to GERD filling (scenarios of more than 9 years) by maintaining a high storage level and adapting the operation to a downstream stress level $WaSSI_{AG}$ of 0.70, HAD can operate normally immediately after filling the GERD without a recovery period (Figure 4.12d). Furthermore, as indicated by the range of the boxplot, streamflow variability in the Nile tributaries (Blue Nile, White Nile, and Atbara) is a crucial factor to the HAD recovery period with longer ranges for short filling scenarios and low HAD initial level. For instance, in case of dry years, HAD can take more than 30 years (or 20 years if HAD is at high initial level) to recover from a 3-year filling scenario. The HAD recovery period highlights the connection between the GERD filling and the time HAD would take to refill its

storage to a normal operation level. The results showed that the GERD filling period cannot offset the HAD recovery period, i.e., short filling will recover in a longer period but with similar overall time when compared to longer filling period with shorter recovery. This longer HAD recovery for the 3-year filling scenario arises from the larger storage volume (larger than GERD storage; 74 km^3) required to recover to its normal operation (175 m) and the less inflow reaching downstream after GERD operation.

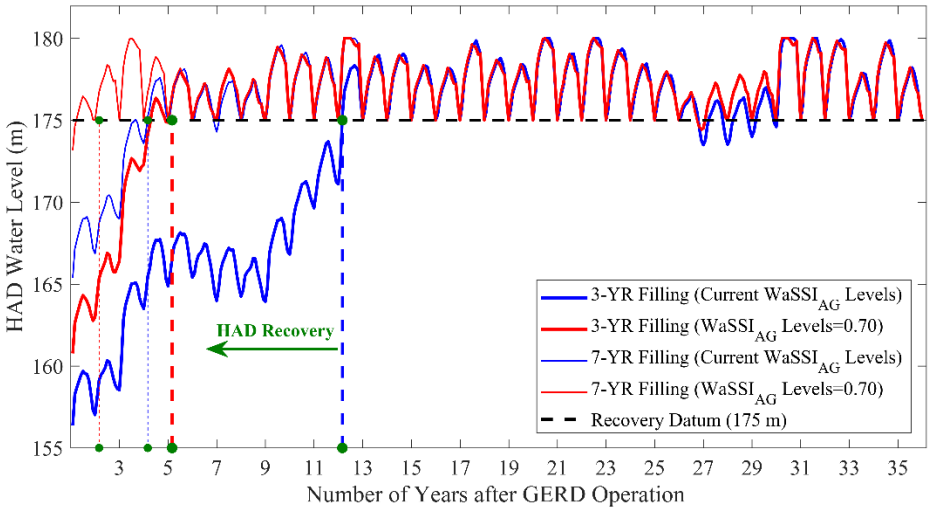

Figure 4.11. Illustrative example of the HAD level recovery during the GERD operation after 3- and 7-year filling scenarios. The recovery period ends when HAD reaches its normal operation level (175) in September.

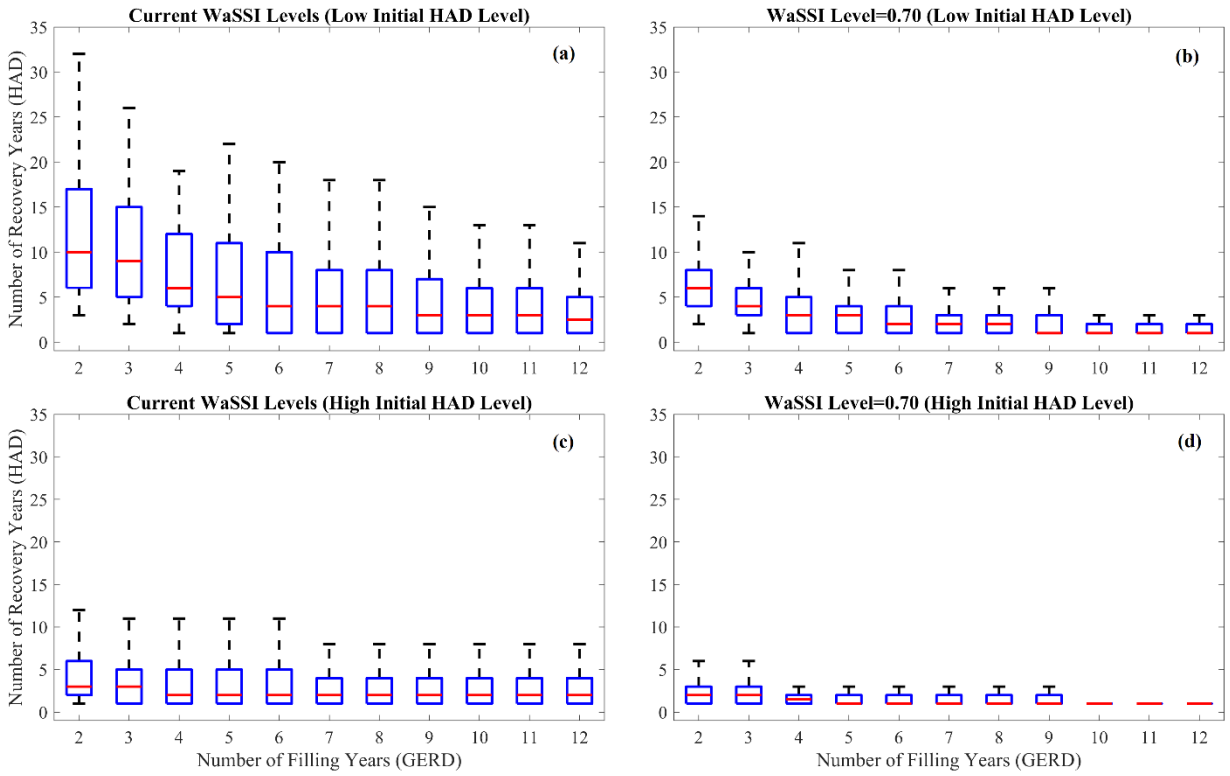

Figure 4.12. The range of HAD recovery years under different GERD filling scenarios when assuming (a & c) current stress levels and (b & d) a predefined stress level ($WaSSI_{AG}$=0.70). The upper and lower panels represent the scenarios of low and high initial HAD storage level, respectively.

Figure 4.13 shows the changes in HAD operation after filling GERD considering both the recovery period of HAD and when reaching its normal operating level (only the results for the 3-year filling scenario with current stress conditions are shown in Figure 4.13). The HAD operation was also compared to the historical HAD operation using a water balance model over the HAD reservoir with inputs from the satellite-based modeling developed by Eldardiry and Hossain (2019). As explained in the GERD operation (Figure 4.10a), the Blue Nile flow downstream of GERD becomes more regulated and therefore alters the HAD inflow hydrograph. Compared to the historical maximum HAD inflow, higher inflows (with more than 3 km^3/month)

are expected during the winter months (December through February). During the GERD storage months (or BNB rainy season; June through September), the HAD inflow is expected to drop with maximum reduction in August (-7.6 km^3/month and -1.40 km^3/month compared to historical average and minimum HAD inflow, respectively). The increase in winter months downstream flow (GERD outflow) maybe favored by Egypt as it will reduce losses due to evaporation in Lake Nasser at HAD dam. However, as indicated in Figure 4.13b, reduction in annual evaporation can be significant only during the recovery period of HAD, i.e., when the HAD storage is below its normal levels. The annual evaporation losses are expected to decrease during the recovery period in a range between 11% (current stresses) and 7% ($WaSSI_{AG}$=0.70) when operating after 3-year GERD filling scenario.

During HAD recovery from a 3-year filling scenario, HAD level will significantly drop down with a monthly average of 170.9 m (Figure 4.13c) compared to an average historical HAD level of monthly average that equals to 175.6 m (about 4.7 m difference). The HAD levels above the historical minimum levels is noticed in all months (with an average of 1.3 m) except for October through December, where still the HAD operation is below the minimum historical levels. These months follow the rainy season in Ethiopia, and therefore this difference reveals the failure of the HAD to recover from the inflow deficit during the summer months where most of the water is stored in GERD. Adopting a higher stress level of 0.70 (Figure not shown) will elevate the water levels in the HAD since we allow for more stressed system downstream. Higher HAD storage levels is noticed for most of the year after the recovery period compared to historical average levels, which reflects an advantage of flow regulation by GERD operation (i.e., higher releases in the winter months). However, it is worth noting that reaching such higher levels will only be achieved after the recovery period, which is driven by the initial HAD storage

level, GERD filling scenario and the streamflow variability. Similarly, comparing the difference between the average monthly storage change of HAD (during GERD operation vs historical average), September and July experience the largest difference with a reduction of -6.5 km^3/month and -3.9 km^3/month, respectively. The results of HAD operation underscores the existence of potential seasons where Egypt can employ more sustainable strategies to better manage the water especially in the months following the BNB rainy season.

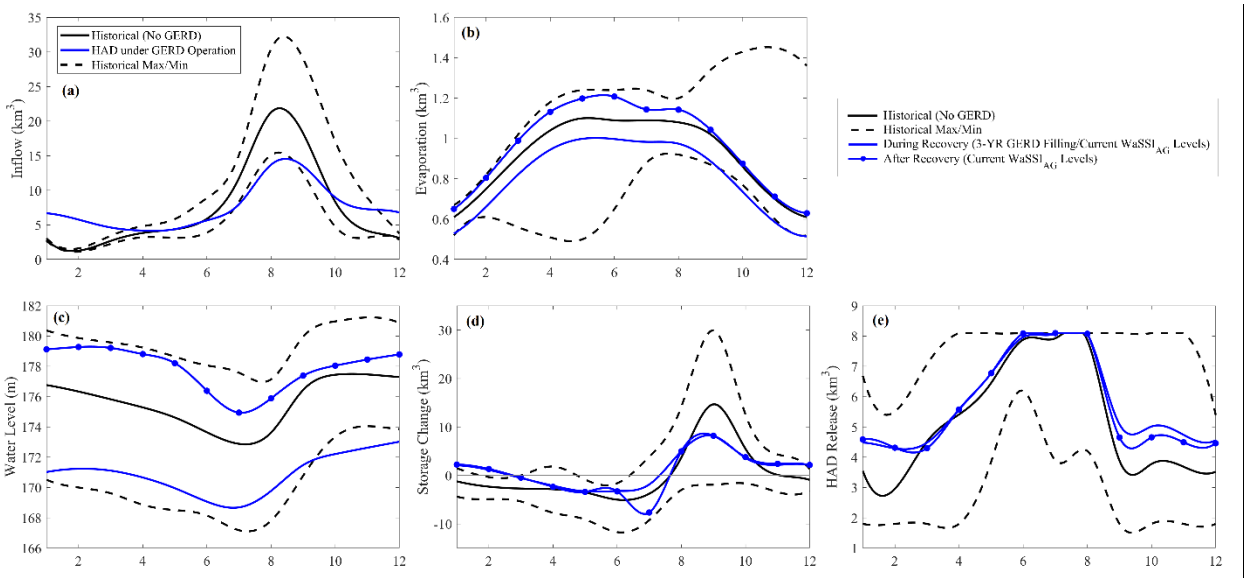

Figure 4.13. Different hydrologic variables (inflow, evaporation, water level, storage change, and release) of the HAD operation during the GERD operation phase.

4.6 Conclusion

The blueprint presented in our study explores the opportunities to adapt the operation of existing dams under the combined impacts of filling/operation of upstream planned dams and water demand in the downstream. Using the HAD-GERD dams as a typical paradigm of large hydropower dams (existing and planned) in a transboundary basin, we examined the impacts of different GERD scenarios on HAD operation. Our key findings can be summarized as follows:

1. The status quo stresses downstream of the HAD reveals a highly stressed system (average $WaSSI_{AG}$ = 0.95) in winter months (November through March) due to water being used for irrigation with less releases from the HAD. The summer months (May through August) experience low stresses with an average of 0.50 when HAD empties its storage to prepare for the Blue Nile rainy season. The seasonal differences in the stresses downstream of the HAD reinforce the importance of considering opportunities to revisit the HAD operation in the summer months to mitigate the expected reduction in water supply during the GERD filling/operation phases.
2. The HAD dam will undergo different operational modes during the filling and operational phases of GERD. The filling scenarios of the GERD dam indicated a smaller impacts on downstream outflow when following a slower filling scenario or by keeping HAD storage at high level prior to GERD filling. A 3-year filling scenario can lead to a significant declining trend in HAD water levels that would be slightly improved if higher stress level ($WaSSI_{AG}$=0.70) are adopted in the summer months. On the other hand following a slower filling scenario, e.g., more than 7-year filling scenario, would lead to an average stabilized HAD levels.
3. The GERD operation will regulate the flow in the Blue Nile and therefore less intra-annual variability in the HAD inflow. When the GERD starts its operation (post-filling phase), the HAD will experience a recovery period to restore its storage to a normal operating level. Such recovery transition will depend on the filling scenario, climate conditions, HAD storage level when GERD starts filling, and the stress level employed downstream of the HAD. Our results concluded that under years of different climate (varies between dry and wet), the HAD would recover to its normal operation after an

average of 7 and 3 years for 3- and 7-year filling scenarios, respectively. This period can significantly drop down if the initial HAD storage is kept at a higher level or by elevating downstream stresses in the summer (e.g., $WaSSI_{AG}$=0.70).

Our study presented a blueprint for the adaptation of HAD to upstream dams under various plausible scenarios, with focus on the GERD dam, currently under construction along the Blue Nile in Ethiopia. The results showed the importance of different decision factors when considering such a transboundary issue. In our analysis, we investigated four factors: GERD filling scenario (or number of years to completely fill the dam to its storage capacity), streamflow variability, HAD initial storage level, and downstream adaptation strategy. Challenges with operating HAD can be alleviated if riparian countries agree upon a coordinated operations of both reservoirs (GERD and HAD). While our analysis considered a unilateral decision for operations, a coordinated approach of operations would help in sharing benefits, particularly during low-flow or high-flow periods (Mulat and Moges 2014; Taye et al. 2016). Whether the GERD will be filled through cooperation or through unilateral determination is a critical factor to consider when deciding an appropriate adaptation strategy.

While Egypt would prefer a slow-paced filling scenario for GERD, e.g., 7 years or more as revealed in our analysis, filling in shorter periods would obviously impact the downstream water use and consequently the operation of HAD. Our results highlighted the opportunities to operate the HAD in a more prudent way that would store more water during the summer, in lieu of historically releasing water during the high flow season (June through September). In addition, preparing in advance for GERD filling by maintaining HAD storage at a high level can significantly mitigate the negative impacts of GERD filling. Such adaptation decisions can also benefit future HAD operation against other upstream dams. Sudan, for instance, has three

planned dams (Shereik, Kajbar, and Dal dams) with a total hydropower capacity of more than 2000 MW. While these dams might operate in the future as only Run-of-the-River hydroelectric systems, HAD has to adapt its operation to expected reduction in the flow reaching downstream, primarily due to evaporation losses in the reservoirs formed by these dams. As demonstrated in our study, a transboundary issue is complicated by the different factors involved in making decision or finding an equitable solution amid riparian countries. While we tested different scenarios of HAD operation, future studies can further explore other decision factors including scenarios for irrigation water use in Sudan and Ethiopia. Thus, a multi-lateral negotiation is a compelling pathway to agree upon various decision factors that would guarantee the development plans of each riparian country.

Our optimal modeling of HAD operation resulted in more HAD releases than what currently released in winter months (from September to March). The higher releases are noticed in both filling and operation phases (Figure 4.9a and Figure 4.13e). This HAD optimal operation indicates that current operation of the dam doesn't exploit the hydropower capacity installed and only hydropower is assumed to be a by-product of the dam release. The lower production of hydropower in HAD is also affirmed by the World Bank statistics, which indicated a drop in the percentage of electricity produced from Hydropower in Egypt from 23.5% in 1990 to only 8% in 2014. This drop is attributed to the increase in power plants fueled by natural gas, which contributes more than 80% of the power generation in Egypt. The decision to optimize the HAD hydropower production or assume a by-product scenario provides another opportunity to HAD operators to control the HAD releases in periods with inflow reduction, as the case during the GERD filling. The integration of hydropower (energy sector) and irrigation (food sector) in our blueprint is important in addressing future challenges facing the Food, Energy, and Water (FEW)

system across transboundary basins, e.g., Nile basin (Al-Saidi et al. 2017; Allam and Eltahir 2019). To further investigate how to adapt the HAD operation to future challenges, the next chapter, Chapter 5, will introduce a Forecast-based Adaptive Reservoir Operation (FARO) approach to explore how HAD can improve its operation by using long-term streamflow forecast.

Chapter 5: The Value of Long-term Streamflow Forecasting in Adaptive Reservoir Operation: The case of High Aswan Dam in the Transboundary Nile River Basin

Note: This chapter has been published mostly in its current form in Journal of Hydrometeorology (Eldardiry and Hossain 2021); **© American Meteorological Society. Used with permission**.

Eldardiry, H., and Hossain, F. (2021). The Value of Long-term Streamflow Forecasts in Adaptive Reservoir Operation: The Case of High Aswan Dam in the Transboundary Nile River Basin. Journal of Hydrometeorology (DOI: https://doi.org/10.1175/JHM-D-20-0241.1).

Abstract

Transboundary river basins are experiencing extensive dam development that challenges future water management, especially for downstream nations. Thus, adapting the operation of existing reservoirs is indispensable to cope with alterations in flow regime. We proposed a Forecast-based Adaptive Reservoir Operation (namely FARO) framework to evaluate the use of long-term monthly forecasts in improving real-time reservoir operations. The FARO approach was applied to the High Aswan Dam (HAD) in the Nile river basin. Monthly precipitation and temperature forecasts at up to 12 months of lead time were used from a suite of eight North American Multimodel Ensemble (NMME) models. The value of NMME-based forecasts to reservoir operations was compared with perfect and climatology-based forecasts over an optimization horizon of 10 years from 1993 to 2002. Our results indicated that the forecast horizon for HAD operation, evaluated using perfect forecasts, ranges between 5- and 12-month lead time at low and high demand scenarios, respectively, beyond which the forecast information no longer improves the release decision. The forecast value to HAD operation is more pronounced in the months following the flooding season (October through December). During these months, the skill of streamflow forecasts using NMME forcings outperforms the

climatology-based forecasts. When considering the operation of upstream Grand Ethiopian Renaissance Dam (GERD), using streamflow forecasts minimally helps to maintain current target objectives of HAD operation and therefore result in higher operation costs as opposed to current conditions without GERD. Our study underlined the importance of deriving a new adaptive operating policy for HAD to improve the value of available forecasts while considering GERD filling and operation phases.

5.1 Introduction

Reservoirs are important water storage infrastructures that can effectively distribute water to serve the demand for hydroelectric energy, irrigation, municipal uses, ecosystem protection, and mitigating floods or droughts (Biemans et al. 2011; Bakken et al. 2016). Meeting such demands becomes more challenging with additional pressures generated by global trends in population growth and competing water demands for food, energy, and water (Brown et al. 2015; Rodell et al. 2018). Hence, maintaining sustainable management of water systems requires further flexibility of reservoir operations to support early actions and decisions. Reservoir operation is determined through a series of decisions over time, based on downstream demands and upstream flow (Labadie 2004). However, making such decisions is governed by the natural uncertainty in the reservoir inflow. Thus, using forecasts of future reservoir inflow can be advantageous to making efficient operating decisions (Ahmadi et al. 2015; Feng et al. 2017; Yang et al. 2020).

Hydrologic forecasts are typically generated via either dynamic, process-based climate models (e.g., Yuan et al. 2015) or ensembles of numerical weather predictions (e.g., Roulin 2007), or via empirical, data-driven models (e.g., Block and Rajagopalan 2007). Both approaches have their limitations, with dynamic models often limited by resolutions and initialization

procedures, while empirical models are constrained by short records and stationarity assumptions (Block and Goddard 2012). This study focused on the use of dynamical forecasts since they can take the underlying physical mechanisms into account, unlike statistical or data-driven models (Candogan Yossef et al. 2017; Woldemeskel et al. 2018). Uncertainties in dynamical forecasts can be reduced through a hybrid approach that benefits from statistical post-processing (Wood and Schaake 2008). However, exploring such a hybrid approach is beyond the scope of our study. In dynamical forecasts, outputs produced by General Circulation Models (GCMs) are typically used as forcing for hydrological models. GCMs outputs are driven by large-scale climate drivers, such as Sea Surface Temperature (SST). Advances in understanding such climate teleconnections have offered a significant improvement in predicting streamflow on a season-ahead and at longer lead times (Hamlet and Lettenmaier 1999; Maurer and Lettenmaier 2004; Georgakakos and Graham 2008).

Skillful streamflow forecasts have proven to be useful for improving reservoir operations (e.g., Hamlet et al. 2002; Nayak et al. 2018; Giuliani et al. 2019; Ahmad and Hossain 2020). Using retrospective streamflow forecasts in operating reservoirs in the Columbia River, Hamlet et al. (2002) showed that long-lead streamflow forecasts can be effectively utilized to obtain increased annual average hydropower. During extreme conditions of droughts and floods, forecasting reservoir inflow informs dam operators how to efficiently manage the reservoir storage levels. While a drought event would require maximizing the storage in the dam (e.g., Golembesky et al. 2009), predicting a flooding event would inform the surplus storage to be released in order to accommodate incoming flow (e.g., Delaney et al. 2020). Furthermore, integrating seasonal climate forecasts with adaptive management schemes has demonstrated potential for improving reservoir operation and provide adequate contingency measures during

hydroclimatic disasters (Anghileri et al. 2016; Turner et al. 2017). Recently, some dam operators in the western United States had adopted a forecast informed reservoir operation approach to improve the reliability of reservoir operation by informing decisions about releasing or storing using forecasts (Jasperse et al. 2017). This forecast-based operation is still under evaluation for other dams before being operationally implemented.

The value of streamflow forecasting in reservoir operations becomes more significant in transboundary basins, where water availability regimes are impacted by water management practices in the upstream riparian countries (Munia et al. 2016; Shumilova et al. 2018). Installing an upstream dam in transboundary basins controls the inflow to existing downstream dams. Thus, the operation of downstream dams is dependent on how a new upstream dam will operate during its filling and post-filling stages. One key question is how forecast value would change with introducing new dams upstream of an existing reservoir system in a transboundary basin. For example, how the forecast value to operating existing reservoirs, will change during the filling and operation of a new upstream dam.

A timely and compelling example is the upstream development in the Nile River Basin (NRB) through the construction of the Grand Ethiopian Renaissance Dam (GERD). The current operation of reservoirs in the NRB is mostly based on rule-curves that were designed from a time series of historical inflows collected during the pre-dam period. The efficiency of such rule curves is naturally limited as inflows substantially change with upstream projects during the post-dam period, e.g., the construction of the GERD. Therefore, informing the operation of downstream dams, e.g., High Aswan Dam (HAD), with streamflow forecasts is one way to address such emerging challenges.

The value of streamflow forecasts can be undermined by limited information on operation of upstream projects. In such cases, when information on upstream dams is not made available or still under negotiations, building scenarios of filling and operation of upstream dam can provide a realistic range of the potential value of streamflow forecasts in improving the operation of downstream existing dams. Consequently, this allows a tangible pathway for risk mitigation under uncertainty of inflow. This study proposes a framework, called Forecast-based Adaptive Reservoir Operation (FARO), to integrate streamflow forecasts in deriving adaptive operating policy. The proposed framework is designed for existing reservoirs to operate in an adaptive manner that accounts for downstream demands while addressing upstream challenges from new transboundary dams. We used the HAD and GERD dams in the Nile river as examples of existing and planned dams, respectively, to test our FARO framework. This study addresses two primary questions: 1) what is the forecast horizon for a reliable inflow forecast to be useful for HAD operations? and 2) what is the potential value of forecast information at long-term scale in adapting the HAD operation to future challenges introduced during filling and operation of GERD? The first question deals with the identification of the HAD forecast horizon and what times of year, i.e., issuing months, when forecasting is more crucial to reservoir operation. Answering the first question allows the application of the FARO framework to assess the value of forecast during the filling and operation of future dams, e.g., GERD.

The rest of the paper is organized as follows. We present the study domain in Section 2. We then describe the FARO framework and the experimental approach to assess the value of streamflow forecast for reservoir operations. In section 4, we discuss the results, highlighting the reservoir operation performance achieved by considering the contributions of monthly forecasts.

We conclude the paper by summarizing the key findings and presenting further research directions.

5.2 Study Area

The Nile River basin (NRB) is a major transboundary basin that extends across eleven countries in northeastern Africa (Figure 5.1a). The NRB comprises two major tributaries, the Blue Nile (originates from Ethiopian plateau) and the White Nile (originates in the Great Lakes region of central Africa). The Blue Nile is the primary tributary to the main Nile River, providing 62% of the flow reaching Aswan (Zaroug et al. 2014), with three rainfall seasons; Bega, which refers to the dry winter season (October - February); Belg, the small rains of spring (March - May); and Kiremt, the wet summer season (June - September). The Kiremt season accounts for about three quarters of total annual rainfall (Tesemma et al. 2010; Taye and Willems 2012). The White Nile rises in the great Lakes region of central Africa, with the most distant source in southern Rwanda and flows north through Tanzania, Lake Victoria, Uganda, and southern Sudan. The Blue Nile and the White Nile meet at the Sudanese capital Khartoum and the Nile river then flows north through Sudan and Egypt to drain into the Mediterranean Sea.

The major dams on the Nile are Roseires Dam (Blue Nile in Sudan), Sennar Dam (Blue Nile in Sudan), High Aswan Dam (Main Nile in Egypt), and Owen Falls Dam (White Nile at Lake Victoria in Uganda). The High Aswan Dam (HAD) regulates the inflow to meet the downstream water supply for irrigation demands and hydropower generation. Lake Nasser (HAD reservoir) is one of the largest man-made lakes in the world and it is vital to Egypt since it stores and regulates the Nile flow upstream of the HAD (Figure 5.1a). The HAD reservoir has a total storage of 162 km^3 with minimum and maximum operating levels of 147 m and 182 m above mean sea level (AMSL), respectively. At the beginning of the water year (1st of August), the

water level is kept at 175 m AMSL (Full Supply Level) to store incoming high flows (Moussa, 2018). The storage increases gradually in the summer and, subsequently, the reservoir levels decrease from January to July as water is released (Figure 5.1b).

The future hydropower dams inventory provided by Zarfl et al, (2015) reveals an increasingly hydropower development in the NRB. One of the ongoing projects is the GERD in Ethiopia that is currently under construction. The GERD construction started in 2011 with a plan to store water up to an elevation of 640 m (Full Supply Level) corresponding to a storage capacity of 74 km^3. The GERD will form the largest hydropower dam in Africa with a total capacity of 5150 MW supplied through 16 installed turbines and it is likely to introduce a significant change in the electricity access for the entire Nile (Mulat and Moges 2014; Wheeler et al. 2016; Eldardiry and Hossain 2020). The GERD basin is the Upper Blue Nile basin located in the western part of Ethiopia (Figure 5.1a), where most rainfall occurs during the summer months between June and September.

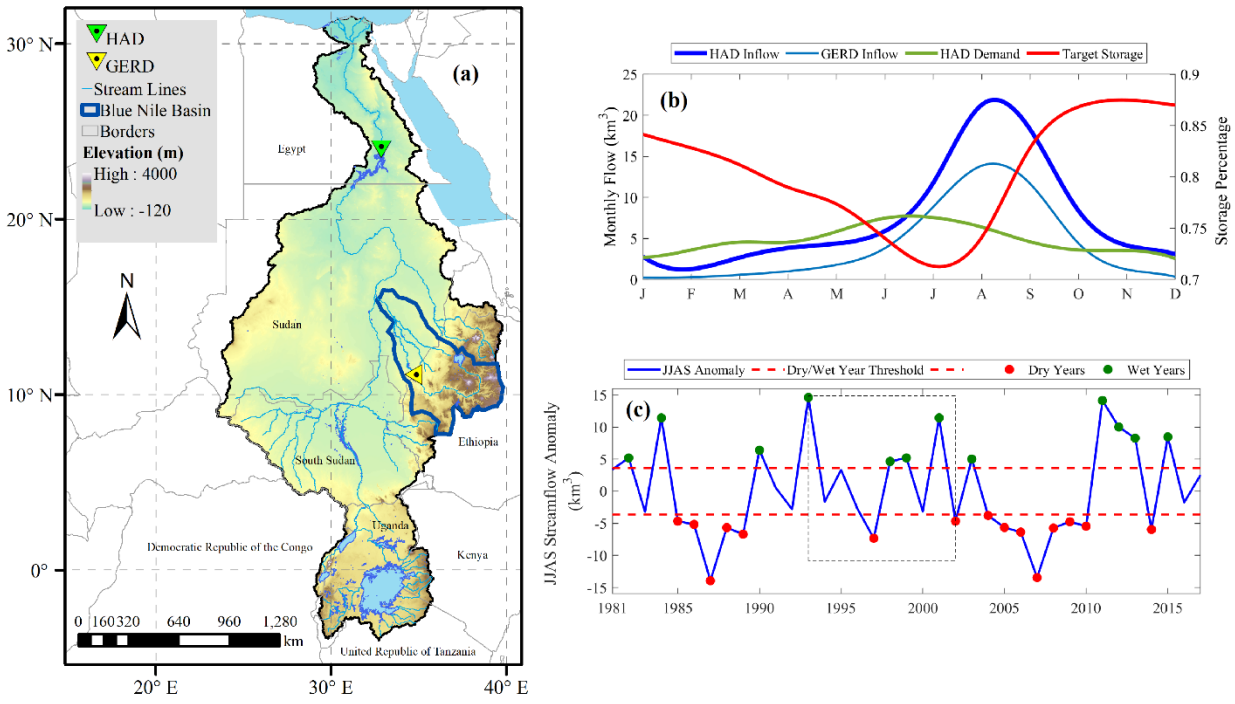

Figure 5.1. (a) The Nile river basin with the location of HAD and GERD dams. (b) Climatological HAD and GERD inflow (averaged over 37 years 1981-2017) as modeled by the satellite-based framework developed by Eldardiry and Hossain (2019). The red and green lines represent the HAD target storage and demand used for deriving HAD optimal operation, respectively. (c) The annual GERD inflow anomalies averaged over the rainy season JJAS (June-July-August-September) during the period (1981–2017). The red dashed line represents the threshold for the dry vs wet year identification at half of the standard deviation of the JJAS total streamflow.

5.3 Methods and Data

Figure 5.2 presents the main components of the Forecast-based Adaptive Reservoir Operation (FARO) framework proposed in our study. First, FARO integrates meteorological forcing data from historical records and General Circulation Models (GCMs) for driving a hydrological model. The hydrological model then produces streamflow for both historical and forecast periods. Second, we used the historical streamflow to define the benchmark streamflow forecasts: perfect forecast (assuming perfect knowledge of reservoir inflow) and streamflow climatology. The streamflow climatology is also used to correct the bias in the operational forecasts based on GCM forcings. Third, the streamflow forecasts are used with a Model Predictive Control (MPC) scheme to optimize the reservoir operation. In MPC, we define different characteristics of the reservoir system, upstream conditions (e.g., introducing new dams), and downstream water system (e.g., demand scenarios). Finally, we assess the value of streamflow forecasting in informing adaptive reservoir operation. The different components of our FARO framework are described in detail in the next sections.

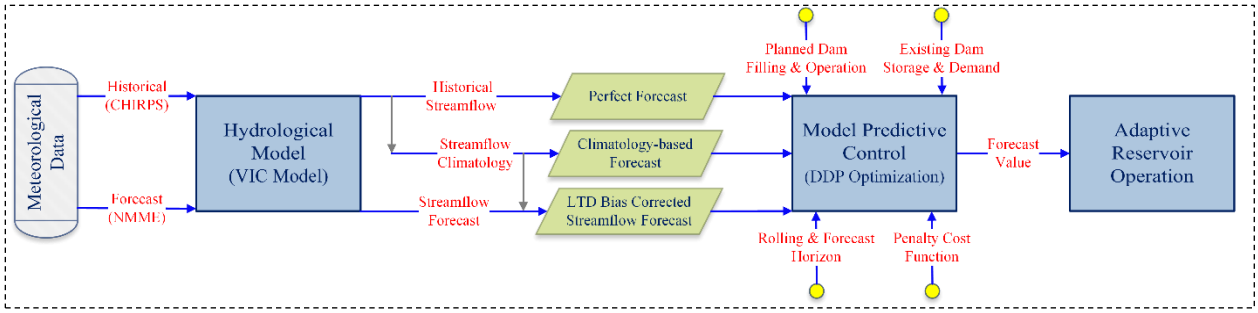

Figure 5.2. FARO framework for deriving adaptive reservoir operating policy using forecast information.

5.3.1 Streamflow Forecasting

a) Benchmark Forecast

To understand the value of a forecast-based operating policy, we need to compare that performance against a benchmark. We applied a benchmark operating schemes using perfect streamflow forecasts. The perfect forecast is based on monthly reservoir inflow using historical simulated streamflow at High Aswan Dam (HAD) for the 10 years from 1993-2002. This ten year period is selected since it includes examples of years with extreme climate conditions in the upstream (e.g., very dry and wet years in 1993 and 1998, respectively). The HAD inflow is simulated using the Variable Infiltration Capacity (VIC) model (described later in 3.1.c) and driven by CHIRPS precipitation. Perfect forecast reflects the theoretical maximum benefit (or potential value) that could be achieved assuming we have full and perfect information on the future in the present when operational decisions are made. We also compare our results when using the climatology of streamflow, i.e., the average monthly streamflow simulated by the VIC model for 37 years from 1981-2017. The climatology infers the absence of information on future forecasts and thus represents a non-adaptive approach to develop the reservoir operational rules.

b) NMME Forecast

We used the predicted monthly precipitation and temperature from North American Multimodel Ensemble (NMME) (Kirtman et al. 2014) to feed the hydrological model and produce streamflow forecasts for the 10 year period from 1993-2002. The NMME real-time forecasts and hindcasts are available through the International Research Institute (IRI) for Climate and Society data portal. Archived forecast variables include precipitation, sea surface temperature (SST), and 2-m air temperature. A detailed list of experimental setup, available models, number of ensembles, and hindcast period can be found in Kirtman et al. (2014). To account for forecast uncertainty, we considered eight NMME models and each model includes between 4 and 24 ensemble members with maximum lead times of 9 (NASA-GEOSS2S), 10 (NCEP-CFSv2), and 12 (all other models) months. In total, multi-model ensemble utilized in this study consists of 90 members (see Table 5.1 for a summary of the eight models). For the hydrological simulations, we used the average precipitation and temperature from each NMME model (over the ensemble members).

Table 5.1. List of NMME models used in this study.

	Model	Available Period	Ensemble Members	Lead Time
1	CanCM4i	Hindcast (1981-2018)	10	12
2	CMC2-CanCM4	Hindcast (1981-2018)	10	12
3	COLA-RSMAS-CCSM4	Hindcast (1982-2019)	10	12
4	GFDL-CM2p5-FLOR-B01	Hindcast (Mar 1980-2019)	12	12
5	NASA-GEOSS2S	Hindcast (Feb 1981-2017)	4	9
6	NCAR-CESM1	Hindcast (1980-2010)	10	12
7	NCEP-CFSv2	Hindcast (1982-2010)	24	10
8	GEM-NEMO	Hindcast (1981-2018)	10	12

c) Hydrological Modeling (VIC)

The predicted surface meteorological conditions (e.g., precipitation and temperature) are used as forcings for the Variable Infiltration Capacity (VIC) model to produce retrospective streamflow forecasts. VIC is a macroscale physically based, semi-distributed hydrology model that closes the energy and water balances and includes subgrid variability in elevation, vegetation, and infiltration (Liang et al. 1994, 1996). The VIC setup used in our analysis was developed by Eldardiry and Hossain (2019) for the Blue Nile Basin (BNB) at 0.1° (~10 km) spatial resolution using high spatial and temporal resolution of satellite observations, e.g., SRTM, CHIRPS, and MODIS. The forcing for historical and NMME forecast runs are both spatially downscaled to the grid scale of 0.1° using inverse distance weighted interpolation method. Eldardiry and Hossain (2019) have demonstrated the skill of the VIC model with satellite observations for simulating streamflow along the BNB (validated at Khartoum and Eldiem stations with a Nash Sutcliff Efficiency of 0.68 and 0.92, respectively). The reader is referred to Eldardiry and Hossain (2019) for further details on the VIC modeling framework over the BNB.

Because of the uncertainty in the hydrologic model and the uncorrected errors in downscaled forcings, a hydrologic post-processing can produce more skillful and reliable hydrologic forecasts (Ye et al. 2014). We employed a Lead Time Dependent (LTD) bias correction method to correct the errors in NMME-based streamflow forecasts (Jabbari and Bae 2020). The LTD bias correction is applied for the streamflow forecast using the ratio between the NMME-based streamflow (for 10-year period 1993-2002) and the climatology of a reference streamflow (average streamflow for 37-year period 1981-2017). In our study, a reference streamflow is produced using VIC simulations that are driven by CHIRPS precipitation for 37 years (1981-2017).

The ability to make skillful hydrological forecasts is determined by different factors including hydrological initial conditions (mostly soil moisture) and the accuracy with which hydrological forcings are known (Lettenmaier 2017). Instead of using observed discharge, we here opted to use streamflow produced from VIC simulations using CHIRPS precipitation as our reference of evaluating the streamflow forecast. This comparison allows focusing our evaluation on the effects of forcing data, i.e., precipitation and temperature, without further including uncertainties associated with hydrologic modeling.

5.3.2 Model Predictive Control (MPC)

To maximize the reservoir releases while incorporating inflow forecasts, we adopted a Model Predictive Control (MPC) formulation. MPC is a well-established optimal control technique that has recently gained increasing attention in the reservoir operation literature (Breckpot et al. 2013; Galelli et al. 2014). MPC is typically implemented in reservoir operations with a rolling horizon decision approach. This approach updates forecasts and decisions with each time step leading to more reliable operation (Zhao et al. 2012; Wan et al. 2016). The steps to derive optimal reservoir operation using MPC are: 1) at each decision time instant (t), a control problem for the reservoir operation (in our study, we used a water balance model controlled by target storage level and downstream demand) is formulated over a finite horizon from (t) to (t+h), where h is the forecast horizon in months; 2) applying a deterministic dynamic programming approach, we used a set of discrete finite horizon of water levels (or storage volumes) with 0.01 m increments to derive alternative sequences of release decisions.; 3) an optimal release decision sequence (R_1,R_2, ….., R_h) is then derived by minimizing the operation cost (i.e., the objective function of the optimization problem) over the forecast horizon h; 4) Only the release decision at the first time step R_1 is used for the next time step (t+1) (since a new

forecast is issued); 5) a new optimization problem is then solved over the next horizon (t+1: t+h+1). Steps (2-5) are repeated (i.e., rolling horizon approach) with updated inflow forecast and reservoir storage until the end of operation horizon.

In our study, the optimization horizon in the MPC model extends for 10 years from 1993 to 2002 (120 months) where we adopted the rolling horizon approach for lead times ranging from one to 12 months. We modeled the HAD operation using a water balance approach that accounts for the reservoir inflow, evaporation losses, storage changes, and reservoir releases. The water balance equation (assuming negligible groundwater interactions) is:

$$\frac{dS}{dt} = I - E - R \qquad \text{(Equation 1)}$$

$$R = I - \frac{dS}{dt} - E \qquad \text{(Equation 2)}$$

where I is the inflow in km^3/month, R is the reservoir release downstream of the HAD in km^3/month, E is the open water evaporation in km^3/month, and dS/dt represents the change in storage volume with time in km^3/month. Reservoir releases are constrained by physical reservoir characteristics, e.g., releasing of excess flow to spillway, minimum and maximum monthly releases (For HAD: R_{min}=1.8 km^3/month and R_{max}=8.1 km^3/month). A key element of the MPC formulation is the definition of the penalty function. The penalty function depends on the characteristics of the system under consideration, i.e., operating objectives of the reservoir. In case of HAD, we accounted for two objectives; 1) target downstream demands (D^{target}) (i.e., supply objective function); and 2) target storage levels (S^{target}) (i.e, storage objective function) to avoid excessive storage or drawdown. In our study, the target flood control levels and downstream demands of HAD operation are defined using the average measured storage levels and outflow (averaged over the 10 year period 1993-2002), respectively (Figure 5.1b) .

To derive HAD optimal releases, we minimized the penalty function using a deterministic optimization method, i.e., Deterministic Dynamic Programming (DDP). The stages of the DDP approach are time periods (monthly in our case), and the states are reservoir water levels (with 0.01 m increments). Thus, an optimal release decision is derived for each time step (t) based on the minimization of the following cost function:

$$R_{1,2,3,\ldots\ldots h}^{optimium} \xrightarrow{min} \{\sum_{t=1}^{h} C_t(R_t, S_t)\} \qquad \text{(Equation 3)}$$

where $C_t(R_t, S_t)$ is the total penalty cost function that is calculated as the summation of the cost incurred if the reservoir failed to meet any of its objectives, i.e., target demand and storage. The following formula is used calculate the total penalty cost at each time step (t):

$$C_t(R_t, S_t) = \left[\max\left(\frac{D_t^{target}}{R_t} - 1, 0\right)\right]^2 + \left[\frac{S_t^{target}}{S_t} - 1\right]^2 \qquad \text{(Equation 4)}$$

For the validation of the MPC model, we forced the model with observed time series of HAD inflows. The reason of using the observed data is to focus our validation only on the performance of the MPC formulation, i.e., the reservoir mass balance and optimization approach, without introducing uncertainties from data sources, e.g., using modeled streamflow or satellite-based water levels. Figure 5.3 shows the comparison of the observed HAD storage levels and outflow with the time series calculated using our MPC formulation during a five year validation period (1998-2002). The comparison depicted a high skill modeling of HAD operation using the MPC formulation with a Nash-Sutcliffe efficiency (NSE), Percentage Bias (PBIAS), and coefficient of determination (R^2) of 0.80, -0.34, and 0.94 for the HAD storage level, respectively (NSE=0.95, PBIAS=2.42 %, and R^2=0.95 for HAD outflow). The slight differences noticed in the storage levels are attributed to the water balance equation used to model the reservoir operation, which cannot perfectly mimic the actual mass balance. For instance, the increase in

HAD storage is attributed to high inflow at the HAD reservoir in 1998 and 1999, that was considered as “high floods” for HAD operation (Mahmoud 2005; Sadek and Medhat 2005). These flooding events led to the formation of Toshka lakes (located at the west of HAD reservoir) and the construction of spillway canals to link HAD reservoir with Toshka lakes (Moussa 2018; Chipman 2019). Overall, the MPC is able to reasonably capture the actual reservoir operation with high skillful predictability of inter-annual and intra-annual storage and flow variations. The ability of the MPC model to simulate the water levels and releases at HAD is critical to further investigate the viability of the forecast information in adapting the HAD operation.

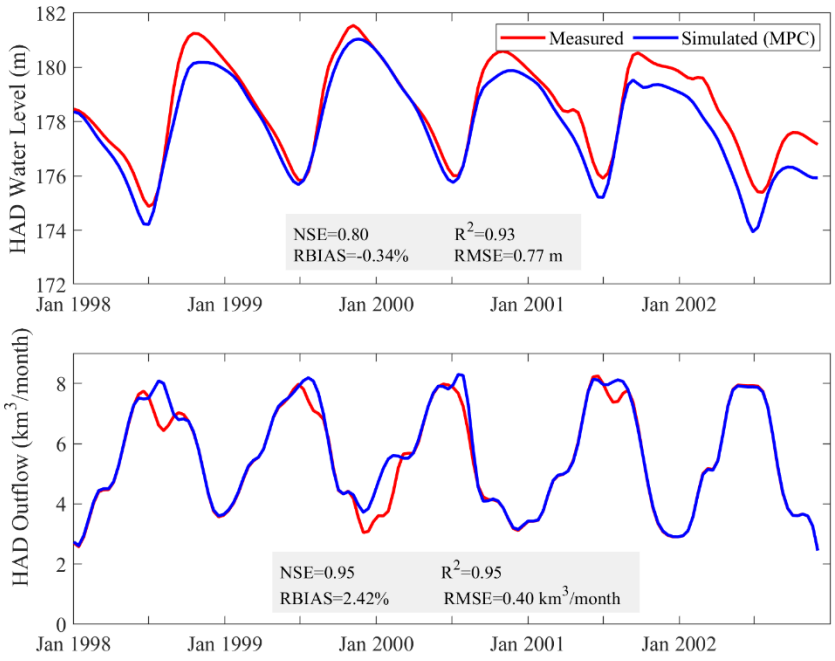

Figure 5.3. Validation of the MPC model for simulating storage water level and outflow of High Aswan Dam (HAD) during the five years (1998-2002).

5.3.3 Upstream Planned Dams

One of the primary questions addressed in our FARO framework is to assess the value of forecast information to operate an existing dam when a newer dam is planned upstream. This value is more substantial during the filling phase of new dam when downstream countries expect a reduction in water supply as water is stored in upstream reservoir. The HAD-GERD case in the Nile river basin typifies a timely example of transboundary challenge where introducing a new upstream dam would require revisiting the operation of existing dams. We used simulated streamflow at Eldiem station (i.e., GERD inflow) during the period 1981 to 2017 to build different scenarios of GERD filling (ranging from 2- to 12-year filling scenarios). The GERD filling scenario follows an approach that assumes monthly filling of the dam in a pattern identical to its inflow, i.e., higher storage in summer months. We considered filling the GERD dam using a moving time window of N years for each N-year filling scenario. For example, for a 3-year filling scenario, we produced 35 possible hydrologic sequence to fill the dam in 3 years (the first window is between 1981 and 1983 and the last window is between 2015 and 2017). The GERD reservoir is considered completely filled when the reservoir storage reaches its maximum capacity of 74 km^3. We here showed only the results when considering the average of the hydrologic sequences produced for 3- and 7-year filling scenarios.

The GERD releases during the filling scenarios are routed downstream to Khartoum station and then added to the flow from the White Nile and Atbara river to form the total inflow into HAD. As future operating rules for the GERD are still under negotiation, we used a discrete dynamic programming approach to derive an operating curve for GERD that is based on optimal hydropower production. More details on the filling and operation scenarios can be found in Eldardiry and Hossain (2020).

5.3.4 Experimental Setup

Our experimental approach considered three forecast alternatives: perfect forecast, streamflow climatology, and actual forecasts using NMME models (Figure 5.2). Perfect forecast is used as our benchmark to assess the forecast value when using NMME- vs climatology-based forecasts. Our scenarios include also testing three demand trajectories: 25th, 50th, and 75th percentiles (calculated as percentiles of measured HAD outflow during the period 1993-2002) to represent low, normal, and high downstream demand patterns, respectively. Table 5.2 summarizes the scenarios included in our FARO experimental setup. The aim of such scenarios is to elucidate the impacts of reservoir operating behavior and upstream conditions on the usefulness of applying long-term forecasts.

Table 5.2. Summary of the scenarios tested for different FARO inputs.

FARO Input	Scenario
Streamflow forecast	Perfect vs climatology vs NMME
Demand trajectory	25th vs 50th vs 75th percentiles
Upstream climate	Dry vs wet years
Upstream planned dam	Filling vs operation phases

5.3.5 Evaluation of Forecast Value and Skill

The streamflow forecast value is quantified using the optimal objective function (i.e., the penalty cost of the MPC model). The forecast value is evaluated using a dimensionless metric by normalizing the optimal penalty cost (units is (km^6); Equation 4) by the square of the reservoir storage capacity. To assess the Forecast Value Added (FVA) when introducing streamflow forecast to reservoir operation, we calculated the percentage of reduction in month-over-month optimal cost, i.e., change in penalty cost between two successive lead times, as follows:

$$FVA_t = \frac{C_{t-1} - C_t}{C_{t-1}} \qquad \text{(Equation 5)}$$

where FVA_t is the forecast value added when introducing streamflow forecast at a t-month lead time to reservoir operation, C_t and C_{t-1} are the optimal penalty cost resulted when using forecasts at (t) and (t-1) month lead time (Equation 3). For example, the FVA for a 3-month lead time is calculated as the reduction in the optimal cost from 2-month lead time to 3-month lead time.

The forecast skill is quantified using a Forecast Skill Score (FSS) that measures how far the value of the streamflow forecast (from climatology-based forecasts or the average of NMME-based forecasts) deviates from the perfect forecast using the following formula:

$$FSS = C - C_{perfect} \qquad \text{(Equation 6)}$$

where $C_{perfect}$ is the total monthly penalty cost when assuming perfect forecast scenario, C is the monthly penalty cost resulted from using the climatology-based forecasts or NMME-based forecasts (using the average of the eight NMME models). A value of FSS below or above zero indicates that streamflow forecasts underestimate or overestimate the optimal cost, respectively.

5.4 Results and Discussion

5.4.1 NMME Streamflow Forecasts

Figure 5.4a shows the relative bias for the monthly streamflow at Khartoum station (the outlet of the Blue Nile) at different lead times ranging from one to 12 months. The NMME models behave differently with wide range of variations when compared to the reference streamflow. The NASA-GEOSS2S model shows an underestimation in monthly streamflow for lead time greater than 2 months.. The largest streamflow overestimation is noticed by the Canadian models: CanCM4i and CMC2-CanCM4 with an average relative bias (averaged over all the lead times) of 430% (16.86 km^3/month) and 428% (16.34 km^3/month), respectively. The

skill performance of NMME forecasts is predominantly driven by strong seasonal- and lead-dependent biases (Slater et al. 2019).

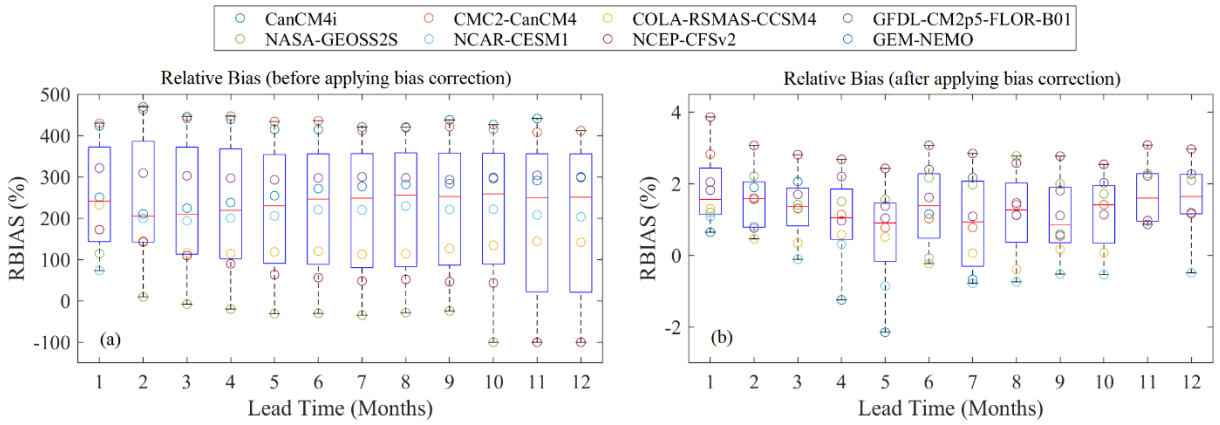

Figure 5.4. Relative bias (%) of monthly streamflow (km^3/month) at Khartoum station simulated in VIC using NMME forcings for the period (1993-2002). The NMME-based streamflow is compared to reference simulated streamflow using CHIRPS precipitation. The left and right panels represent the relative bias before (a) and after (b) applying lead-time dependent bias correction, respectively.

Figure 5.5 shows an example of five year (1998-2002) bias-corrected streamflow for the eight NMME models at three lead time (1-,3-, and 6- months). The bias correction approach resulted in more accurate streamflow with an average relative bias (averaged over both the lead time range and the eight models) of 1.3% (Figure 5.4b). The VIC simulations driven by GEM-NEMO model has the highest performance skill followed by the NCEP-CFSV2 with an average NSE of 0.89 and 0.88, respectively. The high skill of the NCEP-CFSV2 model has also been depicted over other regions, e.g., China (Ma et al. 2015) and the continental United States (Misra and Li 2014). When considering only the flooding season (June through September), we noticed

an overall reduction in the NSE and correlation coefficient with an average of 0.54 and 0.79 (again averaged over the eight models and the lead times).

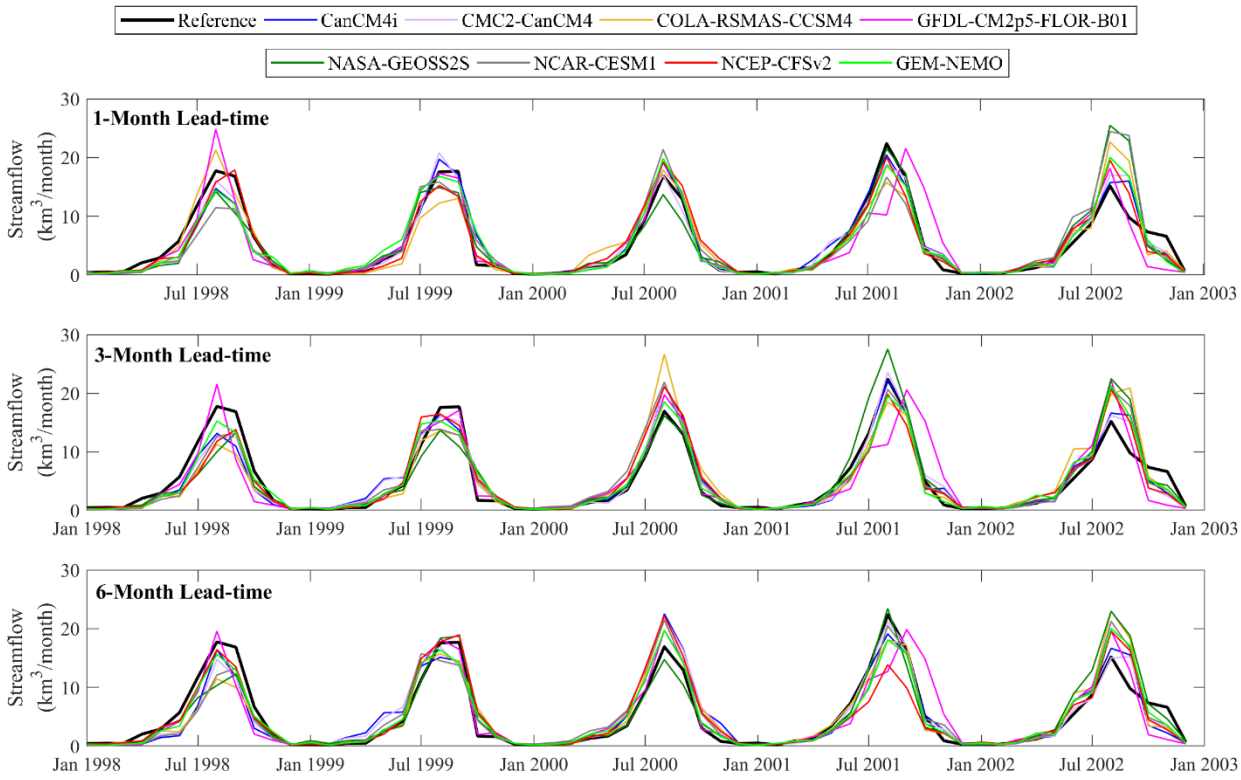

Figure 5.5. Lead Time Dependent (LTD) bias corrected streamflow at Khartoum Station using VIC simulations driven by NMME Forecasts. Each time series is produced by concatenating the NMME-based streamflow at N-lead time (where N is the lead time in months).

5.4.2 Potential Forecast Value for HAD Operation

We here used the perfect forecast benchmark to define the potential forecast value for HAD operation. Figure 5.6 shows the normalized penalty cost (normalized by the HAD storage capacity) for optimal HAD operation under a normal demand trajectory (i.e., 50th percentile) and using perfect forecast at different lead times. For most months, except for flooding season in August and September, lower penalty costs are associated with integrating forecast information

at longer lead time into our reservoir optimal operation. For instance, when using a perfect streamflow forecast in the months following the flooding season (October through December), the average normalized penalty cost ranges between 0.12% (1-month lead time) and 0.02% (12-month lead time). While the penalty cost decreases as streamflow forecast is available for longer lead-time, this pattern is reversed for the HAD in August and September when the peak inflow reaches Lake Nasser. Such a contrasting pattern is attributed to the storage level objective that controls the optimization problem during the flooding season and penalizes the operation for being lower or higher than the target storage level. Thus, when predictions are available during the flooding season, the dam would store more water (i.e., requires higher storage levels exceeding the target storage) to offset the lower future inflows. The requirement of excess storage affirms the HAD being supported with Toshka spillway to the west of Lake Nasser where excess flow can be discharged.

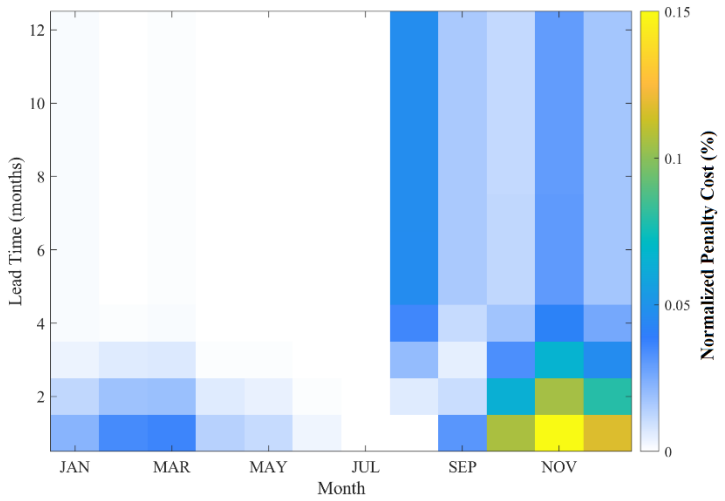

Figure 5.6. Normalized penalty cost for HAD operation using perfect -based forecast (the potential value) averaged over the period 1993-2002 and at a demand trajectory of 50th percentile (x-axis represents the month in which the forecast is issued).

We also considered high and low demand trajectories downstream of HAD, i.e., 25th and 75th quantiles of the HAD outflow to indicate potential levels of stress on the system downstream of HAD. Unsurprisingly, the penalty cost increases with higher demand trajectory since more penalty will be induced to the supply objective function, i.e., less water to meet downstream demands. For instance, the normalized penalty cost increases from 0.06% to 0.17% when operating HAD with changing the demand trajectory from 25th to 75th percentile and using perfect streamflow forecast at a lead time of two months.

Figure 5.7 shows the FVA to HAD operation (averaged over the non-flooding season from October through May) when using perfect streamflow forecast under different demand scenarios. The FVA has two main tipping points identifying the forecast lead time when FVA to HAD operation: 1) reaches its maximum value and 2) reaches zero, i.e., reservoir forecast horizon. For the demand scenarios at 50th and 75th percentiles, the maximum FVA is achieved at a forecast of 4-month lead time (e.g., average FVA=52% for 75th percentile demand scenario). At lower than 4-month lead time, the FVA is less significant for higher demand scenarios (e.g., average FVA of 2-month lead-time is 38.3% for 75th percentile demand scenario). This can be explained by the fact that downstream of HAD is subjected to high stress (due to high demand scenario) and therefore adding forecast information at short lead time (up to 3-month) will not significantly impact the operation decision compared to forecasts at longer lead time. Conversely, in case of low demand scenario where downstream system has less stresses, the HAD operation can significantly benefit from short lead time forecasts with high FVA (e.g., average FVA of 2-month lead time is 52.3% for 25th percentile demand scenario). The FVA to HAD operation recedes gradually with longer lead-time forecasts up to a point when it reaches zero. Beyond this point, the reservoir operation cannot be further improved with forecasts at

longer lead time (Figure 5.7). The forecast horizon for HAD operation ranges between 5 and 12-month lead time for low and high demand scenarios.. The long forecast horizon of HAD is attributed to its large storage capacity (average active storage-inflow ratio is equal to 0.95) that is sufficient to regulate the hydrologic variability of inflow and hedge for future demands.

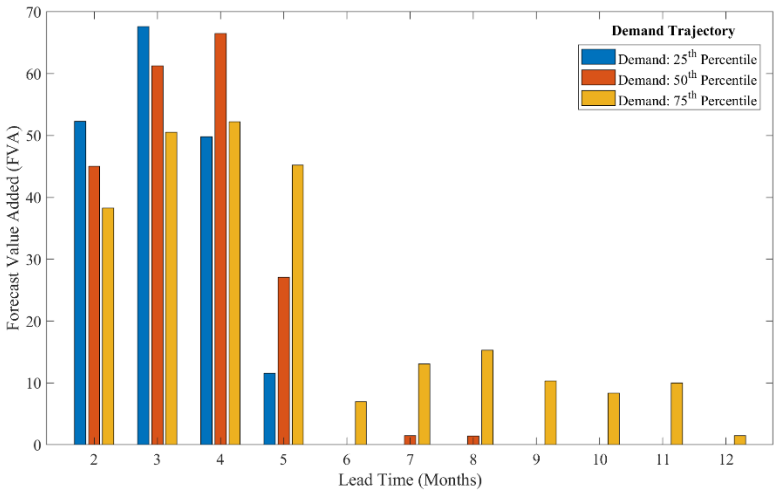

Figure 5.7. Average Forecast Value Added (FVA) calculated as the reduction in month-over-month optimal cost using perfect forecast under different demand trajectories (considering only non-flooding seasons months from October through May).

5.4.3 Skill of NMME-based Forecasts

Figure 5.8 shows the range of the monthly penalty cost based on the actual forecasts from the eight NMME models at different lead times (only 1-, 3-, and 6- month lead times are shown) and compared to the perfect and climatology-based forecasts. The range of penalty cost from the NMME forecasts is able to capture the perfect forecast (blue line in Figure 5.8). For instance, the normalized penalty cost when using NMME-based forecast in November with 3-month lead time ranges between 0.04% and 0.17%, which captures the potential value of the perfect forecast (0.07%). The differences between perfect and NMME forecasts are expected due to the

uncertainty in NMME models that resulted in different forecast quality. Figure 5.9 shows the Forecast Skill Score (FSS; defined in Equation 6) as a function of the lead time (months) and the month during which the forecast is issued. NMME-based forecasts tend to overestimate the operation cost at longer lead times (comparing the average of the eight models with the perfect forecast). Higher skill of NMME forecasts is noticed in the winter months at shorter lead times, i.e., FSS is closer to zero.

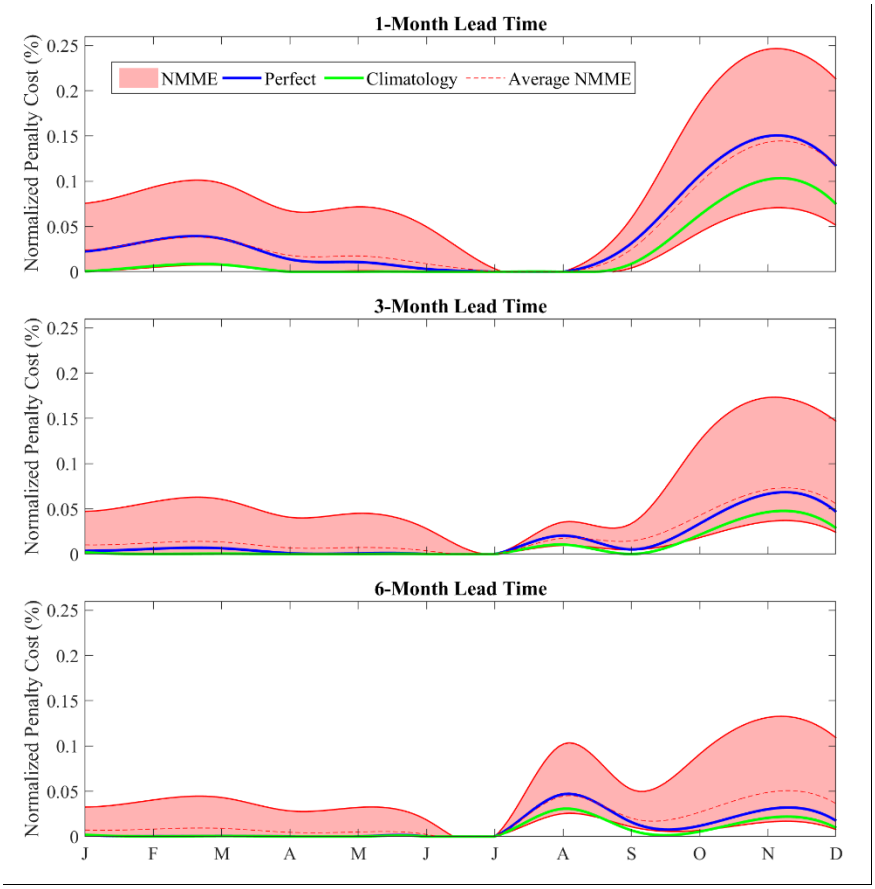

Figure 5.8. Normalized penalty cost of HAD operation (averaged over the years 1993-2002) using perfect and NMME-, and climatology-based streamflow forecasts (only 1-, 3-, and 6-month lead time are shown).

When using the climatology-based forecasts (green line in Figure 5.8), a significant underestimation in the penalty cost is noticed as compared to the perfect forecasts (Figure 5.9a).

For example, the forecast skill in December when using NMME-based forecasts at 1- and 6-month lead time ranges between -0.22 km6 (FSS for climatology-based forecast is -11.1 km6) and 4.9 km6 (FSS for climatology-based forecast is -2.1 km6), respectively. The forecast skill does not decrease uniformly with lead-time, and the selection of a skillful lead time varies as a function of forecast issuing month (flooding vs non-flooding seasons). Overall, when using actual forecasts from NMME models from October through December, HAD operation was improved with an average gain in FSS ranging from 16% (1-month lead time) to 231% (12-month lead time) as compared to the climatology-based forecasts.

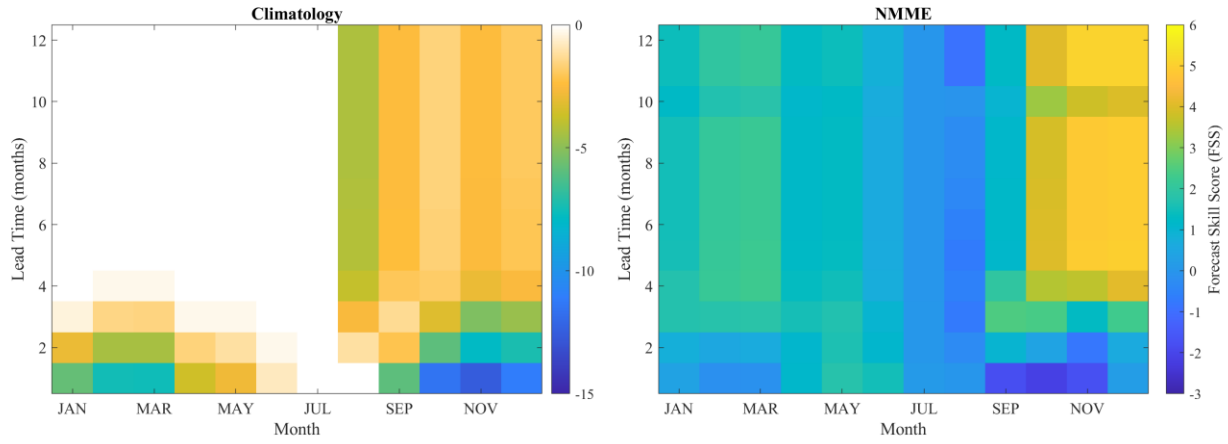

Figure 5.9. Forecast Skill Score (FSS) when using climatology- (left panel) and NMME-based (right panel) forecasts for HAD operation as compared to perfect forecast benchmarking (note that the two panels are represented by different color scale).

5.4.4 Examples for FARO Application

5.4.4.1 Wet and Dry Years

To demonstrate the value of our FARO framework, we evaluated the forecast value when HAD operates in a dry year following a wet year. The dry and wet years are defined at Eldiem station (i.e., at the outlet of the upper Blue Nile basin) by setting a threshold for the total

discharge anomalies of the rainy season (June through September) for a 37-year streamflow record between 1981 and 2017 (Figure 5.1c). The threshold is set as equal to half of the discharge anomaly standard deviation: any discharge anomaly above 3.64 km^3/month is considered as a flooding condition (wet year), and any discharge anomaly below -3.64 km^3/month as a drought condition (dry year). In our example, we showed the forecast-based HAD operation for the two years 2001 and 2002. The two years represent upstream wet (2001) and dry (2002) conditions with a total flow volume at Eldiem station during the rainy season of 49.6 km^3 and 33.6 km^3, respectively (Figure 5.1c). The different climate is also evidenced by the storage water level observed by radar altimetry over lake Nasser (Figure not shown). The water storage reaches its peak in October at a level of 180.59 m and 177.98 m AMSL in 2001 and 2002, respectively.

Following the FARO framework, the MPC model was forced by three streamflow forecast scenarios: perfect, climatology, and NMME-based forecasts, in the wet (2001) and dry (2002) years. As illustrated by Figure 5.10, the streamflow forecasts at longer lead time can substantially ameliorate the dam operation in the dry year by storing more water and thereby reduce the operation penalty cost (when compared to observed operation). For instance, if considering forecasts at 3-month lead time, the total normalized penalty cost (summed for the two years 2001 and 2002), dropped down from 3.20% for the observed HAD operation to 0.91% in case of perfect forecast (and 0.83% for the average of eight NMME models). The reduction in the operation cost elucidates the opportunities to better operate the HAD reservoir using long-term streamflow forecasts to make decisions on storage and releases that would minimize the impact of dry years. For example, an adaptive operation is highly recommended when releasing water in the months preceding the flooding season, i.e., when the reservoir empties its storage.

The HAD operation in 2002, for example, shows a significant drop in storage volume in August (119.10 km^3), while forecast reservoir inflow suggests a higher storage level (132.76 km^3) that can compensate for the inflow reduction in a dry year. Whilst the MPC model with forecast information can potentially improve the HAD operation, slightly higher costs, are produced in the wet year (2001), which is attributed to the uncertainty in the MPC optimization that can also be noticed in the validation of MPC (Figure 5.3). Furthermore, one caveat when using actual forecasts (as the case of NMME forecasts) is to consider the forecast skill due to the inherent uncertainty in the forecasting model, especially when dealing with extremes events (e.g., dry and wet years). A lower forecast skill can significantly reduce the value to reservoir operation, e.g., if a dry year is falsely forecasted as a wet year. Notwithstanding, the improvement of HAD operation, in the example presented, highlighted the value of streamflow forecast to adapt reservoir operation to future challenges, e.g., GERD filling or increasing demands.

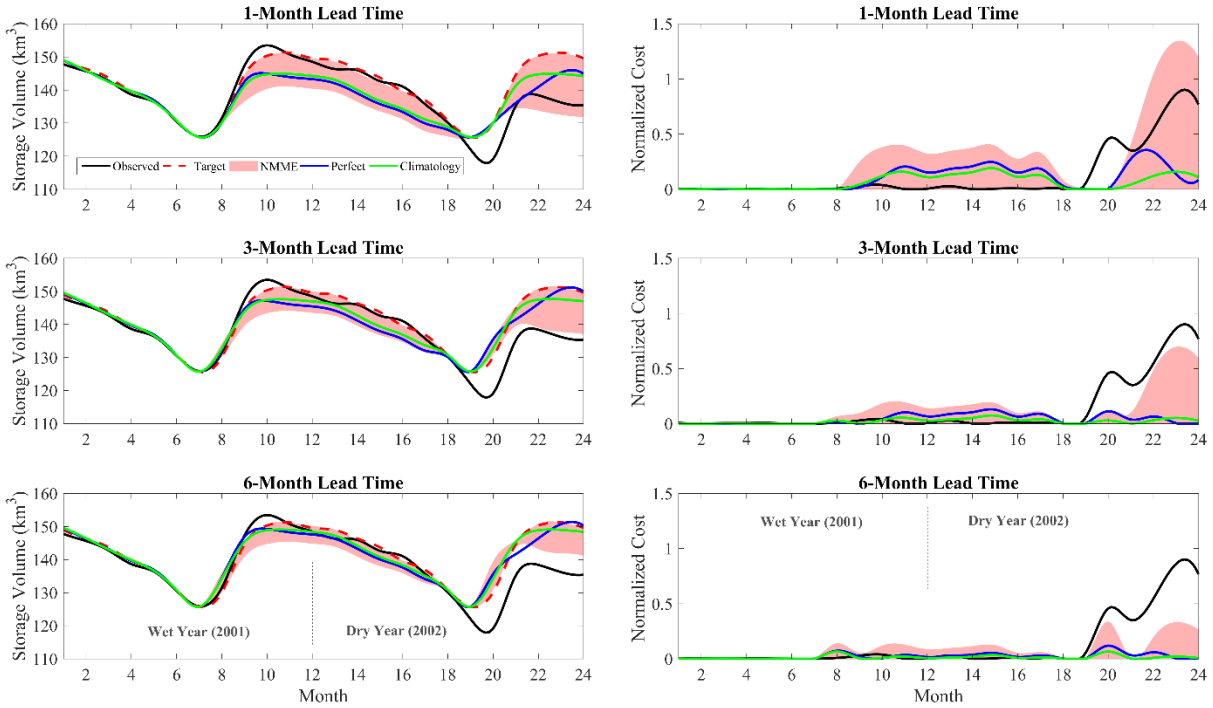

Figure 5.10. The HAD storage volume (Left panels) and penalty cost (right panels) when using streamflow forecast (perfect, climatology, and NMME) in wet (2001) and dry (2002) years (Only 1-, 3-, and 6- month lead times are shown).

5.4.4.2 GERD Filling and Operation Phases

Figure 5.11 shows the normalized change in penalty cost of HAD operation during GERD filling and operation as compared to the current conditions without GERD. Unsurprisingly, the penalty cost increased significantly during the GERD filling, especially at faster filling scenario. For example, when testing a 3-year filling scenario, HAD can operate to meet the current target objectives (i.e., target storage and releases) with an average increase in the normalized optimal cost ranging between 5.1% and 3.8% for 1- and 12- month lead time, respectively (Figure 5.11a). Such increase in penalty cost is attributed to less flow contribution from the Blue Nile as the GERD starts its filling (Figure 5.11d) and therefore penalizes HAD operation to meet its target storage level and demands. With a slower filling scenario, e.g., 7-year filling, streamflow forecasting can have a higher value in HAD operation as indicated by the reduction in the normalized penalty costs (Figure 5.11b). A 7-year filling scenario can improve the forecast value to HAD operation with an average reduction in the operation penalty cost of 85% (averaged for all lead times) as opposed to 3-year filling scenario. This reduction is explained by the higher annual GERD releases with 7-year filling approach that increases by about 60% (37 km^3 compared to only 23.3 km^3 with 3-year filling scenario). During the GERD operation phase, the spatial pattern of HAD operation costs changes with higher penalty cost in the months following the rainy season upstream of GERD (September through November). The maximum operation penalty cost of HAD during GERD operation is noticed in October with an increase of 101.3 $(km^3)^2$ (normalized change in penalty cost =0.39%) and 41.4 $(km^3)^2$

(normalized change in penalty cost =0.16%) for 1- and 12-month lead time, respectively (Figure 5.11c). Such increase follows the significant regulation in the flow downstream of GERD with higher releases in the non-flooding seasons (Figure 5.11d).

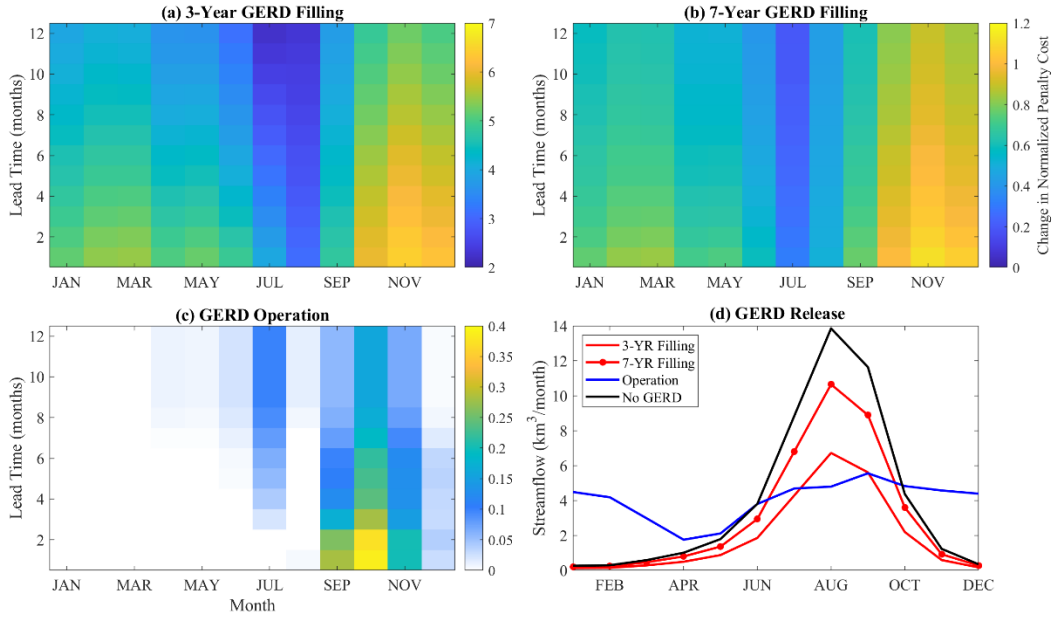

Figure 5.11. Change in normalized penalty cost of HAD operation during GERD filling (a & b) and operation (c) as compared to current conditions without GERD. The penalty cost is calculated using perfect forecast and assuming a demand trajectory of 50th percentile. GERD release for different scenarios including; No GERD, 3- and 7-year GERD filling, and GERD operation (post-filling).

Figure 5.12 compares the FVA as we introduce streamflow forecast at longer lead time to HAD operation under different GERD scenarios. Streamflow forecasting has higher value (i.e., higher reduction in cost) for the current conditions without GERD as compared to GERD filling scenarios. A 3-year filling scenario of GERD has the lowest FVA with an average FVA of 2.5% (averaged for all lead times). This can be explained by the fact that a fast filling scenario will significantly drag the HAD storage to low levels and hence, introducing streamflow forecast

information would minimally help in cost reduction. On the contrary, when adapting a slower filling scenario, e.g., 7-year, HAD can reap the value of streamflow forecasting, especially at shorter lead times, less than 4 months. For instance, a FVA of 6.3% can be attained when operating HAD with a 2-month lead time streamflow forecasting. During GERD operation, the streamflow forecasts tend to benefit the HAD operation at longer lead-times. In addition, the forecast horizon (FVA=0) of HAD operation increases to 9-month lead time (compared to 8 months in case of current conditions without GERD). For example, GERD operates in the future , HAD can benefit from a 8-month lead time streamflow forecasting with a cost reduction of 8.4% compared to only 1.4% for the case without GERD. Overall, maintaining the same target levels of HAD objective during GERD filling and operation would incur more operation penalty costs. This recommends revising the current HAD operating curve to cope with expected changes in upstream flow (Figure 5.11d). The analysis highlighted the months with higher penalty costs (e.g., October during GERD operation), where adaptation of reservoir operation can be employed to better benefit from streamflow forecasts.

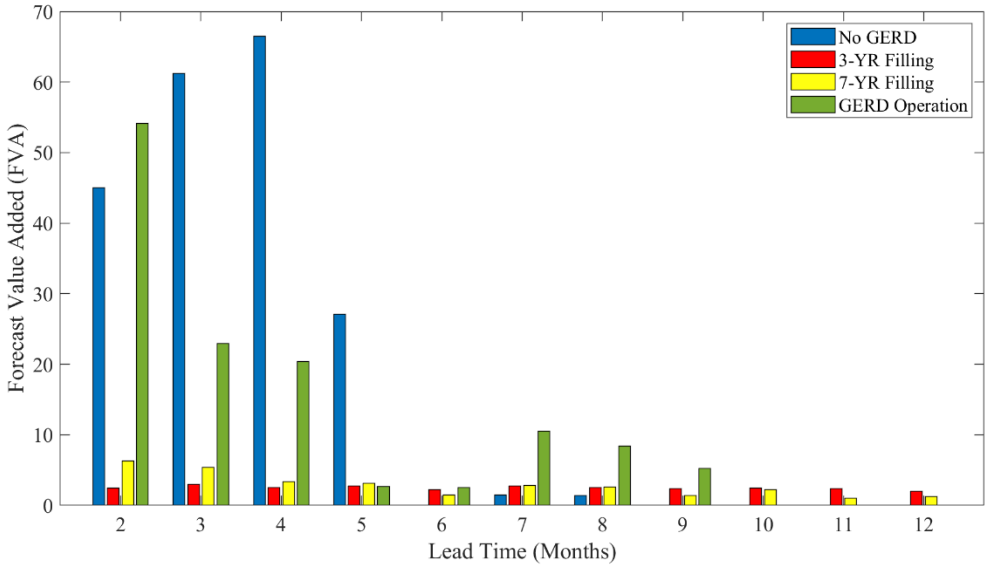

Figure 5.12. Average FVA (i.e., reduction in month-over-month optimal cost) using perfect forecast during GERD filling and operation scenarios and assuming 50th percentile demand trajectory downstream of HAD.

5.5 Conclusion

This study investigated the value of long-term streamflow forecast to improve reservoir operation through a Forecast-based Adaptive Reservoir Operation (FARO) framework. Forecasting streamflow at sub-seasonal (weeks) to seasonal time scales (months ahead) has a prominent role in management of water resources including reservoir operation and management, flood risk planning, and water allocation for crop irrigation. While the value of inflow forecasts in reservoir operation has been capitalized in previous studies, understanding of their precise contribution to adaptive reservoir operation in transboundary basins is limited. Our FARO approach introduces a formalized procedure to quantify the forecast value of long-term streamflow forecasts in adaptive reservoir operation. A forecast-based approach outperforms a traditional static operating policy, with the added benefit from the forecast information. The FARO approach was applied to the High Aswan Dam (HAD) in the Nile river basin to assess the value of streamflow forecasts at different lead time and under expected challenges from upstream planned dams (e.g., Grand Ethiopian Renaissance Dam or GERD).

Our key conclusions are as follows:

1. The FARO modeling framework (i.e., MPC and VIC models) shows a high accuracy in simulating the actual HAD reservoir and capturing the inter-annual and intra-annual storage and flow variations. In our FARO framework, a lead-time dependent bias correction method resulted in highly skillful NMME-based streamflow forecasts

at Khartoum station with an average NSE and correlation coefficient of 0.84 and 0.92, respectively. The ability of both MPC and VIC models to simulate existing reservoir operation and upstream inflow forecasts is critical to evaluating the viability of the forecast information in adapting the HAD operation.

2. The forecast value added (FVA) to HAD operation is more pronounced in the months following the flooding season (October through December). Issuing forecasting in these months is key to HAD operation and can significantly improve the decisions to release or store water in the next water year. When using actual forecasts from NMME models from October through December, HAD operation was improved with an average gain in forecast skill ranging from 16% (1-month lead time) to 231% (12-month lead time) as compared to the climatology-based forecasts. The NMME forecast skill does not decrease uniformly with lead-time, and the selection of a skillful lead-time varies as a function of forecast issuing month (e.g., for winter months, higher skill is attained at shorter lead times).
3. The FARO framework has shown its value in adapting reservoir operation when implemented under different conditions, including varying downstream demands, streamflow climatology during dry vs wet years, and upstream structural features introduced into the water system. The filling of GERD, especially at faster approach, can significantly drag the HAD storage to low levels. During its operation phase, GERD will regulate the HAD inflow throughout the year, i.e., less inflow in the summer months. Hence, introducing streamflow forecast would minimally help to maintain current target objectives of HAD operation and therefore result in higher

operation costs. To improve the forecast value while considering GERD operation, deriving a new adaptive operating policy for HAD is recommended.

Our FARO example on HAD and GERD operation reveals the potential of FARO framework to evaluate the value of streamflow forecast in operation of other dams in the basin, e.g., Sennar, Roseires, and Merowe dam in Sudan. Furthermore, given the advantage of being routinely produced and publicly accessible, NMME forecasts can be implemented operationally to guide water release decisions. Integrating streamflow forecasts into reservoir operations can support water managers and various stakeholders in the Nile region. For a country like Egypt, a FARO framework can be operationalized into a decision support system to monitor reservoir operations, i.e., water storage and release patterns, by upstream riparian countries. Operationalizing long-term streamflow forecasting will have the potential to help negotiate the filling and operation decisions of new dams by estimating annual expectations of streamflow. A major challenge when implementing forecasts in real-time operational applications is the uncertainty involved in streamflow forecasts (Zhao et al. 2011; Chen et al. 2016). Considering forecast uncertainty through model ensembles can compensate for the loss in performance due to forecast inaccuracy. Our study demonstrated that streamflow forecasts based on NMME models can potentially improve real-time reservoir operations. To further enhance the NMME forecast skill, future work can also benefit from hybrid models that integrate both dynamical climate forecasts and statistical or data-driven methods (Slater and Villarini 2018). For example, a hybrid approach can learn from GCM physical-based forecasts to inform the predictors in a statistical forecasting methods (see for example, Robertson et al. 2013 and Humphrey et al. 2016).

Increases in the frequency and intensity of extreme weather events are anticipated to alter streamflow patterns and affect reservoir operation (Asadieh and Krakauer 2015; Ehsani et al.

2017). An extreme event that occurs downstream of an existing dam can lead to a severe flooding or drought if no prior adaptation is implemented to the dam releases. This would imply, for example, releasing less water from the reservoir before it rains. Using short-term forecasts can help to predict downstream extreme events and allow employing an adaptive reservoir operation. In October 2015, Egypt has been subjected to extreme precipitation events in the Nile delta (downstream of HAD) that has resulted in severe flooding of some regions (Zevenbergen et al. 2017). One reason for downstream flooding is the failure of HAD to adapt its operation in a coordinated way that account for downstream precipitation events. The FARO framework can be further extended to benefit from the application of existing numerical forecast models, e.g., NCEP Global Forecast System (GFS), to provide weather forecasts at weekly to sub-daily scales. This would pave the way to derive adaptive operating policy of existing dams while exploiting the value of both long- and short-term forecasts.

Chapter 6: Conclusions

The Nile River Basin (NRB) is home to more than 200 million people sharing the water resources for agriculture, industry, municipal uses, in-stream navigation, and hydropower generation. A central and existential water management issue for the region is maintaining a sustainable supply of water against increasing population, recurring drought, climate change and increasing water demand. Nowhere is this issue of national survival more critical than for Egypt, a populous country of more than 100 million that is singularly dependent on a single river. Such challenges to manage and secure sustainable water are expected to become more acute with the construction of a new large-scale hydropower dam in Ethiopia known as Grand Ethiopian Renaissance Dam (GERD). The GERD will form the largest hydropower dam in Africa with 74 km^3 of reservoir storage and 5150 MW hydropower installed capacity. Therefore, a major concern is what changes the future dams (e.g., GERD) will bring to water security of downstream countries (like Egypt).

The Nile river flow is almost fully controlled by the High Aswan Dam (HAD) once it enters Egypt. Thus, any changes in future water supply will impact the HAD reservoir operation in Egypt, which will need to adapt its operation under a new set of conditions. Addressing such challenges when assessing reservoir operation in developing nations is hindered by lack of data (e.g., operating policy or storage plans) shared among neighboring nations. This dissertation integrated a suite of satellite missions (e.g., TRMM, GPM, Landsat, MODIS) and forecast products (e.g., NMME) with macroscale hydrological modeling (VIC model) to derive an adaptive reservoir operating policy in the transboundary NRB. In particular, the work in this dissertation focused on the adaptation of HAD operation to GERD construction, which typifies

one of the challenges facing dam operators and water managers in downstream Nile riparian countries.

The main findings of this dissertation are as follows:

1. The modeling of HAD operation using satellite observations and macroscale hydrologic model shows a good agreement with measured discharge downstream of the dam. Building a well-established satellite-based modeling framework for monitoring or predicting reservoir operations can benefit water managers and various stakeholders. For instance, policy makers can be supplied with better information of the HAD (and GERD) operations, which subsequently help make more informed decisions about a wide array of water management issues.
2. An assessment of GERD hydropower potential revealed that the hydrology of the Upper Blue Nile can only sustain the inflow to GERD that would produce 13,629 GWh per annum (capacity factor=0.30). Investigations further indicated that the GERD operation under the current design configuration will likely result in eight (out of 14) idle turbines every year. Our study also demonstrated that initial plans to upgrade the GERD capacity (from 5250MW to 6000MW to 6450 MW) have not been beneficial to improving the dam's hydropower production potential.
3. The HAD dam will undergo different operational modes during the filling and operational phases of GERD. A 3-year filling scenario can lead to a significant declining trend in HAD water levels that can be slightly improved if downstream water stress is allowed or by keeping HAD storage at a high level prior to GERD filling. Alternatively, a slower filling scenario that lasts more than 7 years, would lead to a stabilized HAD level on average. The GERD operation will regulate the flow in the Blue Nile with less intra-annual variability

in the HAD inflow. The results concluded that under years of different climate conditions (e.g., dry vs. wet), the HAD would recover to its normal operation after an average of 7 and 3 years for 3- and 7-year filling scenarios, respectively. The recovery period can significantly be reduced if the initial HAD storage is kept at a higher level or downstream water stress is allowed in the summer (e.g., $WaSSI_{AG}$=0.70).

4. Following a Forecast-based Adaptive Reservoir Operation (FARO) approach, the HAD operation shows a higher value of streamflow forecasts in the months following the flooding season (October through December). Issuing forecasting in these months is key to HAD operation and can significantly improve the decisions to release or store water in the next water year. When using actual forecasts from NMME models from October through December, HAD operation was improved with an average gain in forecast skill ranging from 16% (1-month lead time) to 231% (12-month lead time) as compared to the climatology-based forecasts.

Taking advantage of free satellite observations, available globally at high spatial and temporal resolutions, makes the satellite-based framework presented in this dissertation conceptually transferable to other transboundary basins as construction of mainstem and tributary dams becomes more widespread (Kalitsi 2003; Sabo et al. 2017). For instance, more than 20 dams have been built by Turkey in the headwaters of the Euphrates river for hydropower and irrigation. Such dams impact downstream countries (Syria and Iraq) leading to reduced flow and potential desiccation with projected changes in climate (Zeitoun et al., 2013). Similarly, the case of damming the Lower Mekong River is spurring interests in South Asia to investigate how existing dams would operate to sustain the world's largest inland fishery (Hecht et al. 2019). Thus, harnessing the satellite information in transboundary basins of developing countries could provide

more effective and immediately actionable assessments of operations of pre-existing dams while considering the impacts offuture dams.

The satellite-based modeling framework presented in this dissertation has various implications in the management of water resources in the downstream countries of the Nile River. Building upon this framework, long-term sustainability of the Food Energy Water (FEW) security in the Eastern Nile basin can be explored using a nexus approach. Such a FEW nexus highlights the interdependence of the three critical resources and therefore provide an effective way to control the releases from dams in the basin. Changes in the FEW system are more pronounced in the Eastern Nile basin due increasing pressures on water resources from multiple stresses including human-induced land use changes and rapid population growth, rising demand for natural resources, and external factors such as climate change and variability (Al-Saidi et al. 2017).

As the GERD dam is a matter of fact, Egypt has to accept the fait accompli and explore adaptation strategies to face the expected reduction in Nile water supply. While adapting the HAD operation, as suggested in our results, is one approach to alleviate the GERD impacts, it becomes urgent for a populous country like Egypt, to think of alternative resources to support its development plans. For example, importing virtual water (water used in the production of any traded commodity) becomes an integral element in transboundary basin management. Zeitoun et al. (2010) estimated about 41 km^3 of virtual water imported annually by the Nile basin states between 1998 and 2004. This additional water to the basin represents one third of the annual Nile flow and plays a key role in filling the freshwater deficits of downstream countries, Egypt and Sudan. Other alternative measures include, adopting water-efficient agricultural technologies like sprinkler and drip irrigation, building new desalination and water treatment plants, and imposing firm penalties on wasteful irrigation practices or unofficial use of irrigation water. Furthermore, it

becomes highly recommended for Egypt to foster negotiations among riparian countries in the Nile basin to agree upon a long-term framework that explicitly accounts for the impacts of future projects along the Nile. Such a framework should inspire a win-win solution and consider equitable rights of development in all Nile countries.

The work presented in this dissertation aims to advance societal impacts by converting the results from the scientific research into a sound decision support system. The dissertation results will be operationalized through a web portal system (**Ni**le **B**asin **R**eservoir **A**dvisory **S**ystem or **NiBRAS**). The system is currently in the development stage to integrate complex back-end models with front-end user needs. NiBRAS benefits from the growth of open-source and non-proprietary tools, e.g., Google Earth Engine API, which made it possible to build a cost-effective real-time operational system. The system functionality will include different tools to facilitate the understanding of the water management issues associated with reservoir operation in the NRB and provide a basis for evaluating potential solutions. The NiBRAS tools are: 1) Monitoring Reservoir Operation (MRO) tool (status: currently operational); 2) Monitoring Reservoir Initial Impoundment (MRI_2) tool (status: currently beta version is available); 3) Scenarios-based Assessment of Reservoir Operation (SARO) tool (status: currently in progress); and 4) Forecast-based Adaptive Reservoir Operation (FARO) tool (status: currently in progress).

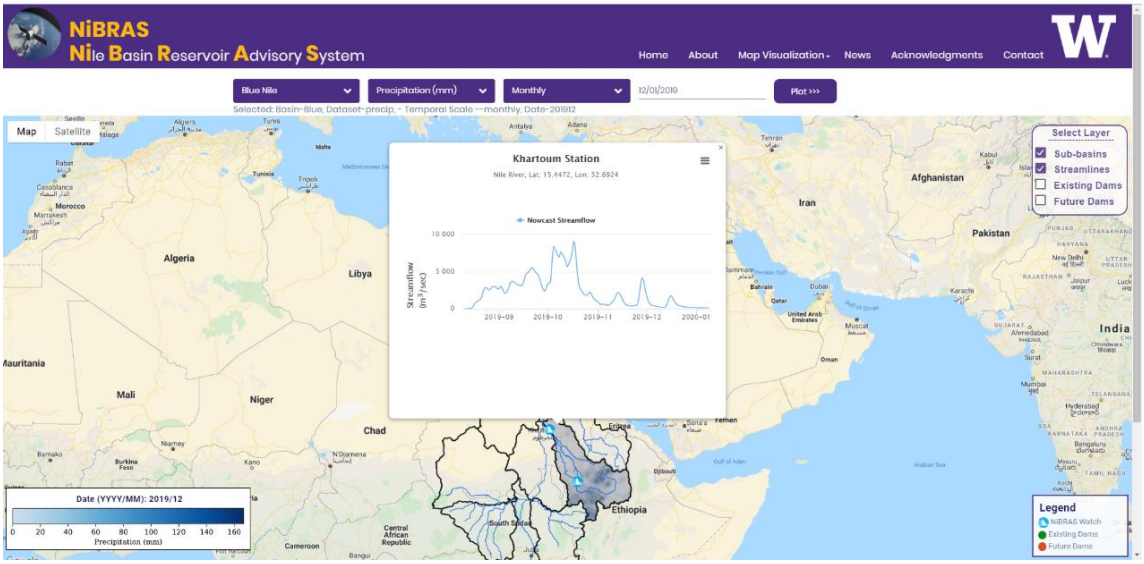

Figure 6.1 Screenshot of the NiBRAS system (in development stage) showing its current functionality (e.g., producing real time streamflow at Khartoum station and map visualization of total monthly precipitation over Blue Nile Basin).

Figure 6.1 shows an example of the current front-end of the system using the MRO tool to provide a real-time monitoring of Blue Nile hydrology (using the modeling framework developed in Chapter 2). Integrating the outcomes of my proposed research studies into the NiBRAS system will promote the societal applications of various water-related satellite/forecast products in the Nile basin; communicate the potential of such products to understand water management issues; and provide a tangible tool forward to facilitate the negotiations for new dam plans. In addition, communicating the scientific findings via the NiBRAS system is a potential pathway to reach a common ground and avoid political tensions in the Nile region that would hinder the successful implementation of adaptive management.

To further promote the stakeholder engagement with the work presented in this dissertation, we organized a three-day workshop (Sensing Rivers 2020 or SR 2020) on satellite remote sensing applications in water resources engineering. More than 20 attendees from the Nile

River countries (particularly from Egypt, Sudan, and Ethiopia) participated in the SR 2020 workshop, where they built their skills with satellite remote sensing datasets and learned about the NiBRAS system. During the workshop, the discussions and feedback from the attendees have been very useful in improving the NiBRAS system functionality so it can better assist water managers and dam operators in making more informed decisions. The experience from SR 2020 workshop and NiBRAS system foster the efforts to develop user-ready, not only use-inspired, research that can lead to more practice-oriented outcomes.

Bibliography

Abd-El Monsef, H., Smith, S. E., and Darwish, K. (2015). Impacts of the Aswan high dam after 50 years. Water Resources Management, 29(6), 1873-1885.

Abtew, W., and Dessu, S. B. (2019). The Grand Ethiopian Renaissance Dam on the Blue Nile. Springer International Publishing.

Abu-Zeid, M. A., and El-Shibini, F. Z. (1997). Egypt's high Aswan dam. International Journal of Water Resources Development, 13(2), 209-218.

Ahmad, S. K., and Hossain, F. (2020). Maximizing energy production from hydropower dams using short-term weather forecasts. Renewable Energy, 146, 1560-1577.

Ahmadi, M., Haddad, O. B., and Loáiciga, H. A. (2015). Adaptive reservoir operation rules under climatic change. Water Resources Management, 29(4), 1247-1266.

Aljefri, Y. M., Fang, L., Hipel, K. W., and Madani, K. (2019). Strategic Analyses of the Hydropolitical Conflicts Surrounding the Grand Ethiopian Renaissance Dam. Group Decision and Negotiation, 28(2), 305-340.

Allam, M. M., and Eltahir, E. A. B. (2019). Water-Energy-Food Nexus Sustainability in the Upper Blue Nile (UBN) Basin. Frontiers in Environmental Science, 7(5).

Allam, M. M., Jain Figueroa, A., McLaughlin, D. B., and Eltahir, E. A. (2016). Estimation of evaporation over the upper b lue n ile basin by combining observations from satellites and river flow gauges. Water Resources Research, 52(2), 644-659.

Allam, M. N., and Allam, G. I. (2007). Water resources in Egypt: future challeges and opportunities. Water International, 32(2), 205-218.

Allen, R. G., Tasumi, M., and Trezza, R. (2007). Satellite-based energy balance for mapping evapotranspiration with internalized calibration (METRIC)—Model. Journal of irrigation and drainage engineering, 133(4), 380-394.

Al-Saidi, M., Elagib, N. A., Ribbe, L., Schellenberg, T., Roach, E., and Oezhan, D. (2017). Water-Energy-Food Security Nexus in the Eastern Nile Basin: Assessing the Potential of Transboundary Regional Cooperation. Water Energy Food Nexus: Principles and Practices, 229, 103.

Alsdorf, D., Birkett, C., Dunne, T., Melack, J., and Hess, L. (2001). Water level changes in a large Amazon lake measured with spaceborne radar interferometry and altimetry. Geophysical Research Letters, 28(14), 2671-2674.

Anghileri, D., Voisin, N., Castelletti, A., Pianosi, F., Nijssen, B., and Lettenmaier, D. P. (2016). Value of long-term streamflow forecasts to reservoir operations for water supply in snow-dominated river catchments. Water Resources Research, 52(6), 4209-4225.

Annys, S., Adgo, E., Ghebreyohannes, T., Van Passel, S., Dessein, J., and Nyssen, J. (2019). Impacts of the hydropower-controlled Tana-Beles interbasin water transfer on downstream rural livelihoods (northwest Ethiopia). Journal of Hydrology, 569, 436-448.

Asadieh, B., and Krakauer, N. Y. (2015). Global trends in extreme precipitation: climate models versus observations. Hydrology and Earth System Sciences, 19(2), 877-877.

Awange, J. L., Forootan, E., Kuhn, M., Kusche, J., and Heck, B. (2014). Water storage changes and climate variability within the Nile Basin between 2002 and 2011. Advances in Water Resources, 73, 1-15.

Awulachew, S. B., Wubet, F. D., McCartney, M., and Shiferaw, Y. S. (2011). Hydrological water availability, trends and allocation in the Blue Nile Basin. In Nile River Basin (pp. 283-296). Springer, Dordrecht.

Bakken, T. H., Modahl, I. S., Raadal, H. L., Bustos, A. A., and Arnøy, S. (2016). Allocation of water consumption in multipurpose reservoirs. Water Policy, 18(4), 932-947.

Balthrop, C., and Hossain, F. (2010). Short note: a review of state of the art on treaties in relation to management of transboundary flooding in international river basins and the global precipitation measurement mission. Water Policy, 12(5), 635.

Barnes, D. F., Golumbeanu, R., and Diaw, I. (2016). Beyond electricity access: output-based aid and rural electrification in Ethiopia.

Basheer, M., Wheeler, K. G., Elagib, N. A., Etichia, M., Zagona, E. A., Abdo, G. M., and Harou, J. J. (2020). Filling Africa's Largest Hydropower Dam Should Consider Engineering Realities. One Earth, 3(3), 277-281.

Basheer, M., Wheeler, K. G., Ribbe, L., Majdalawi, M., Abdo, G., and Zagona, E. A. (2018). Quantifying and evaluating the impacts of cooperation in transboundary river basins on the Water-Energy-Food nexus: The Blue Nile Basin. Science of the Total Environment, 630, 1309-1323.

Bastawesy, M. A., Khalaf, F. I., and Arafat, S. M. (2008). The use of remote sensing and GIS for the estimation of water loss from Tushka lakes, southwestern desert, Egypt. Journal of African Earth Sciences, 52(3), 73-80.

Bastiaanssen, W. G. M., Noordman, E. J. M., Pelgrum, H., Davids, G., Thoreson, B. P., and Allen, R. G. (2005). SEBAL model with remotely sensed data to improve water-resources

management under actual field conditions. Journal of irrigation and drainage engineering, 131(1), 85-93.

Bastiaanssen, W. G., Menenti, M., Feddes, R. A., and Holtslag, A. A. M. (1998). A remote sensing surface energy balance algorithm for land (SEBAL), 1. Formulation. Journal of Hydrology, 212, 198-212.

Bayissa, Y., Tadesse, T., Demisse, G., and Shiferaw, A. (2017). Evaluation of satellite-based rainfall estimates and application to monitor meteorological drought for the Upper Blue Nile Basin, Ethiopia. Remote Sensing, 9(7), 669.

Berga, L., and coauthors (2006). Dams and Reservoirs, Societies and Environment in the 21st Century, Two Volume Set: Proceedings of the International Symposium on Dams in the Societies of the 21st Century, 22nd International Congress on Large Dams (ICOLD), Barcelona, Spain, 18 June 2006. CRC Press.

Beyene, A. (2013). Why is the hydroelectric dam on the Blue Nile, the Grand Ethiopian Renaissance Dam (GERD), sized for 6000 MW? Retrieved November, 25th, 2019.

Biemans, H., and coauthors (2011). Impact of reservoirs on river discharge and irrigation water supply during the 20th century. Water Resources Research, 47(3).

Birkett, C. M., (1998). Contribution of the TOPEX NASA radar altimeter to the global monitoring of large rivers and wetlands. Water Resources Research, 34(5), 1223-1239.

Block, P., and Goddard, L. (2012). Statistical and dynamical climate predictions to guide water resources in Ethiopia. Journal of Water Resources Planning and Management, 138(3), 287-298.

Block, P., and Rajagopalan, B. (2007). Interannual variability and ensemble forecast of Upper Blue Nile Basin Kiremt season precipitation. Journal of Hydrometeorology, 8(3), 327-343.

Block, P., and Strzepek, K. (2010). Economic analysis of large-scale upstream river basin development on the Blue Nile in Ethiopia considering transient conditions, climate variability, and climate change. Journal of Water Resources Planning and Management, 136(2), 156-166.

Block, P., and Strzepek, K. (2012). Power ahead: meeting Ethiopia's energy needs under a changing climate. Review of development economics, 16(3), 476-488.

Bonnema, M., and coauthors (2016). Understanding satellite-based monthly-to-seasonal reservoir outflow estimation as a function of hydrologic controls. Water Resources Research, 52(5), 4095-4115.

Bonnema, M., and Hossain, F. (2017). Inferring reservoir operating patterns across the Mekong Basin using only space observations. Water Resources Research, 53(5), 3791-3810.

Bonnema, M., and Hossain, F. (2019). Assessing the potential of the surface water and ocean topography mission for reservoir monitoring in the Mekong River Basin. Water Resources Research, 55(1), 444-461.

Bormann, B. T. (1994). Adaptive ecosystem management in the Pacific Northwest (Vol. 341). US Department of Agriculture, Forest Service, Pacific Northwest Research Station.

Borrok, D. M., Chen, J., Eldardiry, H., and Habib, E. (2018). A framework for incorporating the impact of water quality on water supply stress: an example from Louisiana, USA. JAWRA Journal of the American Water Resources Association, 54(1), 134-147.

Breckpot, M., Agudelo, O. M., and De Moor, B. (2013). Flood control with model predictive control for river systems with water reservoirs. Journal of irrigation and drainage engineering, 139(7), 532-541.

Brown, C. M., and coauthors (2015). The future of water resources systems analysis: Toward a scientific framework for sustainable water management. Water resources research, 51(8), 6110-6124.

Calmant, S., Seyler, F., and Cretaux, J. F. (2008). Monitoring continental surface waters by satellite altimetry. Surveys in geophysics, 29(4-5), 247-269.

Candogan Yossef, N., Van Beek, R., Weerts, A., Winsemius, H., and Bierkens, M. F. (2017). Skill of a global forecasting system in seasonal ensemble streamflow prediction. Hydrology and Earth System Sciences, 21(8), 4103-4114.

CAPMAS, E. (2014). Annual Bulletin of Statistical Crop Area and Plant Production. The central agency for public mobilisation and statistics.

Cascão, A. E. (2009). Changing power relations in the Nile River Basin: Unilateralism vs. cooperation?. Water Alternatives, 2(2).

Cascão, A. E., and Nicol, A. (2016). GERD: new norms of cooperation in the Nile Basin?. Water International, 41(4), 550-573.

Chen, J., Shi, H., Sivakumar, B., and Peart, M. R. (2016). Population, water, food, energy and dams. Renewable and Sustainable Energy Reviews, 56, 18-28.

Chen, L., Singh, V. P., Lu, W., Zhang, J., Zhou, J., and Guo, S. (2016). Streamflow forecast uncertainty evolution and its effect on real-time reservoir operation. Journal of Hydrology, 540, 712-726.

Chipman, J. W. (2019). A multisensor approach to satellite monitoring of trends in lake area, water level, and volume. Remote Sensing, 11(2), 158.

Chow, V. T., Maidment, D. R., and Mays, L. W. (1988). ‘‘Atmospheric Water’’, in Applied Hydrology, chap. 3, pp. 53–98, International ed., McGraw-Hill, N. Y.

Conway, D. (2000). The climate and hydrology of the Upper Blue Nile River. Geographical Journal, 166(1), 49-62.

Conway, D. (2005). From headwater tributaries to international river: Observing and adapting to climate variability and change in the Nile basin. Global Environmental Change, 15(2), 99-114.

Conway, D. (2017), Water resources: Future Nile river flows, Nature Climate Change, 7(5), 319-320.

Crétaux, J. F., and coauthors (2011). SOLS: A lake database to monitor in the Near Real Time water level and storage variations from remote sensing data. Advances in Space Research, 47(9), 1497-1507.

Decker, M., Brunke, M. A., Wang, Z., Sakaguchi, K., Zeng, X., and Bosilovich, M. G. (2012). Evaluation of the reanalysis products from GSFC, NCEP, and ECMWF using flux tower observations. Journal of Climate, 25(6), 1916-1944.

Degefu, D. M., He, W., and Zhao, J. H. (2015). Hydropower for sustainable water and energy development in Ethiopia. Sustainable Water Resources Management, 1(4), 305-314.

Delaney, C. J., and coauthors (2020). Forecast Informed Reservoir Operations Using Ensemble Streamflow Predictions for a Multipurpose Reservoir in Northern California. Water Resources Research, 56(9), e2019WR026604.

Digna, R. F., Mohamed, Y. A., van der Zaag, P., Uhlenbrook, S., van der Krogt, W., and Corzo, G. (2018). Impact of water resources development on water availability for hydropower production and irrigated agriculture of the eastern nile basin. Journal of Water Resources Planning and Management, 144(5), 05018007.

Dinku, T., Connor, S., and Ceccato, P. (2011). Evaluation of satellite rainfall estimates and gridded gauge products over the Upper Blue Nile region. Nile River Basin (pp. 109-127), Springer, Dordrecht.

Ebaid, H. M., and Ismail, S. S. (2010). Lake Nasser evaporation reduction study. Journal of advanced research, 1(4), 315-322.

EEPCo, Ethiopian Electric Power Corporation (2019), "Grand Ethiopian Renaissance Dam", http://www.eepco.gov.et/abouttheproject.php?pid=1andpcatid=2 (Accessed on November 5th, 2019)

Ehsani, N., Vörösmarty, C. J., Fekete, B. M., and Stakhiv, E. Z. (2017). Reservoir operations under climate change: Storage capacity options to mitigate risk. Journal of Hydrology, 555, 435-446.

ElBastawesy, M. (2014). Hydrological scenarios of the Renaissance Dam in Ethiopia and its hydro-environmental impact on the Nile downstream, Journal of Hydrologic Engineering, 20(7), 04014083.

Eldardiry, H., and Hossain, F. (2019). Understanding Reservoir Operating Rules in the Transboundary Nile River Basin Using Macroscale Hydrologic Modeling with Satellite Measurements. Journal of Hydrometeorology, 20(11), 2253-2269.

Eldardiry, H., and Hossain, F. (2020). A blueprint for adapting high Aswan dam operation in Egypt to challenges of filling and operation of the Grand Ethiopian Renaissance dam. Journal of Hydrology, 125708.

Eldardiry, H., and Hossain, F. (2021). Evaluating the Hydropower Potential of the Grand Ethiopian Renaissance Dam. Journal of Renewable and Sustainable Energy.

Eldardiry, H., and Hossain, F. (2021). The Value of Long-term Streamflow Forecasts in Adaptive Reservoir Operation: The Case of High Aswan Dam in the Transboundary Nile River Basin. Journal of Hydrometeorology.

Eldardiry, H., Habib, E., and Borrok, D. M. (2016). Small-scale catchment analysis of water stress in wet regions of the US: an example from Louisiana. Environmental Research Letters, 11(12), 124031.

Elnmer, A., Khadr, M., Kanae, S., and Tawfik, A. (2019). Mapping daily and seasonally evapotranspiration using remote sensing techniques over the Nile delta. Agricultural Water Management, 213, 682-692.

El-Shabrawy, G. M. (2009). Lake Nasser—Nubia. In The Nile (pp. 125-155). Springer, Dordrecht.

El-Shafie, A., Taha, M. R., and Noureldin, A. (2007). A neuro-fuzzy model for inflow forecasting of the Nile river at Aswan high dam. Water resources management, 21(3), 533-556.

Elshamy, M. E., Seierstad, I. A., and Sorteberg, A. (2009). Impacts of climate change on Blue Nile flows using bias-corrected GCM scenarios. Hydrology and Earth System Sciences, 13(5), 551-565.

Eltahir, E. A., (1996). El Niño and the natural variability in the flow of the Nile River. Water Resources Research, 32(1), 131-137.

Enku, T., van der Tol, C., Gieske, A. S., and Rientjes, T. H. (2011). Evapotranspiration modeling using remote sensing and empirical models in the Fogera floodplain, Ethiopia. In Nile River Basin (pp. 163-178). Springer, Dordrecht.

Epule, T. E., Ford, J. D., Lwasa, S., Nabaasa, B., and Buyinza, A. (2018). The determinants of crop yields in Uganda: what is the role of climatic and non-climatic factors?. Agriculture and Food Security, 7(1), 10.

Eum, H. I., and Simonovic, S. P. (2010). Integrated reservoir management system for adaptation to climate change: the Nakdong River Basin in Korea. Water Resources Management, 24(13), 3397-3417.

Falkenmark, M. (1989). The massive water scarcity now threatening Africa: why isn't it being addressed?. Ambio, 112-118.

Famiglietti, J. S., Cazenave, A., Eicker, A., Reager, J. T., Rodell, M., and Velicogna, I. (2015). Satellites provide the big picture. Science, 349(6249), 684-685.

FAO, 2016: AQUASTAT database, Irrigation and Drainage, Retrieved from: http://www.fao.org/nr/water/aquastat/irrigationdrainage/index.stm, Accessed 29 OCT 2018.

Feng, M., Liu, P., Guo, S., Shi, L., Deng, C., and Ming, B. (2017). Deriving adaptive operating rules of hydropower reservoirs using time-varying parameters generated by the E n KF. Water Resources Research, 53(8), 6885-6907.

Fisher, J. B., and coauthors (2017). The future of evapotranspiration: Global requirements for ecosystem functioning, carbon and climate feedbacks, agricultural management, and water resources. Water Resources Research, 53(4), 2618-2626.

Funk, C. C., and coauthors (2014). A quasi-global precipitation time series for drought monitoring. US Geological Survey Data Series, 832(4).

Funk, C., and coauthors (2015). The climate hazards infrared precipitation with stations—a new environmental record for monitoring extremes. Scientific data, 2(1), 1-21.

Galelli, S., Goedbloed, A., Schwanenberg, D., and van Overloop, P. J. (2014). Optimal real-time operation of multipurpose urban reservoirs: Case study in Singapore. Journal of Water Resources Planning and Management, 140(4), 511-523.

Gao, F., Zhang, Y., Ren, X., Yao, Y., Hao, Z., and Cai, W. (2018). Evaluation of CHIRPS and its application for drought monitoring over the Haihe River Basin, China. Natural Hazards, 92(1), 155-172.

Gaudard, L., and Romerio, F. (2014). Reprint of "The future of hydropower in Europe: Interconnecting climate, markets and policies". Environmental Science and Policy, 43, 5-14.

Gebremichael, M., Bitew, M. M., Hirpa, F. A., and Tesfay, G. N. (2014). Accuracy of satellite rainfall estimates in the Blue Nile Basin: Lowland plain versus highland mountain. Water Resources Research, 50(11), 8775-8790.

Georgakakos, A. P., and coauthors (2012). Value of adaptive water resources management in Northern California under climatic variability and change: Reservoir management. Journal of Hydrology, 412, 34-46.

Georgakakos, K. P., and Graham, N. E. (2008). Potential benefits of seasonal inflow prediction uncertainty for reservoir release decisions. Journal of Applied Meteorology and Climatology, 47(5), 1297-1321.

Gerlak, A. K., Lautze, J., and Giordano, M. (2011). Water resources data and information exchange in transboundary water treaties. International Environmental Agreements: Politics, Law and Economics, 11(2), 179-199.

Giuliani, M., Zaniolo, M., Castelletti, A., Davoli, G., and Block, P. (2019). Detecting the state of the climate system via artificial intelligence to improve seasonal forecasts and inform reservoir operations. Water Resources Research, 55(11), 9133-9147.

Giupponi, C., and Sgobbi, A. (2013). Decision support systems for water resources management in developing countries: Learning from experiences in Africa. Water, 5(2), 798-818.

Golembesky, K., Sankarasubramanian, A., and Devineni, N. (2009). Improved drought management of Falls Lake Reservoir: Role of multimodel streamflow forecasts in setting up restrictions. Journal of Water Resources Planning and Management, 135(3), 188-197.

Gouda, D. M. (2016). Social capital and local water management in Egypt. Oxford University Press.

Grumbine, R. E., and Xu, J. (2011). Mekong hydropower development. Science, 332(6026), 178-179.

Grumbine, R. E., Dore, J., and Xu, J. (2012). Mekong hydropower: drivers of change and governance challenges. Frontiers in Ecology and the Environment, 10(2), 91-98.

Habib, E., ElSaadani, M., and Haile, A. T. (2012). Climatology-focused evaluation of CMORPH and TMPA satellite rainfall products over the Nile Basin. Journal of Applied Meteorology and Climatology, 51(12), 2105-2121.

Hamlet, A. F., and Lettenmaier, D. P. (1999). Columbia River streamflow forecasting based on ENSO and PDO climate signals. Journal of water resources planning and management, 125(6), 333-341.

Hamlet, A. F., Huppert, D., and Lettenmaier, D. P. (2002). Economic value of long-lead streamflow forecasts for Columbia River hydropower. Journal of Water Resources Planning and Management, 128(2), 91-101.

Hecht, J. S., Lacombe, G., Arias, M. E., Dang, T. D., and Piman, T. (2019). Hydropower dams of the Mekong River basin: A review of their hydrological impacts. Journal of hydrology, 568, 285-300.

Hossain, F., and Katiyar, N. (2006). Improving flood forecasting in international river basins. Eos, Transactions American Geophysical Union, 87(5), 49-54.

Hossain, F., Katiyar, N., Hong, Y., and Wolf, A. (2007). The emerging role of satellite rainfall data in improving the hydro-political situation of flood monitoring in the under-developed regions of the world. Natural Hazards, 43(2), 199-210.

Humphrey, G. B., Gibbs, M. S., Dandy, G. C., and Maier, H. R. (2016). A hybrid approach to monthly streamflow forecasting: integrating hydrological model outputs into a Bayesian artificial neural network. Journal of Hydrology, 540, 623-640.

Huntjens, P., and coauthors (2011). Adaptive water management and policy learning in a changing climate: a formal comparative analysis of eight water management regimes in Europe, Africa and Asia. Environmental Policy and Governance, 21(3), 145-163.

Husrt, H. E., Black, R. P., and Simaika, Y. M. (1966). The Major Nile Projects. Nile Control Department - Ministry Of Public Works. The Nile Basin Encyclopedia (Vol.10).

IPOE (2013). International panel of experts for grand Ethiopian renaissance dam. Final Report, Addis Ababa, Ethiopia: IPoE.

Iqbal, N., Hossain, F., Lee, H., and Akhter, G. (2016). Satellite gravimetric estimation of groundwater storage variations over Indus Basin in Pakistan. IEEE Journal of Selected Topics in Applied Earth Observations and Remote Sensing, 9(8), 3524-3534.

Iqbal, N., Hossain, F., Lee, H., and Akhter, G. (2017). Integrated groundwater resource management in Indus Basin using satellite gravimetry and physical modeling tools. Environmental monitoring and assessment, 189(3), 128.

Jabbari, A., and Bae, D. H. (2020). Improving Ensemble Forecasting Using Total Least Squares and Lead-Time Dependent Bias Correction. Atmosphere, 11(3), 300.

Jasperse, J., and coauthors (2017). Preliminary viability assessment of Lake Mendocino forecast informed reservoir operations. Center For Western Weather and Water Extremes.

Jeevalakshmi, D., Reddy, S. N., and Manikiam, B. (2016, April). Land cover classification based on NDVI using LANDSAT8 time series: a case study Tirupati region. In 2016 International Conference on Communication and Signal Processing (ICCSP) (pp. 1332-1335). IEEE.

Ji, L., Senay, G. B., and Verdin, J. P. (2015). Evaluation of the Global Land Data Assimilation System (GLDAS) air temperature data products. Journal of Hydrometeorology, 16(6), 2463-2480.

Kalitsi, E. A. K. (2003). Problems and prospects for hydropower development in Africa. In The Workshop for African Energy Experts on Operationalizing the NGPAD Energy Initiative (pp. 2-4).

Karamouz, M., and Houck, M. H. (1982). Annual and monthly reservoir operating rules generated by deterministic optimization, Water Resources Research, 18(5), 1337-1344.

Karekezi, S., and Kimani, J. (2002). Status of power sector reform in Africa: impact on the poor. Energy Policy, 30(11-12), 923-945.

Kassem, H. S., Bello, A. R. S., Alotaibi, B. M., Aldosri, F. O., and Straquadine, G. S. (2019). Climate change adaptation in the delta Nile Region of Egypt: Implications for agricultural extension. Sustainability, 11(3), 685.

Keys, T. A., and Scott, D. T. (2018). Monitoring volumetric fluctuations in tropical lakes and reservoirs using satellite remote sensing. Lake and Reservoir Management, 34(2), 154-166.

Kibaroglu, A., and Gürsoy, S. I. (2015). Water–energy–food nexus in a transboundary context: the Euphrates–Tigris river basin as a case study. Water International, 40(5-6), 824-838.

Kim, U., Kaluarachchi, J. J., and Smakhtin, V. U. (2008). Generation of Monthly Precipitation Under Climate Change for the Upper Blue Nile River Basin, Ethiopia 1. JAWRA Journal of the American Water Resources Association, 44(5), 1231-1247.

King, A., and Block, P. (2014). An assessment of reservoir filling policies for the Grand Ethiopian Renaissance Dam. Journal of Water and Climate Change, 5(2), 233-243.

Kirtman, B. P., and coauthors (2014). The North American multimodel ensemble: phase-1 seasonal-to-interannual prediction; phase-2 toward developing intraseasonal prediction. Bulletin of the American Meteorological Society, 95(4), 585-601.

Kumagai, J. (2016). The Grand Ethiopian Renaissance Dam Gets Set to Open. IEEE SPECTRUM, 30.

Kummu, M., Gerten, D., Heinke, J., Konzmann, M., and Varis, O. (2014). Climate-driven interannual variability of water scarcity in food production potential: a global analysis, Hydrology and Earth System Sciences, 18(2), 447-461.

Labadie, J. W. (2004). Optimal operation of multireservoir systems: state-of-the-art review. Journal of water resources planning and management, 130(2), 93-111.

Lehner, B., and coauthors (2011). High-resolution mapping of the world's reservoirs and dams for sustainable river-flow management. Frontiers in Ecology and the Environment, 9(9), 494-502.

Lettenmaier, D. P. (2017). Observational breakthroughs lead the way to improved hydrological predictions. Water Resources Research, 53(4), 2591-2597.

Lettenmaier, D. P., Alsdorf, D., Dozier, J., Huffman, G. J., Pan, M., and Wood, E. F. (2015). Inroads of remote sensing into hydrologic science during the WRR era. Water Resources Research, 51(9), 7309-7342.

Liang, X., Lettenmaier, D. P., Wood, E. F., and Burges, S. J. (1994). A simple hydrologically based model of land surface water and energy fluxes for general circulation models. Journal of Geophysical Research: Atmospheres, 99(D7), 14415-14428.

Liang, X., Wood, E. F., and Lettenmaier, D. P. (1996). Surface soil moisture parameterization of the VIC-2L model: Evaluation and modification. Global and Planetary Change, 13(1-4), 195-206.

Liou, Y. A., and Kar, S. K. (2014). Evapotranspiration estimation with remote sensing and various surface energy balance algorithms—A review. Energies, 7(5), 2821-2849.

Lohmann, D., Raschke, E., Nijssen, B., and Lettenmaier, D. P. (1998). Regional scale hydrology: I. Formulation of the VIC-2L model coupled to a routing model. Hydrological sciences journal, 43(1), 131-141.

Longuevergne, L., Wilson, C. R., Scanlon, B. R., and Crétaux, J. F. (2013). GRACE water storage estimates for the Middle East and other regions with significant reservoir and lake storage. Hydrology and Earth System Sciences, 17(12), 4817-4830.

Loveland, T. R., Reed, B. C., Brown, J. F., Ohlen, D. O., Zhu, Z., Yang, L. W. M. J., and Merchant, J. W. (2000). Development of a global land cover characteristics database and IGBP DISCover from 1 km AVHRR data. International Journal of Remote Sensing, 21(6-7), 1303-1330.

Ma, F., Yuan, X., and Ye, A. (2015). Seasonal drought predictability and forecast skill over China. Journal of Geophysical Research: Atmospheres, 120(16), 8264-8275.

Mahmoud, M. K. (2005). Improvement The Efficiency Of Toshka Spillway Canal. Water Science, Issue, (37).

MALR, (2014). The ministry of agriculture and land reclamation, Annual bulletin of indicators of agricultural statistics.

Mataen, D. (2012). Africa--the Ultimate Frontier Market: A Guide to the Business and Investment Opportunities in Emerging Africa. Harriman House Limited.

Maurer, E. P., and Lettenmaier, D. P. (2004). Potential effects of long-lead hydrologic predictability on Missouri River main-stem reservoirs. Journal of Climate, 17(1), 174-186.

Maurer, E. P., Wood, A. W., Adam, J. C., Lettenmaier, D. P., and Nijssen, B. (2002). A long-term hydrologically based dataset of land surface fluxes and states for the conterminous United States. Journal of climate, 15(22), 3237-3251.

Melesse, A. M., Abtew, W., Setegn, S. G., and Dessalegne, T. (2011). Hydrological variability and climate of the Upper Blue Nile River basin. In Nile River Basin (pp. 3-37). Springer, Dordrecht.

Meze-Hausken, E., (2004). Contrasting climate variability and meteorological drought with perceived drought and climate change in northern Ethiopia. Climate Research, 27(1), 19-31.

Misra, V., and Li, H. (2014). The seasonal climate predictability of the Atlantic Warm Pool and its teleconnections. Geophysical Research Letters, 41(2), 661-666.

MIT. (2014). The Grand Ethiopian Renaissance Dam: An opportunity for collaboration and shared benefits in the Eastern Nile Basin: An amicus brief to the Riparian Nations of Ethiopia, Sudan and Egypt from the international, non-partisan Eastern Nile working group. Boston: Massachusetts Institute of Technology.

Mohie El Din, M. O., and Moussa, A. M. (2016). Water management in Egypt for facing the future challenges. Journal of advanced research, 7(3), 403-412.

Molden, D. J., and coauthors (2009). Nile Basin Focal Project. Synthesis report.

Moriasi, D. N., Arnold, J. G., Van Liew, M. W., Bingner, R. L., Harmel, R. D., and Veith, T. L. (2007). Model evaluation guidelines for systematic quantification of accuracy in watershed simulations. Transactions of the ASABE, 50(3), 885-900.

Moussa, A. M. A. (2018). Dynamic operation rules of multi-purpose reservoir for better flood management. Alexandria engineering journal, 57(3), 1665-1679.

Muala, E., Mohamed, Y. A., Duan, Z., and Van der Zaag, P. (2014). Estimation of reservoir discharges from Lake Nasser and Roseires Reservoir in the Nile Basin using satellite altimetry and imagery data. Remote Sensing, 6(8), 7522-7545.

Mulat, A. G., and Moges, S. A. (2014). Assessment of the impact of the Grand Ethiopian Renaissance Dam on the performance of the High Aswan Dam. Journal of Water Resource and Protection, 6(06), 583.

Mulligan, M., van Soesbergen, A., and Sáenz, L. (2020). GOODD, a global dataset of more than 38,000 georeferenced dams. Scientific Data, 7(1), 1-8.

Munia, H., Guillaume, J. H. A., Mirumachi, N., Porkka, M., Wada, Y., and Kummu, M. (2016). Water stress in global transboundary river basins: significance of upstream water use on downstream stress. Environmental Research Letters, 11(1), 014002.

Nachtergaele, F. O., (1999). From the Soil Map of the World to the Digital Global Soil and Terrain Database: 1960-2002. Handbook of Soil Science, CRC Press, Boca Raton, H5-17.

Nasr, H., and Neef, A. (2016). Ethiopia's challenge to Egyptian hegemony in the Nile River basin: The case of the Grand Ethiopian Renaissance Dam. Geopolitics, 21(4), 969-989.

Nayak, M. A., Herman, J. D., and Steinschneider, S. (2018). Balancing Flood Risk and Water Supply in California: Policy Search Integrating Short-Term Forecast Ensembles With Conjunctive Use. Water Resources Research, 54(10), 7557-7576.

Nijssen, B., O'Donnell, G. M., Lettenmaier, D. P., Lohmann, D., and Wood, E. F. (2001). Predicting the discharge of global rivers. Journal of Climate, 14(15), 3307-3323.

Pahl-Wostl, C. (2007). Transitions towards adaptive management of water facing climate and global change. Water resources management, 21(1), 49-62.

Paisley, R. K., and Henshaw, T. W. (2013). Transboundary governance of the Nile River Basin: Past, present and future. Environmental Development, 7, 59-71.

Paredes-Trejo, F. J., Barbosa, H. A., and Kumar, T. L. (2017). Validating CHIRPS-based satellite precipitation estimates in Northeast Brazil. Journal of arid environments, 139, 26-40.

Plengsaeng, B., Wehn, U., and van der Zaag, P. (2014). Data-sharing bottlenecks in transboundary integrated water resources management: a case study of the Mekong River Commission's procedures for data sharing in the Thai context. Water international, 39(7), 933-951.

Qin, P., Xu, H., Liu, M., Du, L., Xiao, C., Liu, L., and Tarroja, B. (2020). Climate change impacts on Three Gorges Reservoir impoundment and hydropower generation. Journal of Hydrology, 580, 123922.

Raadgever, G. T., Mostert, E., Kranz, N., Interwies, E., and Timmerman, J. G. (2008). Assessing management regimes in transboundary river basins: do they support adaptive management?. Ecology and Society, 13(1).

Rahman, M. A. (2013). Water security: Ethiopia–Egypt transboundary challenges over the Nile river basin. Journal of Asian and African Studies, 48(1), 35-46.

Rientjes, T. H., Haile, A. T., Gieske, A. S., Maathuis, B. H., and Habib, E. (2011). Satellite based cloud detection and rainfall estimation in the upper Blue Nile basin. In Nile River Basin (pp. 93-107). Springer, Dordrecht.

Robertson, D. E., Pokhrel, P., and Wang, Q. J. (2013). Improving statistical forecasts of seasonal streamflows using hydrological model output. Hydrology and Earth System Sciences, 17(1).

Rodell, M., Famiglietti, J. S., Wiese, D. N., Reager, J. T., Beaudoing, H. K., Landerer, F. W., and Lo, M. H. (2018). Emerging trends in global freshwater availability. Nature, 557(7707), 651-659.

Rodell, M., Houser, P. R., Jambor, U. E. A., Gottschalck, J., Mitchell, K., Meng, C. J., and Entin, J. K. (2004). The global land data assimilation system. Bulletin of the American Meteorological Society, 85(3), 381-394.

Roulin, E. (2007). Skill and relative economic value of medium-range hydrological ensemble predictions. Hydrology and Earth System Sciences, 11(2), 725-737.

Sabo, J. L., and coauthors (2017). Designing river flows to improve food security futures in the Lower Mekong Basin. Science, 358(6368), eaao1053.

Sadek, N., and Aziz, M. (2005). Flood management of lake nasser after the new toshka barrages construction. In Ninth International Water Technology Conference, IWTC9, Sharm El-Sheikh, Egypt.

Satti, S., Zaitchik, B., and Siddiqui, S. (2015). The question of Sudan: A hydro-economic optimization model for the Sudanese Blue Nile. Hydrology and Earth System Sciences, 19(5), 2275-2293.

Schaefli, B. (2015). Projecting hydropower production under future climates: a guide for decision-makers and modelers to interpret and design climate change impact assessments. Wiley Interdisciplinary Reviews: Water, 2(4), 271-289.

Schulz, C., Martin-Ortega, J., & Glenk, K. (2019). Understanding public views on a dam construction boom: the role of values. Water Resources Management, 33(14), 4687-4700.

Senay, G. B., Friedrichs, M., Singh, R. K., and Velpuri, N. M. (2016). Evaluating Landsat 8 evapotranspiration for water use mapping in the Colorado River Basin, Remote Sensing of Environment, 185, 171-185.

Shahin, M. M., (1985). Hydrology of the Nile basin (Vol. 21), Elsevier.

Sheffield, J., Wood, E. F., Pan, M., Beck, H., Coccia, G., Serrat-Capdevila, A., and Verbist, K. (2018). Satellite Remote Sensing for Water Resources Management: Potential for Supporting Sustainable Development in Data-Poor Regions. Water Resources Research, 54(12), 9724-9758.

Shumilova, O., Tockner, K., Thieme, M., Koska, A., and Zarfl, C. (2018). Global water transfer megaprojects: a potential solution for the water-food-energy nexus?. Frontiers in Environmental Science, 6, 150.

Siam, M. S., and E. A. Eltahir, (2017). Climate change enhances interannual variability of the Nile river flow. Nature Clim. Change, 7(5), 350.

Siddique-E-Akbor, and coauthors (2014). Satellite precipitation data–driven hydrological modeling for water resources management in the Ganges, Brahmaputra, and Meghna Basins. Earth Interactions, 18(17), 1-25.

Slater, L. J., and Villarini, G. (2018). Enhancing the predictability of seasonal streamflow with a statistical-dynamical approach. Geophysical Research Letters, 45(13), 6504-6513.

Slater, L. J., Villarini, G., and Bradley, A. A. (2019). Evaluation of the skill of North-American multi-model ensemble (NMME) global climate models in predicting average and extreme precipitation and temperature over the continental USA. Climate Dynamics, 53(12), 7381-7396.

Sridharan, V., and coauthors (2019). Resilience of the Eastern African electricity sector to climate driven changes in hydropower generation. Nature communications, 10(1), 1-9.

Suberu, M. Y., Mustafa, M. W., Bashir, N., Muhamad, N. A., and Mokhtar, A. S. (2013). Power sector renewable energy integration for expanding access to electricity in sub-Saharan Africa. Renewable and Sustainable Energy Reviews, 25, 630-642.

Sun, G., McNulty, S. G., Moore Myers, J. A., and Cohen, E. C. (2008). Impacts of multiple stresses on water demand and supply across the Southeastern United States. Journal of the American Water Resources Association, 44(6), 1441-1457.

Sutcliffe, J. V., and Parks, Y. P. (1999). The hydrology of the Nile. Int. Assoc. Hydrol. Sci., IAHS Special publication No. 5, Wallingford, UK.

Sutcliffe, J. V., and Y. P. Parks, 1999: The hydrology of the Nile. International Association of Hydrological Sciences, IAHS Special publication No. 5, Wallingford, UK.

Taye, M. T., and Willems, P. (2012). Temporal variability of hydroclimatic extremes in the Blue Nile basin. Water Resources Research, 48(3).

Taye, M. T., Tadesse, T., Senay, G. B., and Block, P. (2016). The grand Ethiopian renaissance dam: source of cooperation or contention?. Journal of Water Resources Planning and Management, 142(11), 02516001.

Taye, M. T., Willems, P. and Block, P. (2015). Implications of climate change on hydrological extremes in the Blue Nile basin: a review. Journal of Hydrology.: Regional Studies, 4, 280-293.

Teferi, E., Uhlenbrook, S., and Bewket, W. (2015). Inter-annual and seasonal trends of vegetation condition in the Upper Blue Nile (Abay) Basin: dual-scale time series analysis. Earth System Dynamics, 6(2), 617.

Tesemma, Z. K., Mohamed, Y. A., and Steenhuis, T. S. (2010). Trends in rainfall and runoff in the Blue Nile Basin: 1964–2003. Hydrological processes, 24(25), 3747-3758.

Thomas Jr, H. A., and Revelle, R. (1966). On the efficient use of High Aswan Dam for hydropower and irrigation. Management Science, 12(8), B-296.

Turner, S. W., Bennett, J. C., Robertson, D. E., and Galelli, S. (2017). Complex relationship between seasonal streamflow forecast skill and value in reservoir operations. Hydrology and Earth System Sciences, 21(9), 4841-4859.

Uria-Martinez, R., Johnson, M., and O'Connor, P. (2018). 2017 Hydropower Market Report Highlights. Oak Ridge National Lab.(ORNL), Oak Ridge, TN (United States).

USBR, (1964). Land and Water Resources of the Blue Nile Basin, Ethiopia. United States Department of the Interior, Bureau of Reclamation.

van der Krogt, W., and Ogink, H. (2013). Development of the Eastern Nile water simulation model. Main Report (Report No. 1206020-000-VEB-0010).

Van der Zwaan, B., Boccalon, A., and Dalla Longa, F. (2018). Prospects for hydropower in Ethiopia: An energy-water nexus analysis. Energy Strategy Reviews, 19, 19-30.

Vörösmarty, C. J., Green, P., Salisbury, J., and Lammers, R. B. (2000). Global water resources: vulnerability from climate change and population growth, Science, 289(5477), 284-288.

Wada, Y., and Bierkens, M. F. (2014). Sustainability of global water use: past reconstruction and future projections. Environmental Research Letters, 9(10), 104003.

Wada, Y., Van Beek, L. P. H., Viviroli, D., Dürr, H. H., Weingartner, R., and Bierkens, M. F. (2011). Global monthly water stress: 2. Water demand and severity of water stress. Water Resources Research, 47(7).

Wan, W., Zhao, J., and Wang, J. (2019). Revisiting water supply rule curves with hedging theory for climate change adaptation. Sustainability, 11(7), 1827.

Wan, W., Zhao, J., Lund, J. R., Zhao, T., Lei, X., and Wang, H. (2016). Optimal hedging rule for reservoir refill. Journal of Water Resources Planning and Management, 142(11), 04016051.

Wang, X., Chen, Y., Song, L., Chen, X., Xie, H., and Liu, L. (2013). Analysis of lengths, water areas and volumes of the Three Gorges Reservoir at different water levels using Landsat images and SRTM DEM data. Quaternary International, 304, 115-125.

Waterbury, J., (2008). The Nile Basin: National determinants of collective action. Yale University Press.

Wheeler, K. G., and coauthors (2016). Cooperative filling approaches for the grand Ethiopian renaissance dam. Water International, 41(4), 611-634.

Wheeler, K. G., Hall, J. W., Abdo, G. M., Dadson, S. J., Kasprzyk, J. R., Smith, R., and Zagona, E. A. (2018). Exploring cooperative transboundary river management strategies for the Eastern Nile Basin. Water Resources Research, 54(11), 9224-9254.

Wheeler, K., and Setzer, S. (2012). Eastern Nile RiverWare planning model. Addis Ababa: Eastern Nile Technical and Regional Office.

Whittington, D. (2004). Visions of Nile basin development. Water policy, 6(1), 1-24.

Whittington, D., Waterbury, J., and Jeuland, M. (2014). The Grand Renaissance Dam and prospects for cooperation on the Eastern Nile. Water Policy, 16(4), 595-608.

Woldemeskel, F., and coauthors (2018). Evaluating post-processing approaches for monthly and seasonal streamflow forecasts. Hydrology and Earth System Sciences, 22(12), 6257-6257.

Wolde-Rufael, Y. (2006). Electricity consumption and economic growth: a time series experience for 17 African countries. Energy policy, 34(10), 1106-1114.

Wood, A. W., and Schaake, J. C. (2008). Correcting errors in streamflow forecast ensemble mean and spread. Journal of Hydrometeorology, 9(1), 132-148.

Wood, A. W., Leung, L. R., Sridhar, V., and Lettenmaier, D. P. (2004). Hydrologic implications of dynamical and statistical approaches to downscaling climate model outputs. Climatic change, 62(1-3), 189-216.

Wulder, M. A., Masek, J. G., Cohen, W. B., Loveland, T. R., and Woodcock, C. E. (2012). Opening the archive: How free data has enabled the science and monitoring promise of Landsat. Remote Sensing of Environment, 122, 2-10.

Yang, G., Guo, S., Liu, P., and Block, P. (2020). Integration and Evaluation of Forecast-Informed Multiobjective Reservoir Operations. Journal of Water Resources Planning and Management, 146(6), 04020038.

Ye, A., Duan, Q., Yuan, X., Wood, E. F., and Schaake, J. (2014). Hydrologic post-processing of MOPEX streamflow simulations. Journal of hydrology, 508, 147-156.

Yihdego, Z., Rieu-Clarke, A., and Cascão, A. E. (2016). How has the Grand Ethiopian Renaissance Dam changed the legal, political, economic and scientific dynamics in the Nile Basin?

Yuan, X., Wood, E. F., and Ma, Z. (2015). A review on climate-model-based seasonal hydrologic forecasting: physical understanding and system development. Wiley Interdisciplinary Reviews: Water, 2(5), 523-536.

Zarfl, C., Lumsdon, A. E., Berlekamp, J., Tydecks, L., and Tockner, K. (2015). A global boom in hydropower dam construction. Aquatic Sciences, 77(1), 161-170.

Zaroug, M. A., Eltahir, E. A., and Giorgi, F. (2014). Droughts and floods over the upper catchment of the Blue Nile and their connections to the timing of El Niño and La Niña events. Hydrology and Earth System Sciences, 18(3), 1239-1249.

Zeitoun, M., Allan, J. T., and Mohieldeen, Y. (2010). Virtual water 'flows' of the Nile Basin, 1998–2004: A first approximation and implications for water security. Global Environmental Change, 20(2), 229-242.

Zeitoun, M., Goulden, M., and Tickner, D. (2013). Current and future challenges facing transboundary river basin management. Wiley Interdisciplinary Reviews: Climate Change, 4(5), 331-349.

Zevenbergen, C., Bhattacharya, B., Wahaab, R. A., Elbarki, W. A. I., Busker, T., and Rodriguez, C. S. (2017). In the aftermath of the October 2015 Alexandria Flood Challenges of an Arab city to deal with extreme rainfall storms. Natural hazards, 86(2), 901-917.

Zhang, W., Liu, P., Wang, H., Chen, J., Lei, X., and Feng, M. (2017). Reservoir adaptive operating rules based on both of historical streamflow and future projections. Journal of hydrology, 553, 691-707.

Zhang, Y., Block, P., Hammond, M., and King, A. (2015). Ethiopia's Grand Renaissance Dam: Implications for downstream riparian countries. Journal of Water Resources Planning and Management, 141(9), 05015002.

Zhao, T., Cai, X., and Yang, D. (2011). Effect of streamflow forecast uncertainty on real-time reservoir operation. Advances in water resources, 34(4), 495-504.

Zhao, T., Yang, D., Cai, X., Zhao, J., and Wang, H. (2012). Identifying effective forecast horizon for real-time reservoir operation under a limited inflow forecast. Water Resources Research, 48(1).

Zhou, T., Voisin, N., Leng, G., Huang, M., and Kraucunas, I. (2018). Sensitivity of Regulated Flow Regimes to Climate Change in the Western United States. Journal of Hydrometeorology, 19(3), 499-515.

Zhu, C., and Lettenmaier, D. P. (2007). Long-term climate and derived surface hydrology and energy flux data for Mexico: 1925–2004. Journal of Climate, 20(9), 1936-1946.